Gas diffusion transport characteristics and mathematical description of membrane systems with application for biogas upgrading.

OGUNLUDE, P.

2023

GAS DIFFUSION TRANSPORT CHARACTERISTICS AND MATHEMATICAL DESCRIPTION OF MEMBRANE SYSTEMS WITH APPLICATION FOR BIOGAS UPGRADING

PRISCILLA OGUNLUDE

PhD 2023

GAS DIFFUSION TRANSPORT CHARACTERISTICS AND MATHEMATICAL DESCRIPTION OF MEMBRANE SYSTEMS WITH APPLICATION FOR BIOGAS UPGRADING

PRISCILLA OGUNLUDE

A thesis submitted in partial fulfilment of the requirements of Robert Gordon University for the degree of Doctor of Philosophy

March 2023

ABSTRACT

Greenhouse gas emissions (GHGs) and their effects have been a matter of global concern over the past decade. With growing energy demands to support developing economies, there has been a challenge of harnessing and utilizing renewable energy to meet these demands. However, despite the effect of global warming and the problems associated with it, the use of fossil fuels is still increasing. This problem has negatively impacted the climate because the greenhouse gases evolved from burning fossils, are increasing the concentration of carbon dioxide in the atmosphere. Thus, this study investigates a method of channelling biogas for use as a renewable energy source using membrane technology which could remedy the situation.

The study began with observing the behaviour of biogas components as they travel selectively through the membrane support. This was done by conducting gas permeation tests to experimentally show how methane and carbon dioxide gases flow distinctively through ceramic membranes having different physico-chemical properties. Permeation tests were carried out under various operating conditions of temperature (up to 100^{o}C) and pressure (up to 3 bar) using membranes of different pore sizes and characteristics to ascertain the influence of these parameters on the membrane perm-selectivity. It was identified that the membranes were operating in a parallel flow regime and gas permeability was a function of viscous and Knudsen flow. A mass transfer model was developed to confirm that mass transfer conditions were not limiting in the boundary layer of the membrane surface. The model incorporates the influence of both structural and fluid properties in characterising diffusive and convective flow through the membrane. The analysis showed that under the same pressure drop across the membrane, the mass flux in porous membrane can be over four orders of magnitude higher than in a silica PDMS membrane with the similar thickness.

Based on these findings, a dynamic approach was considered to modify the membrane by dip coating technique which allows easy manipulation of the deposition quantity and thickness, and it was possible to achieve a finely modified membrane with reduced pore size that improves the perm-selectivity. A methane selectivity of 1.6 was achieved which is of the ideal Knudsen selectivity with a 42% decrease in the CO_2 concentration of the gas mixture.

Permeation studies of the coated membrane shows that gas permeance is dependent on temperature with little impact due to pressure changes which can be attributed to a reduced impact of viscous flow due to the coating. The reduction in pore size due to coating was to a degree that significantly impacts the viscous flow contribution. The characterization results confirm this pore size reduction with the methane gas permeation rates reduced from $6x10^{-6}$ mol/m^2sPa to $1x10^{-6}$ mol/m^2sPa for the support and coated membrane respectively. A numerical method of estimating the pore size of the coated membrane was adopted based on the operating flow mechanism using a series model in conjunction with flow parameters through the layers. It was confirmed that the pore size of the coated membrane was sufficiently reduced to 36nm which is in the dominant Knudsen range. Hence, it was confirmed that by modifying the membranes with this technique, it is possible to increase the selectivity of the methane by Knudsen diffusion.

From this study, it can be established that a membranes' selectivity performance is dependent on an interplay of factors: (i) the structural effect which filters gases based on their interaction with pores; (ii) the thermodynamic equilibrium effect having to do with operating conditions, and (iii) the kinetic effect which considers the different diffusion rates of gas components making them permeate quicker than others.

Keywords: membranes, ceramic, permeance, selectivity, biogas, carbon-capture, separation, renewables

DEDICATION

This work is dedicated to God Almighty who has helped me through each step of the way and to my Dear husband, Ayodeji, for believing in me and ensuring I have everything need to succeed.

DECLARATION

I hereby declare that the material presented in this report is my own work and where this is not the case, the source material has been duly acknowledged.

ACKNOWLEDGEMENT

Heartfelt gratitude to my husband, Ayodeji Ogunlude, for his unwavering support from the PhD application stage to completion, thank you for believing in me and encouraging me even in my lows. I appreciate my children for sharing me with the world of academia and allowing me to pursue my dreams.

To my principal supervisor, Late Professor Edward Gobina, words are not enough to express my appreciation for your support and guidance all through the years that has moulded me to the researcher that I am today. I also appreciate Dr Firdaus Muhammad-Sukki for your co-supervision throughout my studies. Thank you both for your expert guidance.

I whole heartedly appreciate all my lab colleagues, Dr Ofasa Abunumah, Florence Aisueni, Evans Ogoun, Muktar Ramalan, and Idris Hashim for their help and support. Thank you all for being there for me even beyond the academic sphere.

Many thanks to the technical support and administration team of the School of Engineering and the School of Pharmacy and Life Sciences for guidance through health and safety as well as always being available as and when needed for support.

Last but not the least, special thanks to my parents, siblings, and in-laws for all the support and prayers throughout.

I look forward to more accomplishments even in the future.

Contents

LIST OF FIGURES

LIST OF TABLES

LIST OF PUBLICATIONS AND CONFERENCE PROCEEDINGS

OGUNLUDE, P., ABUNUMAH, O., ORAKWE, I., SHEHU, H., MUHAMMAD-SUKKI, F. and GOBINA, E. 2019. Comparative evaluation of the effect of pore size and temperature on gas transport in nano-structured ceramic membranes for biogas upgrading. WEENTECH Proceedings in Energy, 5(1): Proceedings of the 4th International Conference on Energy, Environment and Economics (ICEEE2019), 20-22 August 2019, Edinburgh, UK, pages 195-205.

Available from: https://doi.org/10.32438/WPE.8319

OGUNLUDE, P., ABUNUMAH, O., ORAKWE, I., SHEHU, H., MUHAMMAD-SUKKI, F., and GOBINA, E. 2019. Upgrading biogas to a bio-methane by use of nano-structured ceramic membranes. In Cossu, R., He, P., Kjeldsen, P., Matsufuji, Y. and Stegmann, R. (eds.). Proceedings of the 17th International Waste Management and Landfill Symposium (Sardinia 2019), Cagliari, Italy. Padova: CISA, article 598.

Available from: https://cisapublisher.com/product/proceedings-sardinia-2019/

OGUNLUDE, P., ABUNUMAH, O., ORAKWE, I., SHEHU, H., MUHAMMAD-SUKKI, F. and GOBINA, E. 2020. Upgrading biogas to biomethane by use of nano-structured ceramic membranes. Detritus, 12, pages 73-77.

Available from: https://doi.org/10.31025/2611-4135/2020.13996

OGUNLUDE, P., ABUNUMAH, O. and GOBINA, E. 2020. A study of gas diffusion characteristics on nano-structured ceramic membranes. European Journal of Engineering and Formal Sciences, 4(1), pages 21-23.

Available from: https://doi.org/10.26417/ejef.v4i1.p21-23

OGUNLUDE, P., ABUNUMAH, O., ORAKWE, I., SHEHU, H., MUHAMMAD-SUKKI, F. and GOBINA, E. 2022. An initial study of biogas upgrading to bio-methane with carbon dioxide capture using ceramic membranes. Catalysis Today, 388-389, pages 87-91.

Available from: https://doi.org/10.1016/j.cattod.2020.11.006

OGUNLUDE, P., ABUNUMAH, O., MUHAMMAD-SUKKI, F. and GOBINA, E. 2021. Testing membranes for separation of CO2 from small molecules in landfill gas.

In 2021 TUBA (Turkish Academy of Science) World Conference on Energy Science and Technology (TUBA WCEST-2021) Book of abstracts, 8-12 August 2021. Ankara: Turkish Academy of Sciences, pages 86-87.

Available from: https://doi.org/10.53478/TUBA.2021.017

OGUNLUDE, P., ABUNUMAH, O., MUHAMMAD-SUKKI, F. and GOBINA, E. 2021. A study of gas transport mechanisms for CH4/CO2 using ceramic membranes. Crystals, 11(10): selected papers from 8th International Conference and Exhibition on Advanced and Nanomaterials 2021 (ICANM 2021), 9-11 August 2021, article 1224.

Available from: https://doi.org/10.3390/cryst11101224

OGUNLUDE, P., ABUNOMAH, O., HASHIM, I., AISUENI, F., OGOUN, E., ANTWI, S., RAMALAN, M., WILLIAMWEST, T., SUKKI, F.M. and GOBINA, E. 2022. Mass transfer characteristics through alumina membranes with different pores sizes and porosity. International Journal of Engineering, Science and Technology, 4(1), pages 99-123.

Available from: https://doi.org/10.46328/ijonest.71

OGUNLUDE, P., ABUNUMAH, O., GIWA, A. and MUHAMMAD-SUKKI, F., GOBINA, E. 2021. Predicting CO2 and CH4 transport in landfill gas using porous inorganic membranes operated in the Darcy regime. In Proceedings of 2021 International Congress of Scientific Advances (ICONSAD'21), 22-25 December 2021, Turkey: ICONSAD, pages 770-784.

Available from: https://tinyurl.com/2p8uy2rh

Ogunlude P., Abunumah O., Gobina E., Muhammad-Sukki F. An Experimental Study on the Effect of Methane Potent Biogas Mixture on Gas Permeation Mechanism. In Proceedings of 2022 TechConnect World Innovation Conference and Expo, Washington DC, USA, pages 43-48.

Available from:
https://briefs.techconnect.org/wpcontent/volumes/TCB2022/pdf/188.pdf

LIST OF ACRONYMS

atm	Atmosphere
CH_4	Methane
CO_2	Carbon dioxide
COSHH	Control of substances hazardous to health regulations
EDXA	Energy dispersive x-ray analyser
FTIR	Fourier transform infrared spectrometer
GHG	Greenhouse gases
IUPAC	International Union of Pure and Applied Chemistry
mol	mole
MW	Molecular weight
nm	Nanometre
RA	Risk assessment
SEM	Scanning electron microscopy
SLPM	Standard litres per minute
UNFCCC	United Nations Framework Convention on Climate Change

LIST OF SYMBOLS

μ	Gas viscosity	P_a s
λ	Mean free path	m
α	Selectivity	-
$\emptyset$	Porosity	%
ΔP	Pressure difference	Pa
A	Membrane surface area	m^2
J	Gas flux	mol m^{-2} s^{-1}
P	Permeability	mol m^{-2} s^{-1} Pa^{-1}
Q	Molar flowrate	mol s^{-1}
r	Membrane radius	m
R	Universal gas constant	J kg^{-1} mol^{-1}
r_p	Membrane pore radius	m
T	Temperature	k
δ	Membrane thickness	m

CHAPTER 1: INTRODUCTION AND BACKGROUND

This section gives an overview of membrane application to biogas upgrading. It highlights the importance of mitigating greenhouse gas emissions and how biogas plays a role in reducing these emissions whilst providing an alternative source of energy. The aim and objectives of the research is presented followed by an outline of the thesis.

1.1 GREENHOUSE GASES

The emission of greenhouse gases has been confirmed to be a major factor affecting global warming (Lashof and Ahuja 1990). Greenhouse gases include methane, carbon dioxide, nitrous oxide and chlorofluorocarbons with carbon dioxide, CO_2 and methane, CH_4 being the most potent (Yang, Kathiraser and Kawi 2013). When these gases are released into the atmosphere and accumulate in sufficient quantities, they cause heat to be trapped (i.e. do not allow heat to dissipate into space). This trapping of heat causes an imbalance in the amount of energy that comes from the sun to the earth and back. When this happens, it causes distortion on the earth surface temperature resulting in temperature increments, which subsequently results in global warming.

Global warming is described as an increase in the overall air temperature near the earth's surface. This can have major consequences including higher evaporation rates that occurs as the earth becomes warmer. The increase in temperature causes the ice near the poles to melt at a faster rate. Overtime, this would result in an unbalanced distribution of rainfall implying that some parts of the earth experiencing high rainfall and floods whilst others experience dryness and droughts.

The devastating effects of the extreme conditions of flooding and dryness cannot be over-emphasized. The adverse effects of flooding include, but are not limited to, destruction of farm crops, displacement of people and destruction of properties, waste of man-hours, ultimately affecting the economy. Dryness and drought also cause damaging effects on crop yield and aquatic life. Also as a result of temperature rise on earth, the ozone layer, which prevents the penetration of ultraviolet radiation, is depleted. The depletion of the ozone layer increases the risk of ultraviolet radiation, which may trigger health complications and conditions for the spread of certain diseases such as cancer,

asthma, bronchitis, eye cataracts, etc.

Evidence has shown that there is a direct link between global warming and climate change yet the energy industry which is one of the largest contributors of greenhouse gas emissions still produces power by burning fossil fuels that increase the concentration of greenhouse gas emissions in the atmosphere (Akorede et al. 2012; Pachauri et al. 2014). The by-products of burning fossil fuels include sulphur dioxide, soot, and ash, that also pose a problem and lead to global dimming by altering the properties of the clouds due to a decline in the amount of direct irradiance on the Earth's surface (Wild 2018).

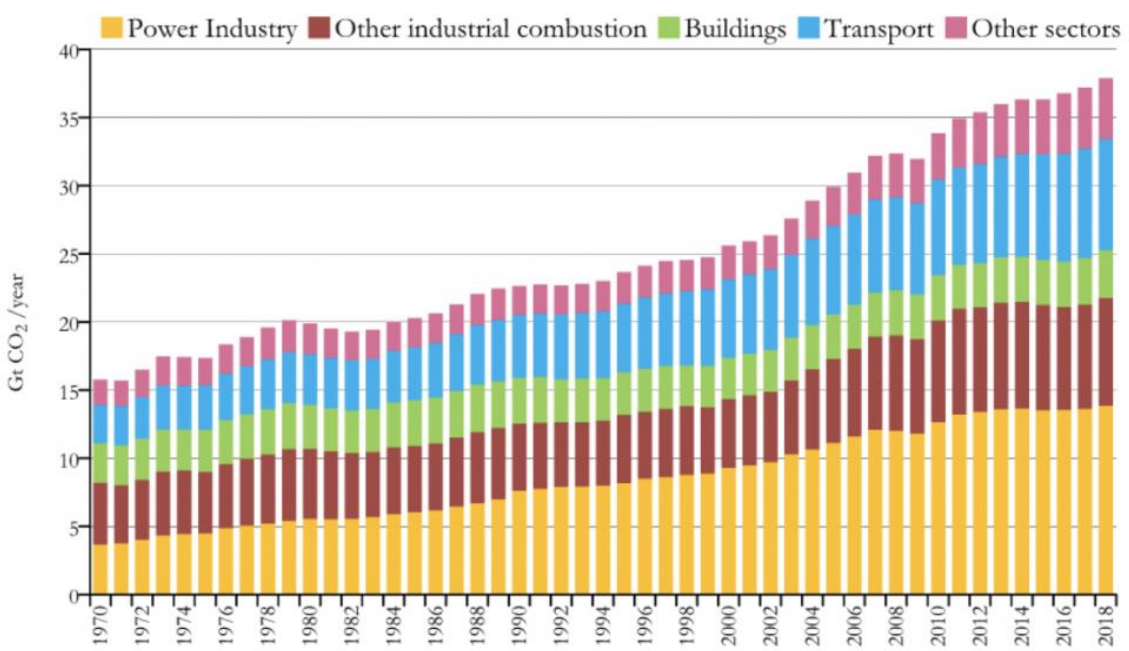

Figure 1 Total global annual emissions of fossil CO_2 in gigatonnes, Gt CO_2/yr by sector ('The Greta Effect: Global CO2 Emissions Increased By 1.9% In 2018' 2019)

As shown in

Figure 1 above, the rise in global GHG emissions shows the huge reliance on fossil fuels (Sokolov et al. 2009). It was reported by the International Energy Agency that CO_2 emissions increases at an annual rate of about 6% due to the reliance on world economies on fossil fuel usage (Dai et al. 2016). This can only begin to change as awareness is increased and the populace, especially stake holders, have a shift in perspective and incorporate green energy into the global

economy. This research therefore plays a vital role by improving existing biogas upgrading technology to provide a simple and cost-effective alternative to fossil fuel usage. Biogas is considered a carbon-neutral energy source because it does not contribute any net greenhouse gas to the atmosphere. The production and use of biogas would, on the other hand, help reduce emissions by capturing methane and carbon dioxide from a waste site before it is released to the atmosphere, and then utilise it as renewable energy that can replace conventional energy sources to fulfil growing energy demands in the economy.

A suitable means of handling emissions has now become a matter of global urgency and this has been proven in recent times by the unfortunate documented events of disasters directly linked to climate change (Quadrelli and Peterson 2007; Seneviratne et al. 2016). For example, in the summer of 2019, Europe experienced a terrible heat wave with Paris reaching its highest ever recorded temperature of 42.5^{o}C (van Oldenborgh et al. n.d.), parts of the United States of America suffered flooding (Gardner 2019), the people of Chennai in India faced droughts ('Viewpoint: Why India's Chennai Has Run out of Water' 2019), Britain's crop shortage posed a problem in the food sector ('Could Climate Change Lead to a Shortage of Food? - CBBC Newsround' n.d.), and Australia experienced a dreadful wildfire ('Australia Bushfires: Cause, Impact, and Restoration' 2020). There has been proposed strategies on how to combat the issue of climate change with various unions organizing international conferences and meetings such as the Kyoto protocol and the intergovernmental panel on climate change (Protocol 1997; Rubin and De Coninck 2005; Zeng, Qu and Zhang 2009). There has also been the introduction of some environmental regulations that encourage the use of sustainable forms of energy which has served as an incentive. Some of these include, the UK net-zero emissions target by 2050 ('UK Becomes First Major Economy to Pass Net Zero Emissions Law' 2020), a cap on the fraction of renewable fuels that are crop based and carbon costing (Fischer and Newell 2005; Michalopoulos 2018).

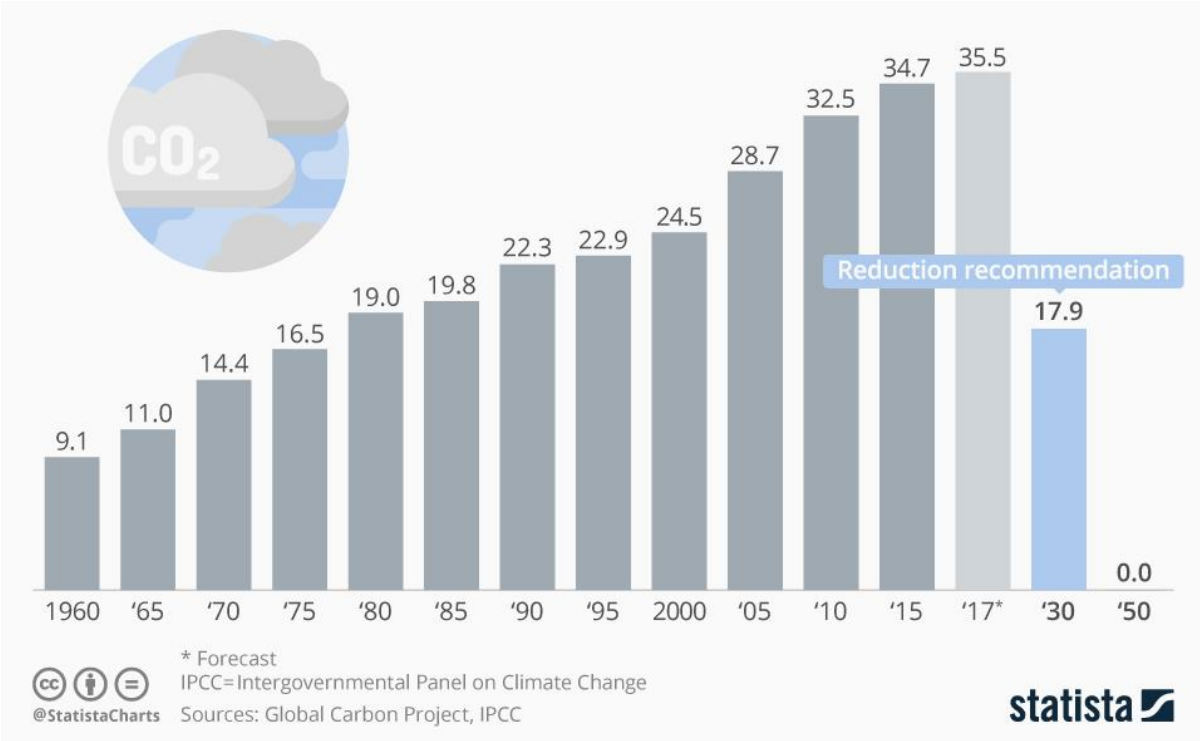

Figure 2 IPCC emissions reduction recommendation in coming decades ('Infographic: IPCC: Pull the Emergency Brake on Global CO2 Emissions' 2020)

Figure *2* shows the recommended reduction in global emissions by the intergovernmental panel on climate change for the year 2030 and beyond. Although, energy production is the largest contributor to GHGs and is a necessity in a growing economy. The energy source can be substituted with a greener choice to mitigate emissions, and this can be realized by capturing and utilizing biogas as a renewable source of energy.

1.2 BIOGAS

In addition to the natural production of greenhouse gases, anthropogenic emissions are caused by daily human activities. Burning of fossil fuels and industrial processes are the major contributors of greenhouse gas emissions resulting in temperature increase and leading to global warming. The challenges posed by global warming have been a cause of serious concern to people, organizations, countries, and the world at large. There are on-going efforts by many nations of the world to significantly reduce emissions from greenhouse gases. These emissions cause environmental pollution because of the toxins produced and released into the atmosphere. This in turn, causes environmental

degradation which poses a threat to the health of living organisms including humans.

Biogas is a mixture that contains mainly carbon dioxide (CO_2) and methane (CH_4). It is evolved from the anaerobic digestion of bio-degradable materials that decompose over time in the digester. These bio-degradable materials include food waste, animal waste, sewage, and other municipal waste. Depending on the biogas source, the conditions in the anaerobic digester such as temperature and several other factors, biogas may also contain other gases like nitrogen (N_2), hydrogen (H_2), ammonia (NH_3), water vapour (H_2O), and siloxanes (Ryckebosch, Drouillon and Vervaeren 2011). The components of biogas can be processed to produce fuels with higher heating values that can be used for various purposes including heating, cooking, transportation, and injection to the national gas grid. This chapter explains the technology behind biogas production and its constituents in the raw state. Figure 3 shows a schematic diagram on how biogas is produced and utilized. The incorporation of biogas utilization technology to the different sectors of the economy would drastically decrease greenhouse gases in the atmosphere as a large percentage of emissions come from the transport and power sectors which largely depend on fossil fuels (Akorede et al. 2012).

Biogas offers numerous advantages over other energy sources. For instance, it does not depend on weather conditions to operate unlike solar or wind. Solar energy depends on sunshine which is usually effective in the summer season and is therefore seasonal. Although solar energy can still be collected on cloudy and rainy days, the efficiency of the system decreases. Similarly, for wind energy, wind strength or speed varies seasonally and cannot be relied upon all through the year. The wind turbines may also not function effectively during certain periods. Biogas on the other hand, can be produced without these limitations and can be easily compressed/stored on a large scale which allows for easy adaptation on demand.

Furthermore, there is a significant reduction in gas emissions compared to other energy sources such as fossil fuels which contribute to anthropogenic emissions in the atmosphere. These emissions pollute and degrade the environment and the effects pose devastating threats to human and other

biological existence.

Additionally, the cost of waste management can be turned into opportunity as the amount of waste going into landfills are reduced while greenhouse gases are captured instead of being released into the atmosphere. This will not only be beneficial to the environmental quality and health of living organisms but could also boost the economy through job creation for the locals and increase potential for revenue generation through export.

Finally, digestate from the biogas digestion process offers an option to recycle nutrients in the food supply chain. This will minimize the use of petrochemical and mined fertilizers (Deepanraj, Sivasubramanian and Jayaraj 2014), thereby promoting production of organic farm produce.

1.3 ANAEROBIC DIGESTION (AD)

Anaerobic digestion is a natural process through which organic matter is broken down by microscopic organisms in the absence of oxygen. The process has been employed as a means for handling waste such as sewage sludge, organic farm waste, municipal solid waste, green/plant waste, organic and industrial/commercial waste (Tomori 2012).

Anaerobic digestion can occur at psychrophilic (below 25^{o}C); mesophilic (25^{o}C – 45^{o}C); and thermophilic (45^{o}C – 70^{o}C) temperature ranges (Al Seadi 2008; Toma et al. 2016). Thermophilic temperatures are very good in terms of biogas formation because of the higher temperatures used. However, maintaining this temperature range is costlier than generation in the mesophilic and psychrophilic temperature ranges which can happen in nature.

The four key phases of anaerobic digestion include hydrolysis, acidogenesis, acetogenesis and methanogenesis (Cappenberg 1975; Deepanraj, Sivasubramanian and Jayaraj 2014).

Hydrolysis: Biomass comprises a range of organic polymer chains which must be broken down for the microscopic organisms in digesters to get to the energy capability it contains. The process of breaking down these polymer chains is known as hydrolysis. Thus, the first phase in anaerobic processing is the hydrolysis of high molecular weight polymeric components, amino acids and

fatty acids. Acetate and hydrogen obtained from hydrolysis can be directly acted upon by methanogens while molecules like volatile fatty acids (VFAs) with more extended chain lengths than acetate would need to be further broken down for utilization by methanogens. Methanogens are the microorganisms that produce methane as a metabolic by-product.

Acidogenesis: This phase continues to break down the large chain lengths by acidogenic or fermentative microscopic organisms and form volatile fatty acids, alkali, carbon dioxide, and hydrogen sulfide.

Acetogenesis: Products from the acidogenesis stage are further processed by acetogens. Acetogens are microorganisms that produce acetate as a result of carbon dioxide reduction as shown in the equation below.

$$2CO_2 + 4H_2 \rightarrow CH_3COOH + 2H_2O$$

Methanogenesis: The final stage uses the transitional products of the prior stages and convert them into methane, carbon dioxide, and water which makes up most of the biogas emitted from the system. The process of methanogenesis is sensitive to high and low pH and typically occurs between pH 6.5 – 8. Finally, the leftover material which organisms cannot act upon, and any dead bacterial remains, constitute the digestate.

A simple equation for the whole process is given by the following equation:

$$C_6H_{12}O_6 \rightarrow 3CO_2 + 3CH_4$$

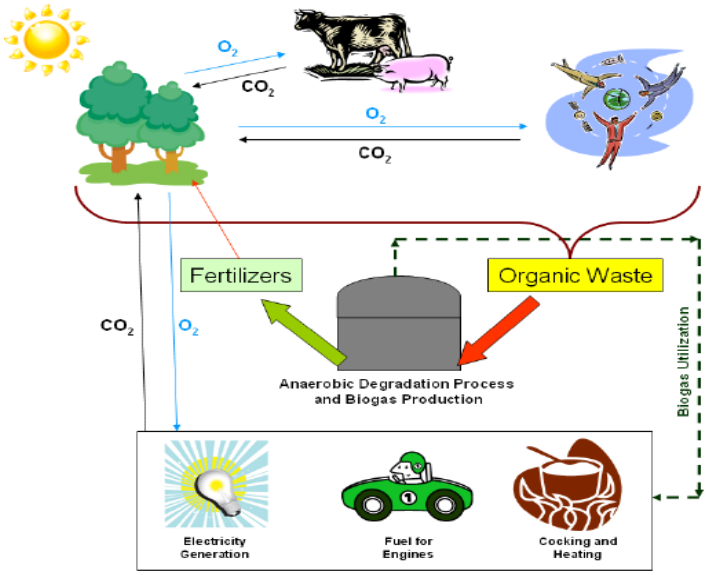

Figure 3 Simple flow diagram showing how biogas is produced and utilized (Minde, Magdum and Kalyanraman 2013)

Figure 3 shows that organic material or waste is fed into the digestion tank where anaerobic digestion takes place producing biogas which may be used for a variety of purposes. To further improve the heating value of this fuel and widen its applicability, upgrading biogas has become a subject of interest.

1.3.1 Factors that influence Anaerobic Digestion

There are various factors that affect the rate at which organic material is broken down which in turn determines the volume of biogas that is produced. These factors ought to be observed and adjusted to achieve the optimum results from an anaerobic digestion process. A fundamental factor is the temperature within the digester as shown in **Figure 4** below. The higher the temperature (thermophilic range), the higher the growth of the methane-forming microorganisms that produce methane compared to the psychrophilic and mesophilic ranges.

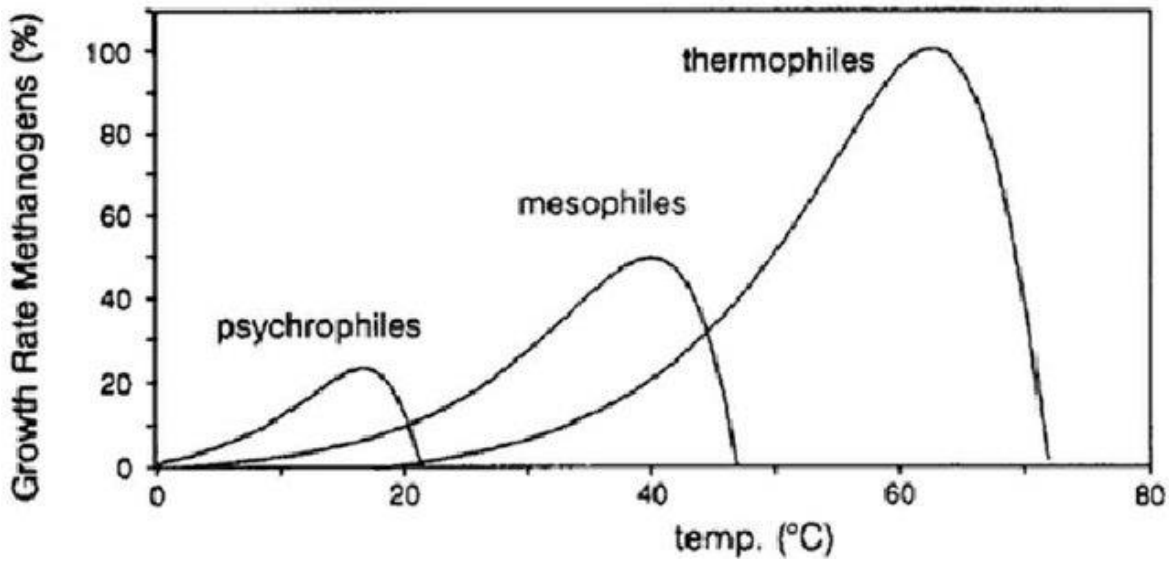

Figure 4 Methane production rate at various temperatures (Dincă et al. 2014)

1.3.1.1 Temperature

The temperature within the anaerobic digester is an essential factor as it affects the rate of methane production. Digesters may operate at mesophilic, psychrophilic, or thermophilic conditions. The temperature within an anaerobic digester also has an impact on the time needed for the digestion process, for instance, at thermophilic conditions, the time taken for methane formation is less, methane generation is higher and there is more reduction of pathogens compared with when processing at psychrophilic conditions (Damle 2014; Toma et al. 2016).

1.3.1.2 pH

The pH in an anaerobic digester influences the adequacy of the methane-forming-bacteria which are pH sensitive and operate at levels between 6.5 and 8 when converting volatile fatty acids to methane. This underscores the importance of monitoring the pH levels of an operating digester (Deepanraj, Sivasubramanian and Jayaraj 2014).

1.3.1.3 Mixing

Mixing within a digester creates intimate contact between microscopic organisms and the substrate. Mixing also inhibits the formation of temperature gradients that allow uniform processing all through the digester to reduce the formation of scum (Stafford 1982).

1.3.1.4 Retention Time

Retention time is the standard time that the substrate spends in a digester during processing. There are two categories of retention times in an anaerobic digester which are the solids retention time (SRT) and hydraulic retention time (HRT). Solids retention time (SRT) is the average time that solid bacteria spend in the anaerobic digester while hydraulic retention time (HRT) is the average time that soluble compounds spend in a reactor (Climenhaga and Banks 2008; Kinyua, Cunningham and Ergas 2014).

1.3.1.5 Toxicity

Some elements influence the formation of pathogens in a digester. Little amounts of mineral particles and heavy metals support the growth of microscopic organisms, while higher amounts of these mineral particles may hamper their growth. These factors are essential to the development of microscopic organisms and the generation of methane (McCarty and McKinney 1961; Lawrence and McCarty 1965).

1.3.1.6 Feedstock/Loading rate

This refers to the quantity of organic material fed into a digester per time. The suitable loading rate is dictated by the size of the digester and the type of organic material being utilized. If the digester is overloaded, there may be acid accumulation and hindrance of methane generation, likewise, a starved digester brings about low methane creation (Liu et al. 2009).

1.3.1.7 Carbon/Nitrogen (C/N) proportion

The Carbon/Nitrogen proportion is key as the pathogens require both components in exact amounts for metabolic responses. Research shows that the process can be optimized at a C/N ratio of about 8:20, however, this may vary depending on the substrate nature (Krishania et al. 2012).

Although biogas has shown to be a very attractive biofuel that would compete with conventional energy sources. To improve its efficiency, it needs to be upgraded to bio-methane. Membrane technology has been identified as a method through which biogas can be effectively upgraded to a high value fuel and has several advantages over conventional upgrading methods including low maintenance, low energy requirements, minimal labour requirements, compact modular design that allows easy expansion for changes in capacity

requirements, and environmentally friendly processing. The membranes act as a selective filter that allows the flow of one gas whilst limiting the flow of other gases thus purifying a gas mixture. The effectiveness of a membrane is a measure of its permeability and selectivity which defines how much and how well a membrane separates the mixture. Membranes may be tested using several static and dynamic characterisation techniques such as microscopy, spectroscopy, physisorption, and permeation measurements which are detailed in the following chapters.

1.4 AIM AND OBJECTIVES

The main goal of this research is to deliver a methodological analysis of membrane systems that can be integrated for use in biogas production facilities. The objectives include:

1. To measure the permeability and selectivity of biogas components through ceramic membranes and monitor the effect of changes in membrane structural and fluid properties on perm-selectivity
2. To determine and compare the flow or transport mechanisms of biogas components using data derived from experimental analysis and mechanistic transport calculations
3. To develop a method that can be used in estimating the mass transfer properties of different pore sized membranes that can be applied to describing fluid transport in porous media
4. To fabricate an additional layer on the ceramic support using chemical agents to achieve biogas upgrading by modifying the membrane properties
5. To characterize the support and modified membranes using gas permeation test, scanning electron microscopy (SEM), energy dispersive x-ray analyser (EDXA), Fourier transform infrared spectronomy (FTIR) and liquid nitrogen desorption analyser and compare the effect of changes in their properties on biogas upgrading

1.5 CONTRIBUTION TO KNOWLEDGE

Aggressive methane mitigation is acknowledged as the key to avoiding risky levels of global warming (Kuylenstierna et al. 2011; Shindell et al. 2012; Kim et al. 2013). This research aims to aid the net-zero emissions target which has been set and develop a technique that converts the "would have been emitted" GHGs to a sustainable energy form reducing the reliance on carbon-intensive forms of energy such as fossil fuels.

The research carried out analysed the structural, fluidic, and operating conditions of membranes systems to ascertain the optimum conditions for biogas upgrading and proposed a method of preparation of the ideal membrane that allows for high permeance and selectivity of the desired gas. The originality of the membrane unit is in the way in which the biogas is upgraded. This is separated by means of an imposed pressure difference over the membrane which has been textured to enhance gas permeation. Using membranes with high separation efficiency allows the recovery of the highest possible methane yield. Depending on the grid or user requirements, the gas can be upgraded to the preferred methane concentration.

Carbon capture and storage (CCS) technologies are currently being developed to address compliance issues related to the intensification of environmental regulations and policies. The impact of our membrane technology will also be felt in carbon capture from exhaust gases including post-combustion, pre-combustion and oxycombustion. CO_2 separation in gas processing is also a viable application that employs alternatives that are commonly used in post-combustion thus sharing developments and consolidating innovations (additional to innovations driven by knowledge from basic and applied science research). The high volume of produced exhaust gases and the expanding reserve of natural gas conquers the state-of-the art chemical and physical absorption (the most widely used mature technology). Moreover, the study of mass transfer characteristics in the core samples can be applied to fluid behaviour in porous media and would be particularly useful in the oil and gas industry for geological and carbon capture applications. The work has identified the gaps in technology and drivers of innovation in the biogas upgrading chain. In this context this work represents a recent and massive niche technology for commercial use of membrane-based processes and impacts both energy

security and climate change.

1.6 OUTLINE OF THE THESIS

The aim of this research is to create wealth from waste by utilizing greenhouse gases - CO_2 and CH_4, that would otherwise be polluting the environment. As a renewable source of energy, it will reduce reliance on and importation of fossil fuels thereby creating an alternative source of energy. This alternative source of energy can support the world's ever-growing population and economy whilst limiting greenhouse gas emissions and aiming for the net-zero emissions target to minimize the effect of global warming.

This thesis would explain the various aspects that pertain to the research goal, beginning with the need for reducing greenhouse gas emissions with an option of utilizing renewable energy which in this case is biogas.

In this chapter, biogas is promoted as an alternative to the conventional forms of energy such as coal and oil. It was found that the percentage of methane gas in a biogas mixture is dependent on some factors which can be optimised during the production process.

Chapter 2 would give an overview of the current state of the art technologies available for upgrading biogas, their pros and cons and why membrane technology is the technology of choice for this research. Furthermore, this section introduces membrane technology, its features, advantages as well as the major transport mechanisms that may be expected as gases flow through the membrane layer. It was noted that the ceramic membranes offer advantages over the conventional polymeric membranes with the ability to withstand much higher temperature and pressure conditions.

Chapter 3 makes available the methodology of the research including the various apparatus used and provides a detailed experimental procedure. Silica membranes were prepared using the sol-gel technique and tested for performance enhancement.

Chapter 4 provides data derived from experimental studies to determine the factors that increase selectivity of the membranes having different physical properties. This was achieved by gas permeation studies under various

operating conditions and data evaluation. A gas transport model is also put forward for comparative analysis. Further work was done to design a membrane that fits the expected requirements for gas separation membranes. Silica was used as the agent to prepare the separation layer for analysis. It was observed that membrane performance was impacted by structural, thermodynamic, and kinetic effects.

Chapter 5 summarises the thesis and concludes with recommendations. Membrane technology shows promising results for utilisation in biogas upgrading.

1.7 RESEARCH ETHICS

The Robert Gordon University's Research Ethics Students and Supervisors Appraisal (RESSA) was completed prior to commencing this research. The research governance policy was followed to ensure the research was fulfilled with high standards and codes of practice. This was put in place to:

- Protect the researcher by clarifying the responsibilities of all parties involved including the student, supervisory team, and the university
- Protect any other individual that may be affected by the research by considering the overall impact of the work
- Protect fellow researchers by minimizing the risks to others as well as recognizing the input of other researchers and securing confidentiality of any results
- Improve the quality of the research by fostering high standards and efficient practice

1.8 HEALTH AND SAFETY

The Robert Gordon University's Health and Safety Policy was strictly adhered to throughout the research. The policy includes:

- Guidance on handling and disposal of hazardous substances
- Minimizing any associated risk to the barest minimum
- Ensuring all researchers work in a responsible and safe manner
- Statement on lone working and out of hours access

Gas Handling training was done before proceeding with the experiments. Personal Protective Equipment (PPE), such as safety boots, lab coat, gloves, and goggles, were always worn. Electrical and gas leak checks and equipment functionality checks were done before the start of every run and shut down. Gas cylinders were properly secured. The laboratory was always adequately ventilated and exit gases were appropriately exhausted to a functional fume cupboard. An oxygen detector was in place to measure the safe oxygen level in the laboratory when working with toxic gases. Fire extinguishers were in place all through the experiment. In addition, at least one trained gas handler was required to be always in the laboratory during the experiment. The opening and closing hour policy of the University laboratory was strictly followed.

Whilst processing biogas, the safety aspects also need to be considered, some of which include flammability, poisoning, suffocation, and the other risks associated with high pressures and temperatures. It is very crucial to be aware of the associated risks and to minimise them. Laboratory risk assessments, control of substances hazardous to health regulations (COSHH), and gas handling certifications were completed prior to performing experiments. Nevertheless, the advantage of dealing with biogas is that it is lighter than air and thus any gas leakage would rise upward. Upgraded biogas also has a greater temperature of ignition than both petrol and diesel so the risk of a fire or explosion is reduced.

In conclusion, the impact of greenhouse gas emissions in today's world cannot be overemphasized. Membrane technology can compete with the conventional gas separation processes to mitigate emissions and upgrade biogas to bio-methane for use as an alternative source of fuel.

CHAPTER 2: LITERATURE REVIEW

The previous chapter highlighted membrane technology as an attractive alternative to other methods of biogas upgrading. In this chapter, a review on the current separation technologies is presented and more detail on membrane technology is provided as well as its advantages over the existing methods.

2.1 BIOGAS UPGRADING TECHNOLOGIES AND COMPARISON

Biogas in its pure natural state as an alternative source of energy may be significantly inefficient if not upgraded to bio-methane. Thus, upgrading of biogas is required because: (i) the presence of CO_2 in the gas reduces the power output from the engine and occupies significant space when biogas is compressed for storage. (ii) It also causes freezing problems when the compressed gas undergoes expansion at valves and metering points (iii) Carbonic acid from CO_2 may be formed which causes corrosion of pipes and fittings (iv) moisture reduces the heating value of the biogas and enhances corrosion (Vrbová and Ciahotný 2017; Cheng et al. 2020). Moreover, the pipeline specification for CO2 content is slated at around 2 mol% (Ji et al. 2010).

There are four (4) major technology pathways currently being used to upgrade biogas to biomethane. They are: (i) absorption (ii) adsorption (iii) membrane separation (iv) cryogenic separation (Petersson and WeLLInGer 2009; Niesner, Jecha and Stehlík 2013). **Figure *5*** shows the current state-of-the-art technologies for biogas.

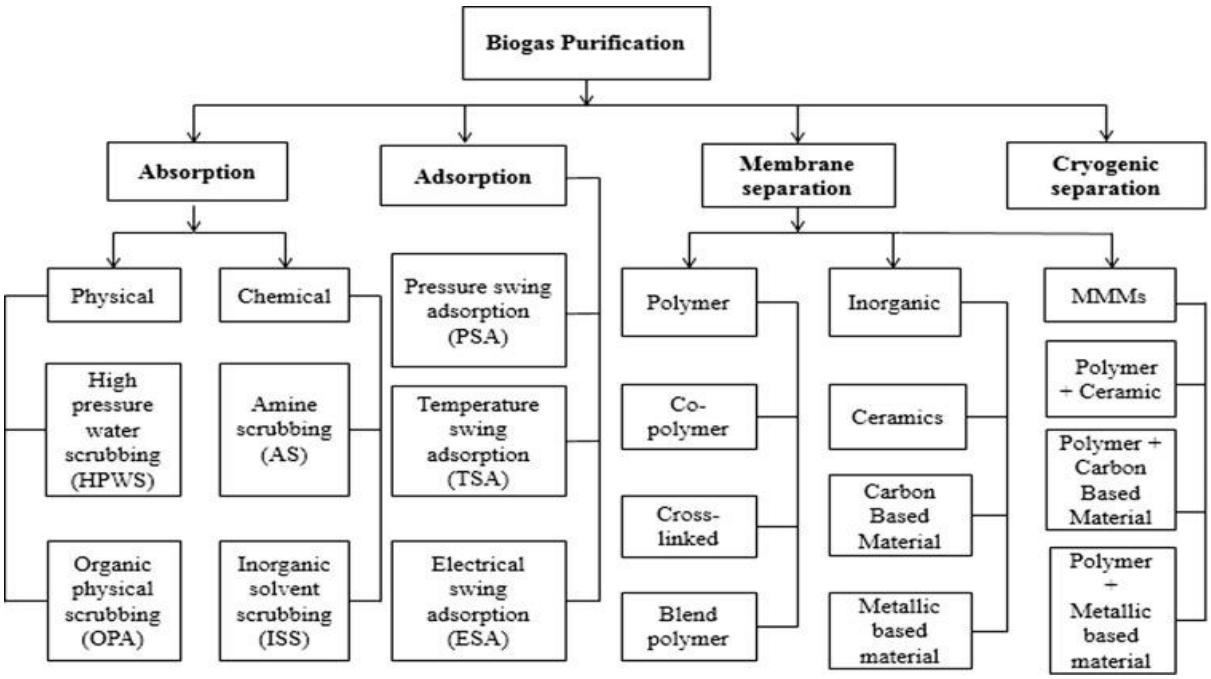

Figure 5 Current Technologies for Biogas Upgrading (Ullah Khan et al. 2017)

2.1.1 Absorption by Scrubbing

Absorption can be done using water or chemicals. **Figure *6*** shows a schematic flow diagram of a water/chemical scrubbing system for carbon dioxide removal. Water scrubbing is used to eliminate both carbon dioxide and hydrogen sulphide (CO_2 and H_2S) from the mixture using the principle of preferential solubility as they are more soluble in water than methane. The absorption procedure is purely physical, biogas is pressurized and passed through the base of a packed column while water is sustained above it. The process is carried out counter-currently. The water exits the bottom of the column with absorbed CO_2 and/or H_2S and can be recovered for reinjection again to the scrubber. Recovery/Regeneration is done by de-pressuring or stripping with air in a similar manner (Baena-Moreno et al. 2019). However, stripping with air is not suggested when high amounts of H_2S are handled because it is heavier than air and volatile. In a case where cheap water can be utilised for instance, water channel from a sewage treatment plant, the most cost-effective technique is to eliminate the recovery and reinjection of the water (Yuan Chen et al. 2015).

On the other hand, chemical scrubbing is done using organic solvents like mixtures of methanol and dimethyl ethers of polyethylene glycol (Angelidaki et al. 2018). This method also relies on the principle of solubility and is similar to the process of water scrubbing. The disparity between water and polyethylene

glycol is that CO_2 and H_2S are more soluble in polyethylene glycol which results in lower solvent demand and reduced pumping (Sahota et al. 2018). The use of chemical scrubbers for absorption includes the development of reversible chemical bonds between the solute and the solvent. This requires a relatively high energy input to break the bonds for recovery of the solvent (Angelidaki et al. 2018). Regeneration is done by reducing the chemical gradient (Shimekit and Mukhtar 2012). To make this technology more attractive, strategies to reduce energy requirements and environmental friendliness of the process should be pursued.

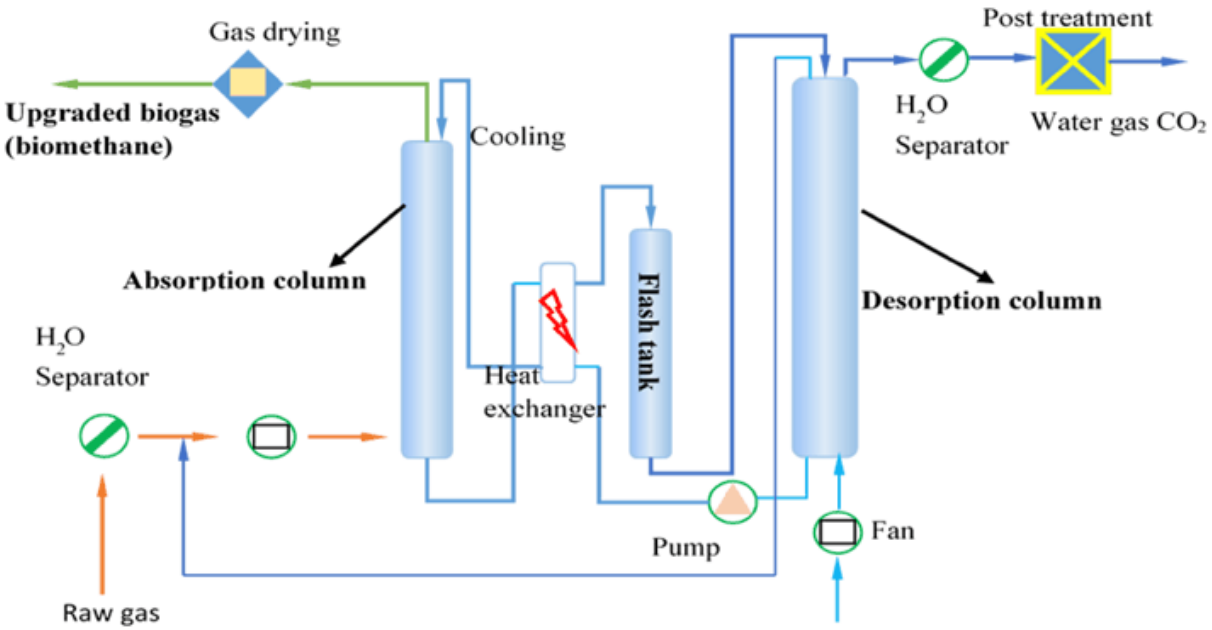

Figure 6 Water and Organic Solvent Scrubbing for CO_2 Removal (Awe et al. 2017)

2.1.2 Pressure Swing Adsorption (PSA)

Figure *7* shows a schematic diagram describing the pressure swing adsorption for CO_2 removal. Pressure swing adsorption (PSA) is used to separate gas mixtures according to the molecular characteristics of the components and their attraction to an adsorbent material. Adsorption materials, such as zeolites or activated carbon, are utilized as a molecular sieve in adsorbing the target gas at high pressure then the system swings to low pressure to desorb contents in the adsorbent material. This process hinges on the principle that under high pressure, gases tend to be pulled onto solid surfaces or are "adsorbed" (Sun et

al. 2015; Baena-Moreno et al. 2019). Pressure swing adsorption processes can be used to separate gas mixtures because each component would be adsorbed at different paces. Operating two vessels simultaneously leads to a consistent build-up of the target gas and permits uniform pressure distribution throughout the process as the gas flowing out of the vessel being depressurised is utilised to pressurise the next vessel (Angelidaki et al. 2018; Sahota et al. 2018). However, the high-pressure requirements of the process make operating costs very high. Reducing these operational costs and the compactness of the unit will make this technology more appealing.

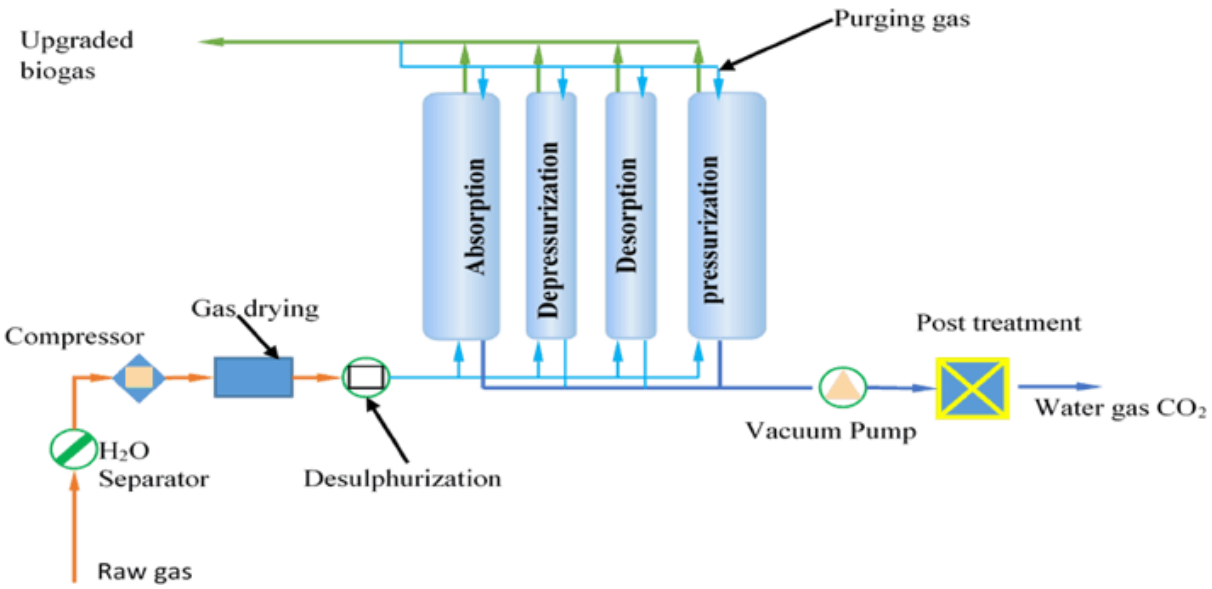

Figure 7 Pressure Swing Adsorption Technology for CO_2 Removal (Awe et al. 2017)

2.1.3 Membrane Separation

Figure *8* shows a schematic diagram describing the membrane separation process. In this process, the gas mixture is passed through a thin film which restricts the passage of other components (Baena-Moreno et al. 2019). There are two membrane separation strategies: High Pressure Gas Separation and Gas-Liquid Adsorption. The high-pressure separation simply separates hydrogen sulphide and carbon dioxide from methane while the gas-liquid adsorption uses micro-permeable hydrophobic films to break up the carbon dioxide and hydrogen sulphide into a fluid while methane remains as gas and is collected (Angelidaki et al. 2018; Sahota et al. 2018). By improving the permeability and selectivity of biogas separation membranes, this technology will be more

adopted.

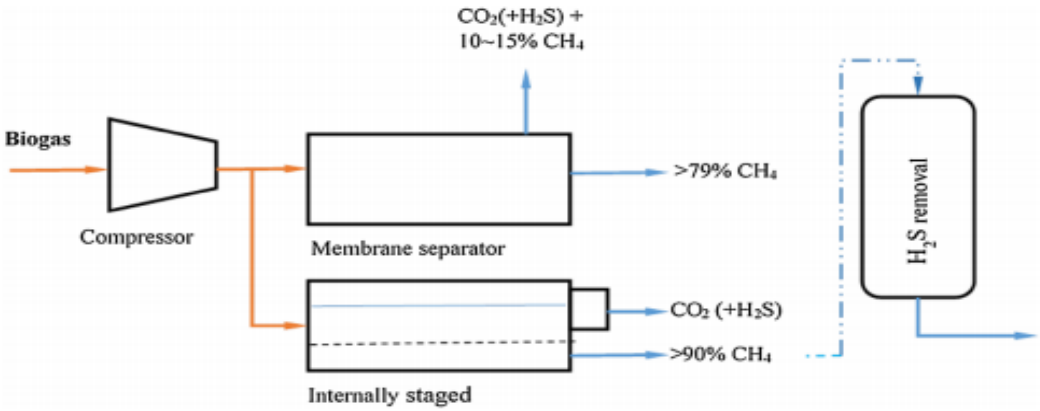

Figure 8 Membrane Separation Process (Awe et al. 2017)

2.1.4 Cryogenic Separation

Figure 9 shows a flow diagram describing the cryogenic separation process for gas separation. This purification process separates methane from carbon dioxide, hydrogen sulphide and other biogas contaminants. This is possible because every contaminant condenses at an alternate temperature-pressure domain. The process works at low temperatures, close to -100^{O}C, and at high pressures of close to 40 bars. Operation requirements are maintained using a specified arrangement of compressors and heat exchangers. However, this process is very expensive relative to other means of gas separation and undergoes significant loss of efficiency with streams of low CO_2 concentration. There is also a high likelihood of pore blockage and risk of flammability/toxicity of some cryogenic fluids (Shimekit and Mukhtar 2012; Angelidaki et al. 2018; Sahota et al. 2018). Techniques to improve the start up and running costs of this technology need to be advanced.

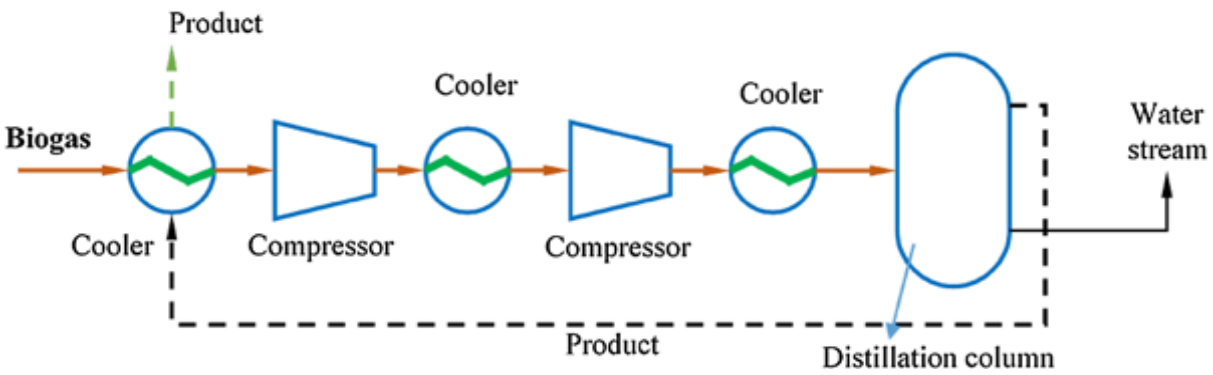

Figure 9 Cryogenic Gas Separation Process (Awe et al. 2017)

Table 1 Comparison of different Pilot and Commercial Biogas Upgrading Technologies (Angelidaki et al. 2018)

	Cryogenic	**PSA**	**Water Scrubbing**	**Chemical Absorption**	**Membrane Separation**
Consumption for raw biogas (kWh/Nm^3)	0.76	0.23-0.30	0.25-0.30	0.05-0.15	0.18-0.20
Consumption for clean biogas (kWh/Nm^3)	na	0.29-1.0	0.3-0.9	0.05-0.25	0.14-0.26
Heat consumption(kWh/Nm^3)	na	none	none	0.50-0.75	none
Heat demand (^oC)	-196	na	na	100-180	na
Cost	high	medium	medium	high	high
CH_4 losses (%)	2	<4	<2	<0.1	<0.6
CH_4 recovery (%)	97-98	96-98	96-98	96-99	96-98
Pre-purification	yes	yes	optional	yes	optional
H_2S co-removal	yes	possible	yes	contaminant	possible
N_2 and O_2 co-removal	yes	possible	no	no	partial
Operation pressure (bar)	80	3-10	4-10	atmospheric	5-8
Pressure at outlet (bar)	8-10	4-5	7-10	4-5	4-6

na: not available

A comparison of the different biogas upgrading technologies are presented in

Table *1*. Compared to other methods, chemical absorption and membrane separation consume a nominal amount of biogas during operation

with high recovery and minimal losses of methane during the upgrading process. However, membrane separation is an energy efficient single-pass process that doesn't require sorbent regeneration or desorption at varied temperature and pressure (An et al. 2011).

Water scrubbing has many disadvantages including high energy consumption, large processing units and increased risk of corrosion, making chemical scrubbing the preferable method (AL MAMUN and TORII 2016). Currently, chemical scrubbing is the most widely used on an industrial scale taking up around 90% of the CO_2 separation market (Dai et al. 2016). However, the process of using scrubbers is highly energy consuming, takes up more than 70% of the total cost of carbon sequestration, and requires the use of toxic chemical. These toxic chemicals are non-recyclable resulting in a significant amount of waste products that need to be properly disposed of, thereby increasing costs and posing environmental and health hazards (Brunetti et al. 2010; Shimekit and Mukhtar 2012). Additionally, issues relating to flooding, foaming entraining, and channeling are prevalent in this method. Therefore, the use of membrane technology is proposed as an effective and efficient means of upgrading biogas because it is a simple process where the use of toxic chemicals is avoided making it an environmentally friendly process. Also, energy consumption is relatively lower than the conventional upgrading processes as they do not consume energy in the latent heat of evaporation (Shimekit and Mukhtar 2012). To enable the full emergence of membrane technology, the separation performance needs to be further improved. This involves considering techniques such as surface modification to improve pore-molecule interaction, with a view to enhancing the overall flow/separation mechanism market (Dai et al. 2016; Ozen and Ozturk 2019).

2.2 PROPOSED TECHNIQUE: MEMBRANE TECHNOLOGY

A membrane may be defined as a permeable or semi-permeable layer which controls the flow of compounds. Therefore, it delivers one product with less of another component, resulting in the product concentration in those components (Beil and Beyrich 2013). This process is used in industry for recovery of reactants and valuable gases, isolation of products and pollution control

(Sridhar, Bee and Bhargava 2014). The flow of gases is based on their differences in permeability which is a function of membrane properties and the nature of gases (Wiheeb et al. 2015). Generally, the performance of a membrane is defined by its permeability and selectivity, and a good indication is with high values of both achieved for efficiency in commercial applications. However, in practicality, there is a trade-off between these parameters. Nonetheless, in any given process, there is an economic optimum in the combination of selectivity and permeance.

Permeance/Permeation is a measure of the amount of permeate that flows through the membrane and is evaluated by the amount of fluid that passes through the area of the membrane in a given time for a given pressure difference. It is given as:

$$\mathrm{P} = \frac{F}{A\Delta P_d} \tag{2.1}$$

obtained from,

$$Q = \frac{F}{A} \tag{2.2}$$

where,

F gas molar flow rate, mol/sec

Q Molar flux

A membrane surface area, m^2

ΔP_d pressure difference across the membrane, Pa

Permeability is the permeance normalized against thickness and can be used to compare data

$$P_e = \frac{Fl}{A\Delta P_d} \tag{2.1}$$

l Membrane layer thickness, m

Selectivity refers to the ability of the membrane to separate gases and

gives a measure of the purity of the permeate gas and losses. It is evaluated by the ratio of gas permeation rates. (Havas and Lin 2017).

2.2.1 Classification of Membranes

Membranes may be classified as either polymeric or inorganic. Polymer membranes can be subdivided into porous and non-porous membranes and their use in industrial processes depend on the properties of the membrane and the intended application. Even though polymer membranes have been studied over time for use in gas separation, their constraints of low chemical and thermal stability have limited their usage in factual industrial application as depicted by Robeson (Liu et al. 2006). Zeolite and carbon molecular sieve membranes suffer limitations including poor processibility, scalability, low permeation as a result of membrane thickness and susceptibility to cracking or undesirable intercrystalline porosity that impede selectivity (Xomeritakis et al. 2003). These membranes cannot achieve high permeability due to their disordered pore structures that cause high diffusion resistance (Sedigh et al. 1998; Li et al. 2012).

Recently, inorganic membranes have been gaining interest as they supersede polymer membranes in terms of chemical and thermal stability, they also have well-specified pores, molecular filtering properties, and wide pore size availability (Pakizeh, Omidkhah and Zarringhalam 2007a; Shimekit and Mukhtar 2012; Wei et al. 2019). These membranes are used as a support for separation and reaction processes that require high pressure drops, variable pH and temperatures even above 1000^{o}C. Due to their versatility, they can be combined with other materials to form composites that are tailored to certain reactions such as desalination of water, hydrogenation, oxidation, CO_2 reforming, hydrogen separation and H_2O_2 synthesis (Hsieh 1996; Fain 2000; Kanellopoulos 2000; Oyama 2011). Inorganic membranes may be made up of: (i) the support layer which is usually macro-porous and provides high tensile strength with mechanical support; (ii) one or two intermediate layers that may be mesoporous (linking the pore size differences between the layers allowing for pressure control); and (iii) a top layer that is microporous and acts as the reaction site for achieving the desired products (Bhave Ramesh 1991; Vercauteren et al. 1998; Benito et al. 2005; Li 2007).

Some types of inorganic membranes include ceramic membranes formed by combining a metal and non-metal oxide, nitride or carbide; glass membranes which are made by leaching on de-mixed glasses; and metallic membranes obtained by sintering of metal powders. Although the initial cost is high, the many advantages of the technology make the cost appreciable. Moreover, the development of low-cost ceramic membranes and recycling of support using heat treatment to decompose the coatings on the support can diminish costs (Sainan et al. 2013).

Ceramic membranes are typically made from one or a combination of metal oxides such as alumina (Al_2O_3), silica (SiO_2), zirconia (ZrO_2), titania (TiO_2) depending on the specific process requirement. They may also be in plate, disc or tubular form. However, the tubular form is typically used because it offers more separation area per unit volume for reaction to take place. These membranes may be porous or non-porous. Porous membranes contain fixed pores and their selectivity is dependent on the pore size distribution. Their physical and chemical properties which interpret the permeability depend on the material used and method of preparation. They usually exhibit good permeance but low selectivity and are characterized by pore size, porosity and tortuosity with pore sizes ranging from microporous ($dp<2nm$), mesoporous ($2nm<dp<50nm$) and macroporous ($dp>50nm$) (Ghasemzadeh, Basile and Iulianelli 2019; Nagy 2019). On the other hand, non-porous membranes depend on the intrinsic properties of the material and the solubility. They are highly selective but permeance is low; molecules of similar size can be separated if they have significantly different solubility in the material.

Compared to polymeric membranes, inorganic ceramic membranes offer superior permeabilities-selectivity combinations. They show enhanced mechanical strength with chemical stability thereby able to withstand higher pressure differences and harsh/corrosive operating conditions for a given wall thickness. The same support material can be used to develop different membranes having varied permeation characteristics for different gas mixtures. Their structural properties can be adjusted by simple thermochemical processes and adapted for specific separation requirements. Although there are many advantages to ceramic membranes over polymeric membranes, it has been highlighted from literature that for the successful implementation of a supported

inorganic membrane, the following key issues need to be addressed (Chang et al. 2006; Ismail, Khulbe and Matsuura 2015):

- Good interfacial bonding of the membrane layer and the support to further improve the permeability and achieve long-term performance
- Production of a defect-free membrane layer to improve its selectivity by eliminating the passage of impurities through the defects
- Matching thermal and chemical performance of the membrane layer and support to provide superior quality membranes that are durable.

2.2.2 CO_2/CH_4 Separation Membranes

As described earlier, membranes may be classified as polymeric (or polymeric blends), inorganic (such as, zeolite, carbon molecular sieves, or silica), and composite (organic-inorganic, or mixed matrix). Inorganic membranes have been proven to deliver the best results for CO_2/CH_4 separation performance due to their (molecular sieving and surface diffusion) gas flow mechanism compared to the solution-diffusion characteristics of polymeric membranes.

Commercial polymeric membranes are typically non-porous and have an asymmetric structure displaying a solution-diffusion mechanism and delivering low permeance and moderate selectivity. However, they are attractive for their low cost and ease of maintenance. Despite many attempts to improve the perm-selectivity of these membranes over the years, their performance has not been able to overcome the limitations highlighted by Robeson (Robeson 1991). Although, some research has been done on blending polymers to achieve the desired membrane characteristics. For instance, a glassy polymer (with high selectivity) embedded in a rubbery polymer matrix (to deliver high permeability) to combine their strengths.

Zeolite membranes normally compose of a zeolite layer on an alumina or stainless-steel support. The mechanism of gas flow is typically molecular sieving or surface diffusion, and separation can take place at low temperatures by preferential adsorption. Carbon membranes are usually made by pyrolysis of thermosetting polymers to achieve narrow pore size distributions that contribute to molecular sieving flow mechanism. The gas molecules need to possess

sufficiently high activation energy to pass through the pores. Carbon membranes with larger pores can also operate by surface diffusion mechanism. However, zeolite and carbon membranes are very expensive and difficult to produce and manage and are therefore unattractive for commercial use. However, research has shown that membranes prepared on alumina supports deliver higher permeance rate and this is as a result of the large and asymmetric pore structure of the alumina supports (Shekhawat, Luebke and Pennline 2003; Shimekit et al. 2009).

For silica membranes, standard precursors such as tetraethyl orthosilicate (TEOS) OR tetramethyl orthosilicate (TMOS) are used. Reports show that higher permeances were achieved by sol-gel processing compared to chemical vapour deposition. The challenge with silica membranes produced by sol-gel is the reproducibility as the performance is largely dependent on the synthesis conditions (such as defect formation and particle contamination from the atmosphere) (Shekhawat, Luebke and Pennline 2003; Shimekit et al. 2009).

Mixed-matrix membranes, also called composite organic-inorganic membranes, are made up of inorganic particles embedded in a polymer matrix. The inorganic particles behave as molecular sieves to enable the combination of their excellent separation characteristics with the simplicity of producing polymer materials. At low to moderate loadings of the inorganic phase, gas flow diffuses across the polymer and through the inorganic phase. At high loadings, flow is mainly through the inorganic phase. Some mixed-matrix membranes act on the selective adsorption in the inorganic phase.

Table 2 Comparison of membrane types (Stern 1994; Shekhawat, Luebke and Pennline 2003; Shimekit et al. 2009; Sridhar, Bee and Bhargava 2014)

CH_4/CO_2 Separation Membranes	**Permeance**	**Selectivity**	**Advantages**	**Disadvantages**
Polymeric	low	moderate	low cost	Trade-off between permeability and selectivity
Inorganic	moderate	high	Durability under harsh conditions	Difficult to produce

2.2.3 Advantages of Membranes

The advantages of utilising membrane technology for industrial processes include but are not limited to (Schell and Houston 1983; Scott and Hughes 2012):

- Its compact size that makes it attractive especially for offshore facilities
- It does not involve phase changes
- Possibility of product loss is minimal
- They are suitable with temperature sensitive materials and are not chemically altered
- Possible re-use of CO_2
- They have high selectivity and permeation rate
- They are simple to operate
- Efficiency of raw materials and potential for recycling by-products
- Operation is usually under continuous steady-state conditions
- Scale up is relatively easy

2.3 MEMBRANE PREPARATION METHODS

Membranes can be prepared by several methods in order to give the desired separation/reaction characteristics. Some of the methods include but are not limited to (Tasselli 2015):

- **Sintering:** In this method, the particles of the material are compressed, and heat is applied to cause sticking of the particles that form pore sizes equal to the particle size. Sintered membranes can operate under harsh conditions due to their resistive materials and they are suitable for microfiltration processes.
- **Extrusion:** The technique involves stir mixing powder with plasticizers, binders and other ceramic additives and then taking the mixture through a series of treatments such as vacuum purging and aging, and finally passing it through the die nozzle under a certain pressure (20–180 MPa) to extrude the required shape of the support.
- **Acid leaching:** Alkali borosilicate systems are combinations which comprise the chemical species SiO_2, B_2O_3 and R_2O, where R may be sodium, potassium, or lithium. The components of the mixture are tuned to specific concentrations and subsequently heated. Then, the whole mixture experiences an amorphous phase separation, meaning, the mixture transforms into two distinct phases - One of which is an alkali-rich borate phase, and the other a silica-rich glassy phase. The borate phase can be dissolved in acid, while the silica phase cannot, thus, after the heat treatment, a hot-acid solution can be used to leach out the borate phase and what is left is an exceptionally pure and porous silica glass skeleton with greater surface area, that is, porous glass.
- **Stretching:** Pores are formed by stretching the film perpendicularly to the direction of extrusion until there is some rupture on the film structure. These membranes are suitable for microfiltration processes.
- **Track-etching:** Here, radiation which damages the film is followed by chemical treatment to eradicate the damaged material and create uniform pores. These are suitable for ultrafiltration and microfiltration processes.
- **Phase Inversion:** A polymer dissolved in solvent changes form from fluid to solid state under controlled conditions to produce a desired

membrane morphology. These membranes are suitable for a variety of processes.

- **Solution Coatings:** A dilute polymer solution in an easily evaporated water-insoluble solvent is spread over the surface of a support. Preparation of composite membranes is achieved by this method and they are suitable for nanofiltration and gas separation processes.

2.4 MEMBRANE CHARACTERIZATION METHODS

Membrane materials may be characterized by static techniques or dynamic techniques. Static characterisation methods provide morphology related parameters concerning both active and inactive pores. On the other hand, dynamic characterisation methods where membrane permeability is involved, provides permeation related parameters and occasionally morphology related parameters regarding active pores only (Julbe and Ramsay 1996). In using these characterisation techniques, the following factors should be considered (Rouquerol et al. 1994):

- The selection of an ideal characterisation method depends on the nature of material and its intended use
- In selection, the method chosen must be able to assess a parameter directly related to the phenomena involved in its intended use or application
- The complexity of porous material texture, even on theoretical grounds, can be explained by the introduction of simplifying assumptions
- Absolute values of parameters such as porosity, pore size, surface area, etc cannot be obtained rather a characteristic value is provided which depends on the principles involved and the test used
- A perfect agreement between parameters is not expected, thus an awareness of the precise, limited, and corresponding significance of the information delivered by each characterization technique is expected

Static Methods

This section describes the static characterisation methods of a porous structure which includes (Burggraaf and Cot 1996):

- Stereology

- Intrusive methods such as Hg porosimetry, physiosorption, calorimetric methods, NMR
- Non-intrusive methods including radiation scattering, wave propagation

2.4.1 Stereology

Microscopy can be used to provide visual details of a membrane surface as well as cross-section morphology and the image analysis for quantitative data. *Optimal microscopy* is used to observe large defects on the surface of the membrane using magnification of 500-1000 but a higher resolution is required for the observation of fine texture. *Scanning electron microscope (SEM)* can produce higher resolution information than optical microscopy due to the much shorter wavelength of electrons compared to light photons and can obtain magnifications of 10^5 with resolution that can reach 5nm. SEM forms an image from its emitted electrons as a result of its interaction with the atoms of the specimen. *Field emission scanning electron microscope (FESEM)* is an improved SEM that can reach resolution around 1.5nm due to the cold cathode electron source used rather than thermionic source. FESEM samples can be observed at low accelerating voltage and lighter metallization which is essential for examining fragile membrane structures. *Transmission electron microscopes (TEM)* in some cases may provide close to 1nm resolution. However, the electrons must go through the specimen which limits the sample thickness. Thus, only unsupported, or stripped membrane layers can be analysed. *High resolution transmission electron microscopy (HRTEM)* can reach a resolution of 0.3nm. *The Z-contrast scanning transmission electron microscopy (STEM)* is a new approach to HRTEM that produces a direct image of material atomic structure and composition where the intensity of the image is proportional to the square of the atomic number (Z). *Scanning probe microscopies* such as *Atomic force and Scanning tunnelling electron microscopies (AFM/STEM)* can image angstrom to micron sized surface features and require only little sample pre-treatment. Furthermore, *Image analysis* may be performed on micrographs to obtain quantitative data such as pore size, pore area, pore density and porosity. This allows enhancement of the image for analysis prior to measurement.

2.4.2 Intrusive Methods

Mercury porosimetry uses mercury (a non—wetting liquid) and forces it into the

pores of a dry sample and measures the volume of mercury entering the sample porous structure for each applied pressure by measuring the reduction in height of the mercury column which is connected to the measuring cell. The Laplace equation is used to determine the relationship between pressure and pore radius. Then, the membrane weight and the pore size of the support can be used to determine the porosity of the support layer*. Gas adsorption /desorption isotherms (physisorption)* is an extensively used method in characterisation of porous materials and can be used to determine pore volume, pore size distribution and specific surface area. The adsorption isotherm is obtained by measuring the quantity of gas adsorbed as a function of relative pressure (p/p_o) by a gravimetric/volumetric method or using a surface acoustic wave device. *Calorimetric methods* include *immersion calorimetry and thermophotometry.* Immersion calorimetry uses the measurement of the heat of immersion of a dry material in different liquids to determine surface area and pore size distribution below 10 angstroms. Thermophotometry is based on the thermal analysis of the liquid-solid phase transformation of capillary condensate in a porous structure and is based on the principle that the equilibrium state of the fluid of a highly dispersed pure substance is determined by the curvature of interfaces. *Nuclear magnetic resonance (NMR)* uses two main techniques, one which is based on the study of NMR relaxation times of a fluid within the pores. This lies on the principle that pore fluid near a pore wall experiences spin lattice and spin-spin relaxation in a magnetic field at a faster rate than the bulk fluid. The other technique is based on the chemical shift of ^{129}Xe trapped in the material.

2.4.3 Non-intrusive Methods

Radiation scattering measures variations in the angular distribution of scattered intensity. This may be obtained from the scattering length of solid materials that occur over normal distances that surpass the normal interatomic spacings. The process does not require sample pre-treatment and uses two techniques known as small angle x-ray (SAXS) and neutron scattering (SANS) which can provide unique microstructural information from small angle scattering measurements that cannot be obtained from bulk measurements. SANS can be used to analyse material microstructure even in the wet state due to the very high penetrating power of neutrons. However, the subtraction of flat incoherent contribution in heterogeneous materials poses a challenge. On the other hand, sample size,

thickness and containment are limited with x-rays because of the adsorption of radiation. *Wave propagation* is another non-intrusive method of characterization which uses techniques. One which is ellipsometry, based on the change in polarization characterised by two elliptical angles obtained from light that is reflected at the boundary of different optical media. The other is ultrasonics which is based on variations in the attenuation of ultrasonic velocity. *Ion-beam analysis* studies the effect of stimulating a resonance in a sample to obtain the nuclei energy distribution of elastically backscattered ions that may be used in calculating pore size. *Positron lifetime spectroscopy* studies radiation derived from positronium decay and the time spectrum of positron annihilation when a positron enters a condensed medium.

Dynamic Methods

This section describes the dynamic characterization methods of a porous structure which includes (Burggraaf and Cot 1996):

- Rejection measurements
- Liquid displacement techniques
- Fluid flow measurements including liquid, gas, permporometry

2.4.4 Rejection measurements

Rejection measurements are done with reference to standard molecules using a parameter known as "cut-off" value. This the lower limit of solute molecular weight for which the rejection is at least 90%. These measurements depend on the type of solute, its interaction with the membrane and other process parameters.

2.4.5 Liquid displacement techniques

This may include liquid/gas methods (bubble point, liquid expulsion permporometry) and liquid-liquid displacement porosimetry (or biliquid permporometry). The former uses a principle that relates pressure required to force air through a liquid-filled membrane and pore radius (i.e., Laplace equation). The rate of pressure increases as well as pore length influence these measurements. Mean pore size and pore size distribution can be derived from flow distribution curves which include the "wet curve" (that is, the measurement of gas flow across the wet defect-free membrane) and the "dry curve" (that is, gas flow through the same membrane in a dry state). The latter involves

measuring the flowrate of the fluid displacing a non-miscible more wetting liquid that is impregnated in a membrane as a function of the pressure difference.

2.4.6 Fluid flow measurements

This involves the measurement of permeability to a fluid to obtain the mean pore radius of the membrane. The flux is sensitive to all structural aspects of the material. Thus, very high uncertainties are expected depending on the models and approximations used. Hence, calculation of parameters can be obtained from *liquid permeability, gas permeability or permporosimetry* measurements.

2.5 MEMBRANE ADSORPTION PHENOMENA

2.5.1 Types of Isotherms

From literature, there are different types of adsorption isotherms as shown later in chapter 3 (**Figure *21***). Type I and II are the most encountered in adsorption systems. Type I which is the Langmuir isotherm assumes monolayer adsorption while the Type II undertakes multilayer adsorption followed by capillary condensation. Types II and III are very similar to Types IV and V except that for Type IV and V, adsorption increases as the adsorbate gas reaches its vapour pressure while for Type II and III, a maximum adsorption is attained (Burggraaf and Cot 1996).

2.5.2 The Langmuir Isotherm

The statistical thermodynamic derivation assumes the surface consists of a given number of adsorption sites, S_0 and the number of sites occupied by adsorbate molecules is S_2, thus the number of unoccupied sites is $S_1 = S_0 - S_2$. Assuming, the rate of adsorption is proportional to the number of unoccupied sites and gas pressure and that, the rate of desorption is proportional to occupied sites and at equilibrium, the rate of adsorption equals the rate of desorption

$$K_1 S_1 p = k_1 p(S_0 - S_2) = K_2 S_2 \qquad (2.2)$$

dividing the equation by $S_{0,}$ we have the Langmuir equation as

$$\theta = \frac{bp}{1+pb} \tag{2.3}$$

Where, $\theta = S_2/S_0$ and $b = k_1/k_2$ which is the Langmuir constant and can also be written as n/n_0, where n is the kg-moles adsorbed per kg of adsorbent and n_0 is the saturation capacity. The equation becomes

$$n = \frac{n_0 bp}{1+bp} \tag{2.4}$$

At low pressures, the equation becomes $n = n_o bp$ while at high temperatures, n approaches the saturation value of n_o.

The Langmuir equation can be rewritten as

$$\frac{p}{n} = \frac{1}{bn_0} + \frac{p}{n_0} \tag{2.5}$$

2.5.3 The BET Isotherms

The BET equation is a widely used method in determining surface area from adsorption data for Type I, II, III isotherms.

Assuming that the Langmuir equation applies to each layer and:

(1) the heat of adsorption for the first layer has a unique value while for other layers is equal to the heat of condensation of the liquid adsorbate

(2) adsorption and desorption can only occur at the exposed layer

then the BET isotherm equation is obtained

$$\frac{n}{n_0} = \frac{cx}{(1-x)[1+(c-1)x]} \tag{2.6}$$

Where, x is the relative pressure, p/p_0 where p equals the pressure of the adsorbate and po equals the vapour pressure of the adsorbate; $c=e^{\Delta Q/RT}$ with ΔQ being the difference between the heat of adsorption and the latent heat of condensation.

The BET equation can be rewritten as

$$\frac{x}{n(1-x)} = \frac{1}{cn_0} + \frac{(c-1)x}{cn_0} \tag{2.7}$$

2.5.4 Isotherms derived from the Equation of State

This derivation is based on the assumption that the adsorbed layer can be treated as a two-dimensional phase. At constant temperature, the Gibbs adsorption isotherm becomes

$$Ad\pi = nd\mu \tag{2.8}$$

Where, A is the surface area, π is the spreading pressure, n is the number of moles adsorbed per unit mass of adsorbent and μ is the chemical potential of the adsorbate. Assuming the gas phase behaves as an ideal gas

$$d\mu = RTd\ lnp \tag{2.9}$$

Combining equations, the basis for derivation of adsorption isotherms from equations of state is

$$\frac{d\pi}{dlnp} = \frac{n}{A}RT \tag{2.10}$$

2.5.5 The Potential Theory

In multilayer adsorption, this theory assumes that dispersion forces play a determining role in adsorption that results in the existence of a potential field in the area of the adsorbent surface.

$$W = f(\varepsilon) \tag{2.11}$$

Where, W is the adsorbed volume above the surface with potential energy field ε.

From the dispersion interaction theory, the ratio of forces of attraction of different molecules equals to that of polarizability of the vapor molecules. Thus, the function introduces this ratio which is called the affinity coefficient, β and a factor showing the function of the size distribution of pore volume, k, to give the Dubinin-Radushkevich (DR) equation

$$W = W_0 E^{-k\frac{\varepsilon^2}{\beta^2}} \tag{2.12}$$

Where, W_0 is the limiting volume of the adsorbent sites representing the volume

of the micropores of the adsorbent.

Experimental Techniques

2.5.6 Adsorption Isotherms Determinations

This method uses volumetric and gravimetric techniques. The former is commonly used by measuring the pressure-volume relation to establish the amount of adsorbate gas on an adsorbent at different relative pressures (p/p_0). On the other hand, the latter uses electro microbalances or transducers and records the adsorbate weight gain as a function of time which makes the technique adaptable for the measurement of adsorption kinetics and diffusion coefficients(Burggraaf and Cot 1996).

2.5.7 Surface Area Determinations

The equilibrium adsorption capacity of the solid can be related to actual surface area using an appropriate theory such as the BET isotherm. The BET equation can be written in terms of volume as

$$\frac{x}{v_a(1-x)} = \frac{1}{v_m c} + \frac{(c-1)x}{v_m c} \tag{2.13}$$

Where, V_a and V_m are the volume of gas adsorbed and the volume of gas at the monolayer coverage respectively (Burggraaf and Cot 1996).

2.5.8 Pore Size Distribution

A major characteristic of pore sizes having a wide range of pore size distribution is the presence of a hysteris loop where the adsorption and desorption branches do not match within a range of relative pressures. The phenomenon is attributed to capillary condensation where the pores are modelled as a bundle of capillaries and the radius of the pores is related to relative pressure by the kelvin equation

$$RT\ ln\frac{p}{p^0} = \frac{\gamma V}{r} \tag{2.14}$$

Where, Υ is the surface tension and r is the pore radius

Both branches of the hysteris loop can be applied to the equation but the desorption branch is more appropriate. Thus, at each desorption pressure, the capillary radius can be calculated. Furthermore, specific assumptions and equations have been adapted for the determination of pore size for micro-, meso- and macro-pore materials (Burggraaf and Cot 1996).

A summary of the commonly used characterisation methods is shown in ***Table 3*** below. A combination of the results from these measurements provides tangible information about the membrane's physico-chemical properties.

Table 3 Commonly used membrane characterisation methods (Zioui et al. 2015)

Type	Instrument	Information
Performance test	Membrane filtration setup	Permeability, rejection, and pore-size distribution
Membrane porometry	Bubble point, mercury intrusion, gas adsorption, permporometry	Information on membrane pore structure
Microscopic methods	SEM	Surface/cross-section features
	TEM	Cross section of membrane/foulant
	AFM	Roughness, surface morphology
Spectroscopic methods	FTIR	Membrane/foulant functional groups
	XPS	Elements/chemical binding
	EDX	Elemental mapping of foulants
	EIS	Structural information of sublayers
Other methods	Goniometer	Hydrophobicity
	Streaming potential	Surface charge
	AFM force measurement	Interaction force

2.6 MEMBRANE GAS TRANSPORT MECHANISMS

The mechanism of gas transport in membranes are derived from Graham's law and Fick's law. The diffusion and concentration gradient play a role in the rate of permeation of gases and the selectivity of the membrane is altered by pressure, temperature, and concentration gradient of species along the membrane.

Graham's law states that the rate of diffusion of a gas is inversely proportional to the square root of its molecular weight (Ismail, Khulbe and Matsuura 2015). In mathematical form,

$$\frac{Rate\ a}{Rate\ b} = \left(M_b/M_a\right)^{1/2} \tag{2.17}$$

where,

$Rate\ a, b$	the rate of diffusion of the first gas and second gas respectively
M_a, M_b	the molar masses of gases a and b in g mol^{-1} respectively

Fick's law relates the molar flux through the membrane to the concentration gradient through the membrane thickness. It postulates that flux flows from regions of high concentration to low concentration with a magnitude proportional to the concentration gradient (Ismail, Khulbe and Matsuura 2015). This can be written in mathematical form as,

$$F_i = \frac{P_e}{L}(P_1 - P_2)A \qquad (\frac{mol}{s}) \tag{2.15}$$

where,

P_e	permeability, mol m^{-1} s^{-1} Pa^{-1}
L	length, m
$P_1\ and P_2$	pressure at point 1 and 2 respectively, Pa
A	permeation area, m^2

Gas transport in membranes can take place through several mechanisms including Hagen-Poiseuille flow, Knudsen diffusion, surface diffusion, capillary condensation, and molecular sieving. The transport mechanism can occur

depending on the membrane pore size, the molecular size of permeating species, the interactions between permeating molecules, membrane material, and operating conditions.

2.6.1 Hagen-Poiseuille

This mechanism comes to play when the pore diameter is large compared to the mean free path of the gas molecules ($\lambda/r_p < 1$). Therefore, intermolecular collisions are strongly dominant leading to bulk flow through large pores. The mean free path is the average distance a particle will travel without collision. This means that the gas molecules collide together more frequently than they collide with the pore walls, thus there can be no separation of mixed gases. In this regime, the gas permeance is proportional to the radius squared and the mean pressure; and inversely proportional to the gas viscosity (Oyama 2011; Domenico De Meis 2017). Flow may be expressed by Darcy's law. Regime is proportional to porosity and varies inversely with tortuosity (Pakizeh, Omidkhah and Zarringhalam 2007b).

$$P_e = \frac{\varepsilon \eta r^2}{8\mu RT} P_{av} \qquad (mol\ m^{-1} s^{-1}\ Pa^{-1}) \tag{2.16}$$

where,

ε	porosity, %
μ	viscosity, Pa s
η	shape factor assumed equal to the reciprocal tortuosity
R	universal gas constant, J K^{-1} mol^{-1}
r	pore radius, m
T	temperature, K
P_{av}	mean pressure, Pa

2.6.2 Knudsen Diffusion

This may occur when the pore size is larger than that of the gas molecules but smaller than its mean free path (λ) ($r_p/\ \lambda < 1$). There is more elastic collision between the gas molecules and the pore wall compared with interaction between the molecules. With each collision, the gas molecules are absorbed fleetingly and then reflected back in a random direction. The molecule to wall collisions are more dominant thereby, allowing lighter molecules preferentially diffuse

though the pores (Sridhar, Bee and Bhargava 2014). The permeance is given as (Oyama 2011; Domenico De Meis 2017):

$$P_e = \frac{2\varepsilon\eta r v}{3RT} \qquad (mol\ m^{-1}s^{-1}\ Pa^{-1}) \tag{2.17}$$

and,

$$v = \left[\frac{8RT}{\pi M}\right]^{0.5}$$

The equation shows that the permeation varies proportionally to the average pore radius and inversely with $M^{0.5}$ and independent of pressure distinguishing it from the viscous flow regime.

where,

ε	porosity, %
η	shape factor assumed equal to the reciprocal tortuosity
R	universal gas constant, J K^{-1} mol^{-1}
r	pore radius, m
T	temperature, K
v	molecular velocity, ms^{-1}
M	molar mass of the gas, g mol^{-1}

Additionally, the mean free path may be expressed mathematically as:

$$\frac{\mu}{P}\sqrt{\frac{\pi k_B T}{2M}} \tag{2.18}$$

where,

μ	viscosity of the gas at atmospheric temperature and ambient pressure, P_a s
k_B	Boltzmann constant J K^{-1}
T	temperature, K
M	molecular weight, g mol^{-1}

P pressure within the membrane pores, P_a

Knudsen number is a value used to characterise flow regimes which is defined as the ratio of the molecular mean free path of gas (λ) to a characteristic dimension of flow domain such as pore size. The mean free path (λ) is the average distance travelled by a molecule between collisions with another molecule. The larger the size of the molecule, thus, the shorter its mean free path. This is related to the Knudsen number (Kn) by:

$$K_n = \frac{\lambda}{d_p} \tag{2.22}$$

where,

d_p membrane pore diameter, m

λ Mean free path of the gas, m

2.6.3 Surface Diffusion

This mechanism is achieved by gas-membrane pore interaction which produces a concentration gradient that causes diffusion in the direction of lower concentration – both pore size and physico-chemical make-up of the pore surface determine the membranes' separation efficiency (Sridhar, Bee and Bhargava 2014). The porous medium acts as a semi-permeable membrane where gas molecules with high adsorption capacity or strong affinity for the membrane surface are preferentially adsorbed on the pore surface; reducing flow and diffusion of the weakly adsorbing gases. This mechanism usually occurs at low temperatures (due to decreased adsorption at high temperatures) and smaller pore sizes or non-porous membranes where contact between the gas molecules and inner surface is so strong compared to their kinetic energy such that the molecules cannot escape (Tüzün and Arçevik 2010). The permeance is given as (Oyama 2011; Domenico De Meis 2017):

$$P_{SD} = P_O \exp\left(\frac{-\Delta Ha - \Delta Esd}{RT}\right) \tag{2.23}$$

where,

P_O pressure, Pa

$(-\Delta Ha - \Delta Esd)$	energy barrier for diffusing molecules to permeate through the membrane, J m^{-1} s^{-1}
R	universal gas constant, J K^{-1} mol^{-1}
T	temperature, K

2.6.4 Capillary Condensation

Capillary condensation is a form of surface flow where one of the gases is condensable. It usually occurs at higher gas pressures with temperatures lower than the critical temperature. The condensed gas molecule fills the pores at certain critical relative pressures, blocking/ limiting the flow of the non-condensable gas, whilst the condensable gas dissolves therein and are transported across the pores of the membrane (Uhlhorn, Keizer and Burggraaf 1992; Uchytil et al. 2003; Shimekit and Mukhtar 2012).

$$\frac{\rho RT}{M}\ln\frac{P_t}{P_o} = -\frac{2\sigma cos\theta}{r} \tag{2.24}$$

where,

ρ	density, kg/m^3
M	gas molecular weight, kg mol^{-1}
θ	contact angle
P_t	total pressure, Pa
σ	interfacial tension, N/m
r	radius, m
R	universal gas constant, J K^{-1} mol^{-1}
T	temperature, K
P_o	vapor pressure, Pa

2.6.5 Molecular Sieving

This mechanism is based on size and shape exclusion of gas molecules (Sridhar, Bee and Bhargava 2014). It involves separation of the molecules by their particle size using membrane pores of similar size of the molecules. The typical pore sizes for molecular sieving are less than 2nm (Rackley 2017; Nagy 2019).

$$J_s\,(T) \sim \rho q_{sat} D_S^{O}\,(0)(1-\theta)^{-1}\ \exp(-E_{D,S}/RT)d\theta/dx. \tag{2.25}$$

where,

$J_s\ (T)$	flux at temperature T, mol/s
ρ	density, kg/m^3
q_{sat}	saturated molar volume, m^3/mol
$D_S^O\ (0)$	limiting surface diffusivity, m^2/s
θ	fraction of available adsorption sites that are occupied, dimensionless
$E_{D,S}$	surface diffusion activation energy, kJ/mol
R	universal gas constant, J K^{-1} mol^{-1}
T	temperature, K

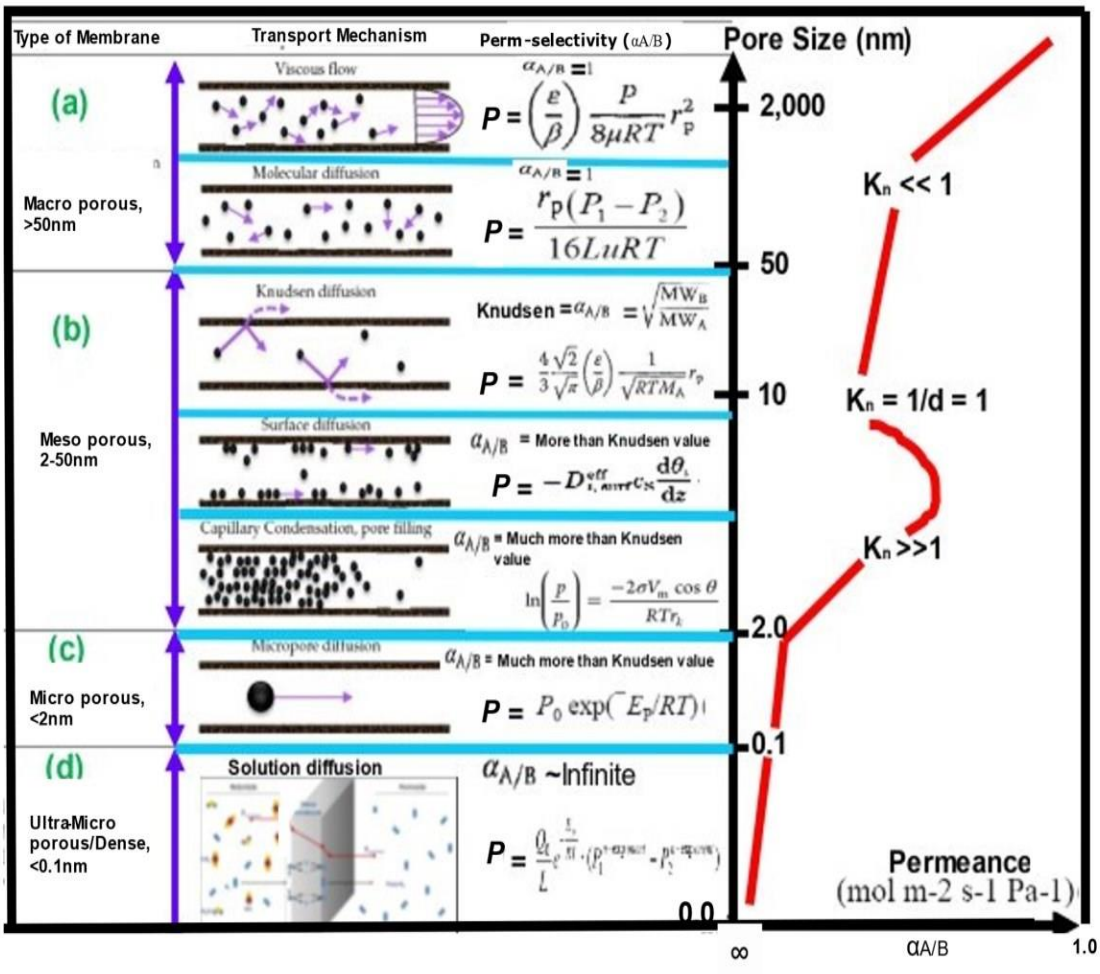

Figure 10 Gas transport mechanism in porous materials and their perm-selectivity. Adapted from (Ghasemzadeh, Basile and Iulianelli 2019)

Figure *10* describes the different mechanisms of flow and relates them to their pore size ranges – in each range, different transport mechanisms dominate. Interestingly, within 2 – 50nm, laminar flow, Knudsen diffusion, and

surface diffusion can take place (Domenico De Meis 2017). Furthermore, where there is a wide distribution in pore sizes (say from 1nm to 6000nm) all the above-mentioned mechanisms will occur to some extent depending on the temperature and pressure in operation. The general idea is to tailor the membrane to be able to take advantage of the gas properties and their interaction with the surface of the membrane to enhance the separation.

$$P_T = P_{H\text{-}P} + P_{Kn} + P_{SD1} + P_{CC} + P_{MS} + P_{SD2} \quad (2.26)$$

$$F_T = (P_T/\delta) \quad (2.27)$$

where,

P_T	Total permeability, mol m m^{-1} s^{-1} Pa^{-1}
$P_{H\text{-}P}$	Hagen-Poiseuille permeability, mol m m^{-1} s^{-1} Pa^{-1}
P_{Kn}	Knudsen permeability, mol m m^{-1} s^{-1} Pa^{-1}
P_{SD1}	Surface diffusion permeability, mol m m^{-1} s^{-1} Pa^{-1}
P_{CC}	Capillary condensation permeability, mol m m^{-1} s^{-1} Pa^{-1}
P_{MS}	Molecular sieving permeability, mol m m^{-1} s^{-1} Pa^{-1}
P_{SD2}	Solution diffusion permeability, mol m m^{-1} s^{-1} Pa^{-1}
F_T	Total permeance, mol m^{-1} s^{-1} Pa^{-1}
δ	Membrane thickness, m

In this case, with pore sizes in the macro/mesoporous range

$$F_T = F_{LF} + F_{KN} = k_1 r_{p1} + k_2 r_{p2} \quad (2.28)$$

2.7 CHARACTERISATION OF SEPARATION PROPERTIES

In order to make efficient use of resources and achieve effective membrane separation, high permeability and selectivity are required. There are several factors that have been identified by previous authors to affect gas flow in porous media (Pillalamarry, Harpalani and Liu 2011; Liu and He 2017; Peng and Li 2018; Chen et al. 2020). This can be classified into fluid properties and structural parameters.

2.7.1 Fluid Properties

These include the properties of the fluid that affect the movement or rate of flow of fluids through the membrane.

2.7.1.1 Molecular Weight

Molecular weight can be defined as a measure of the total atomic weight values of atoms present in each molecule. In relation to this work, we examine methane and carbon dioxide gases which have molecular weights of 16 g/gmol and 44 g/gmol, respectively, and try to describe how this fluid property affects the flow of gases through the membranes. In other words, how the weight of atoms present in each molecule of CH_4 and CO_2 changes the rate at which they flow through. Some authors have stated that flux is inversely proportional to the square root of the gas molecular weight. It is, therefore, expected that in a separation process, CH_4 (16 g/gmol) would be more selectively convened than CO_2 (44 g/gmol).

2.7.1.2 Kinetic Diameter

Kinetic diameter is an indication of the size of a molecule (3.3 and 3.8 for CO_2 and CH_4, respectively), which estimates the possibility of a molecule colliding with another. Thus, it is associated with the mean free path of molecules in a gas. That is, the average distance that a particle will travel without collision. This is imperative when discussing the behaviour of gases, as it plays an important role in the determination of the gas flow mechanism. For instance, in viscous flow, the pore diameter is large compared to the mean free path of the gas molecules, and there is frequent collision between the molecules. Whereas, in Knudsen flow, the pore size is larger than that of the gas molecules but smaller than its mean free path. Thus, there is elastic collision between the gas molecules and the pore wall but no interaction between the molecules. Hence, the molecule-to-wall collisions are frequent, thereby allowing lighter molecules to preferentially diffuse through the pores.

2.7.1.3 Flowrate

Flowrate is a quantification of bulk fluid movement. In terms of this research, we consider volumetric flow rate to be the rate at which a volume of fluid moves per unit time. The rate at which CH_4 and CO_2 gases flow through the membrane is strongly related to acting pressure and temperature. The faster a gas flows,

the higher the flux and permeance, which increases the selectivity of that gas in each membrane.

2.7.1.4 Pressure

Pressure is an important engineering quantity that affects many aspects of fluid mechanics. The research carried out by Pillalamarry et al indicates that pressure significantly affects CH_4 diffusion at lower pressure rather than high pressure (Pillalamarry, Harpalani and Liu 2011). However, the authors did not relate this to the CO_2 diffusion rate and other system factors, which are crucial to a biogas separation unit. Hence, these experiments used up to eight isobars to investigate the effect of the coupling of pressure and other parameters on the separation process.

2.7.2 Structural Parameters

These are the inherent properties of the membrane matrix system that affect the mode at which fluids pass through based on its components, symmetry, and general make-up.

2.7.2.1 Pore Size

Pore size is the distance between two opposite walls of a pore; thus, it is a measure of how large or small each pore within a material is. Due to the nature and mode of membrane preparation, we generally have a non-uniform range of pores, and hence, the mean pore size is used. Pore size is characterised in the laboratory using nitrogen physisorption, where the sample is degassed by loading the insulated sample-containing cell into the degassing station (for 3 hours at 300 $^{\circ}$C) of the physisorption equipment to remove any moisture and impurities. The degassed samples are re-weighed and moved to the analysis station where the sample-containing cell is immersed into a liquid nitrogen dewar and analysed at 77 K to provide pore size measurements. The effect of pore size to flowrate has been studied extensively. However, only limited studies have touched on it from the perspective of gas separation. From literature (Liu and He 2017; Peng and Li 2018), it can be deduced that displacement of CH_4 by CO_2 in coal bed reservoirs is affected by pore size. Another investigation (Pillalamarry, Harpalani and Liu 2011; Chen et al. 2020), revealed that pore size significantly affects the diffusion and separation of N_2/CO_2. Drawing an analogy from these authors, it is expected that pore size would affect biogas separation.

Thus, in this study, different pore sizes were experimentally tested to identify separation effectiveness.

2.7.2.2. Surface Area

The effect of surface area is also examined to ascertain if, and to what extent, this improves the performance parameters (permeability and selectivity) of the membrane system. Generally, higher surface area leads to a higher rate of reaction due to more acting sites for reaction progression. With this in mind, this work proceeded to utilise two membranes with the same mean pore size (15 nm) and similar characteristics but different surface area and thickness (3 mm and 5 mm) to confirm this in relation to fluid flow in porous media.

2.7.2.3. Operating Temperature

Consequently, the experiment included varying temperatures of the core sample to investigate the effect of the coupling of temperature and other parameters on the separation process.

In summary, membrane technology has shown good prospects for gas separation and its application to biogas separation can be improved by overcoming the limitations of adhesion and production of defect free membrane surface. The following chapter provides details on the methods of preparation and testing of an enhanced membrane system for biogas upgrading.

CHAPTER 3: METHODOLOGY

3.1 BASIC OVERVIEW

Ceramic membranes have been chosen for application in this study due to their unique and exceptional characteristics when compared to other gas separation membranes. They are made up of materials belonging to the inorganic group of materials and stable with use of biogas components. Ceramic membranes have well-specified pores, good molecular filtering property, wide pore size availability, and high durability (as the material does not age with time like other adsorbents do). In addition, these membranes show enhanced performance, high tensile strength, reduced energy consumption, and superior chemical, mechanical and thermal resistance that does not restrict its application in acidic, corrosive, high temperature and pressure environments that are prevalent in industry. In this chapter, the technique of preparation and characterisation of the ideal membrane for biogas upgrading was presented. A series of experiments to evaluate the membrane's performance of were carried out.

3.2 EQUIPMENT AND APPARATUS

The equipment and apparatus used for the experimental process include:

1. Weighing balance
2. Beakers
3. Measuring cylinders
4. Magnetic stirrer
5. Rotary dryer
6. Retort stand
7. Thermocouple
8. Thermometer
9. Flow meter
10. Pressure gauge
11. Venier calliper and ruler

12. Mortar and pestle
13. Hand tools including screw drivers, spanners, allen keys
14. Electric oven by Carbolite
15. Scanning Electron Microscope by Zeiss, model number EVO LS-10
16. Energy Dispersive X-ray Detector by Oxford Instruments, model number INCAx-act 51-ADD0020
17. Automated Gas Sorption Analyser by Quantachrome Instruments
18. Nicolet i S 10 FT-IR Spectrometer by Thermo Scientific
19. Laser Gas Analyser
20. One Attension ThetaLite Optical Tensiometer
21. Gases supplied by BOC gases, UK
22. 2-methyl butane supplied by Fisher Scientific, UK
23. Silicon elastomer SLYGARD 184 supplied by Dow Corning, UK
24. SLYGARD 184 curing agent supplied by Dow Corning, UK
25. Graphite seals supplied by Gee graphite
26. Membrane supplied by Ceramiques Techniques et Industielles (CTI), France
27. Heating tape supplied by RS component
28. Laboratory fabricated membrane unit

3.3 EXPERIMENTAL PROCEDURES FOR MEMBRANE CHARACTERISATION

Membrane permeation tests were carried out using the experimental set-up shown in **Figure 11** and **Figure *12*** below. Ideally, the gases will be separated into (i) a low pressure permeate containing the more permeable gas of the mixture and (ii) a high-pressure residual gas (retentate) which contains the less permeable component of the mixture. The set-up consists of a gas cylinder (labelled 4) with regulator (labelled 3) which contains the feed gas. It also comprises a heat regulator to adjust settings for the various temperature ranges studied (labelled 5), a pressure gauge to monitor the system pressure (labelled 1), a temperature indicator to display working temperature (labelled 7), a volumetric meter for flow measurements (labelled 6), the membrane module (that has been sealed to prevent leakage of gas and covered in glass fibre heating tape for insulation) (labelled 2), and an exit line through which the

outlet gas flows to the fume cupboard.

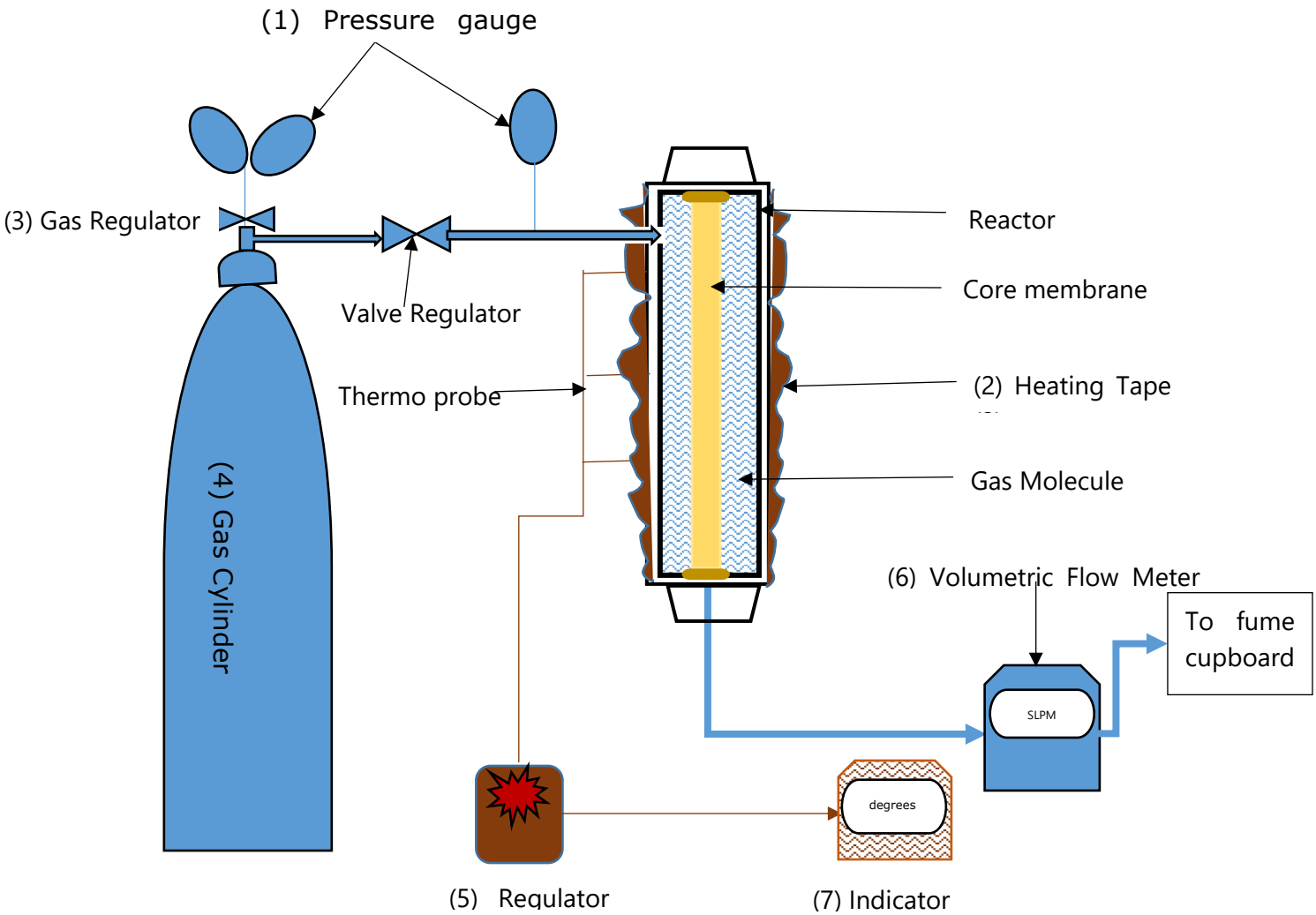

Figure 11 Schematic diagram of experimental set-up

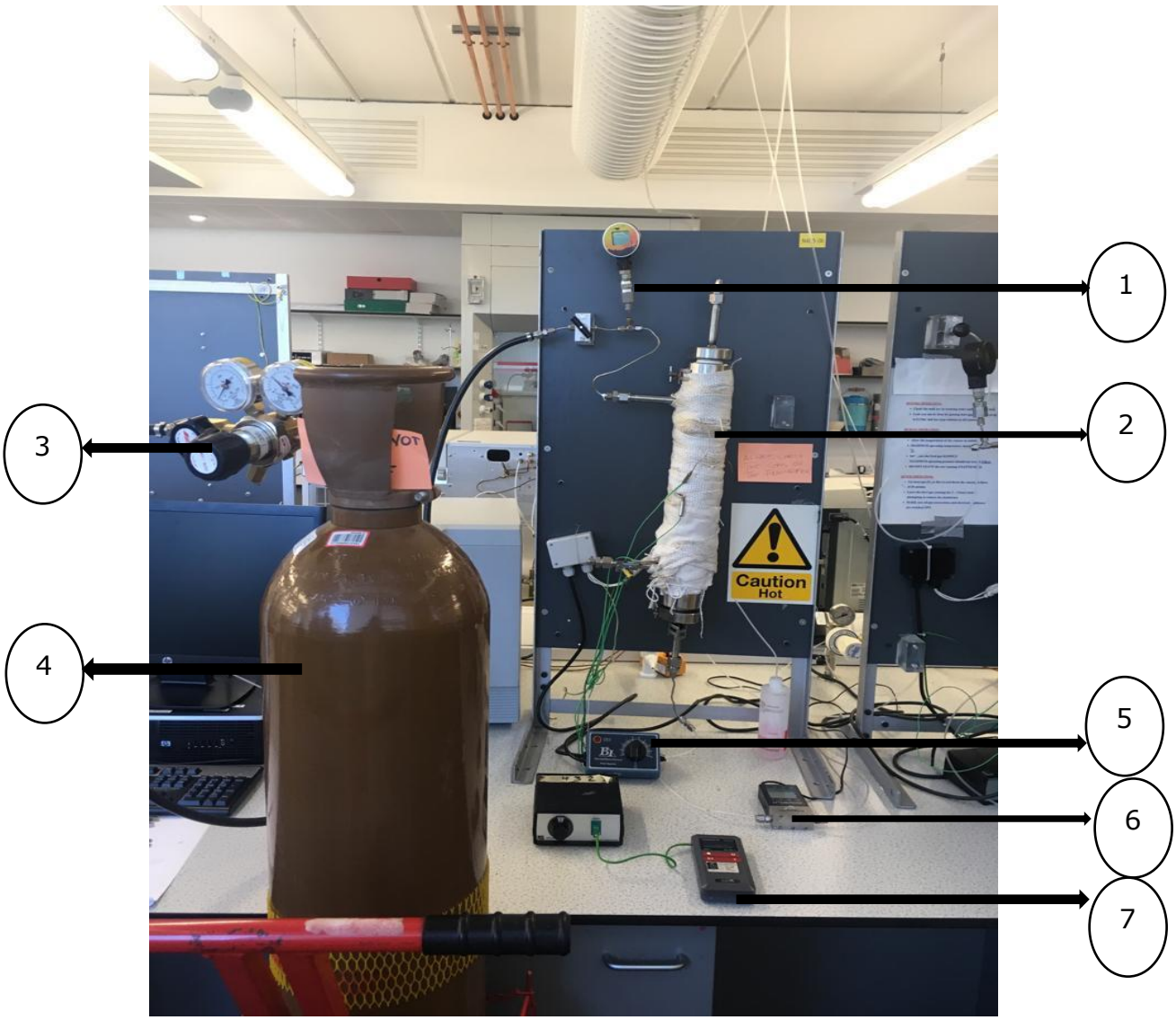

Figure 12 Experimental set-up showing all equipment including; pressure gauge (1), membrane module covered with heating tape (2), gas regulator (3), gas cylinder (4), heat regulator (5), volumetric meter (6) and temperature indicator (7)

The required specifications were provided to BOC for blending and delivery of the pure and binary gas mixtures. The membrane was inserted into a core holder, sealed on both ends, and mounted onto the rig. The core holder was designed and fabricated to high standards with stainless steel to accommodate the pressure ranges studied. A more detailed view of the rig is shown in **Figure 13**.

Figure 13 Membrane core holder

The configuration is like a shell and tube having a central annulus through which the membrane may be inserted with detachable covered ends that may be removed for easy insertion and removal of the membrane. It is equipped with feed, retentate and permeate ports for gas flow through the membrane. The laser gas analyser shown in **Figure *14*** was connected to the permeate stream and used to check the concentration of CO_2 gas through the membrane.

Figure 14 Laser gas analyser

The membranes were primarily made of alumina having pore sizes of 15nm, 200nm, and 6000nm. The membranes were produced with intermediate layers, starting with very coarse layers followed with layers of decreasing pore sizes being added until the designated pore sizes are reached as shown in **Figure *15***. The figure shows a scanning electron micrograph and an illustration of a typical structure of the different layers. For example, to achieve a membrane with a pore size of 6000nm, the support will have a support layer (layer 1) to achieve a macroporous membrane, while a membrane with pore size of 200nm also macroporous will have the support plus another layer (layer 1 and layer 2). Again, to achieve a membrane with mesoporous size of 15 nm, we will have the support plus two other layers (layers 1, 2 and 3). The layers are usually made from different materials such as aluminum oxide (Al_2O_3), titanium oxide (TiO_2), zirconium oxide (ZrO_2), silicon dioxide (SiO_2), silicon carbide (SiC), Zeolite or a hybrid mixture of two or more materials of their oxides. Given the specifications of the membranes, different analysis and comparison of gas transport behaviour and flow mechanism were established for the purpose of this work.

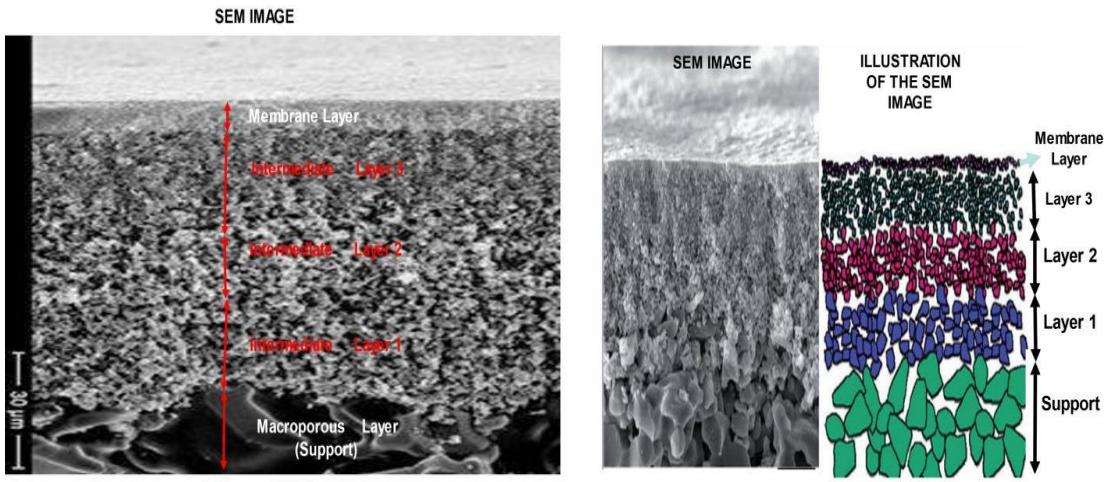

Figure 15 Sample micrograph (left), and SEM illustration of the layered arrangement of a typical ceramic membrane structure (right) (De Meis 2017)

The ceramic membrane was fitted into the centre of the annulus and both ends sealed with graphite seal to avoid gas slip, retain a pressure tight system, and isolate the high-pressure feed from the low pressure permeate. A graphite

seal is used because it is compressible, inert, temperature resistant and cost-effective. A leak test was conducted prior to each experimental run by pressurising the permeation rig at double the pressure required for the experiments and checking for any pressure drops along the lines. A snoop solution was also used as an indicator for leaks.

The membrane core holder was wrapped in heating tape with fire resistant glass fibre insulating material and thermocouples were attached at various points to maintain the temperature of the unit. This was connected to a temperature controller and the thermocouple selector switch that monitors the temperature throughout the unit.

At the inlet, the gas to be analysed was fed in and the flow meter confirmed that a steady constant driving force was being maintained. At the outlet, there was also a flow meter to measure the flowrate of the outgoing gas after passing through the membrane. The membrane module was then flushed to enable measurement of the flow characteristics of another gas by repeating the procedure. By comparing the flow characteristics of the different gases, the perm-selectivity of the membrane was measured.

The experiments followed the use of imposed pressure difference on the feed and permeate side by maintaining the permeate side at atmospheric pressure meaning that the transmembrane pressure equaled the feed side pressure. Operating conditions were stabilised for each experiment run, this was confirmed using a pressure gauge and temperature indicator connected to the reactor chamber. The resultant gas flow gives an estimate of how much methane versus carbon dioxide is evolved and this is used to estimate how well the membrane will separate the gases.

Additionally, membrane characterisation was done using static and dynamic methods to analyse and determine the membrane properties. The scanning electron microscope (SEM) equipment shown in **Figure *16*** was used to characterise the membrane sample by providing high resolution images that show the membrane topography (including defects) and measures surface thickness. The scanning electron microscope was equipped with an energy dispersive x-ray analyzer (EDXA) that show the composition of elements present within the membrane. The sample to be analysed was placed on a stub, set

firmly with an adhesive and loaded onto the SEM/EDXA equipment to produce micrographs of the sample at different magnifications using a finely focused beam of electrons that scans the sample.

Figure 16 Scanning Electron Micrograph with Energy Dispersive Analyzer

SEM analysis was carried out using a Zeiss Evo LS10 S with an Oxford Instruments INCA System Energy Dispersive X-ray Analyser. The microscope was used to obtain magnified images of the membrane surface for each sample while the EDXA was employed to provide data on the elemental composition of compounds in the scanning area.

Samples were prepared by freezing in liquid nitrogen and then carefully fracturing to prevent any distortion of the samples to be analysed. The pieces were carefully picked with a tweezer, mounted on a stub, and then inserted into the instruments' analysis chamber.

In order to allow us to combine both chemical and visual information on a microscopic scale, further characterisation was carried out by the fourier transform infrared spectrometer (FTIR) shown in **Figure *17*** where the functional groups of the membrane were determined to show the different bonds present in a membrane sample and its composition.

Figure 17 FTIR Spectrometer

The functional groups of the membrane are determined using an attenuated total reflection (ATR) Nicolet I S 10FT-IR spectrometer in the range 400-4000cm^{-1} to show the different bonds present in a compound. Spectroscopy is the study of the interaction of light and matter and is used to gather data about what the structure of a molecule might be.

By irradiating a molecule with infrared light, there is some interaction with the compounds in the sample that reaches the detector and shows the rate of absorbance of light by the sample, if any, to give information about the structure of the molecule. When a specific wavelength is absorbed, the identity of the molecules affects the photon of absorption, and the information is used to generate an IR spectra. The wave number illustrates the energy of infrared light and the transmittance gives the percentage of the wave number that reaches the detector.

A 100% transmittance means that all the infrared light corresponding to that wave number is passing through the sample without being absorbed to reach the detector. On the other hand, peaks show a reduction in this transmittance and means that the infrared light of a certain wave number is being absorbed by a particular functional group within the sample and therefore not reaching the detector. This gives information on the type of bond that is

present within that compound.

Furthermore, droplet permeation measurements were done toanalyse the absorption rate and pore size difference for each membrane sample. This was done using the One Attension ThetaLite Optical Tensiometer shown in **Figure *18***.

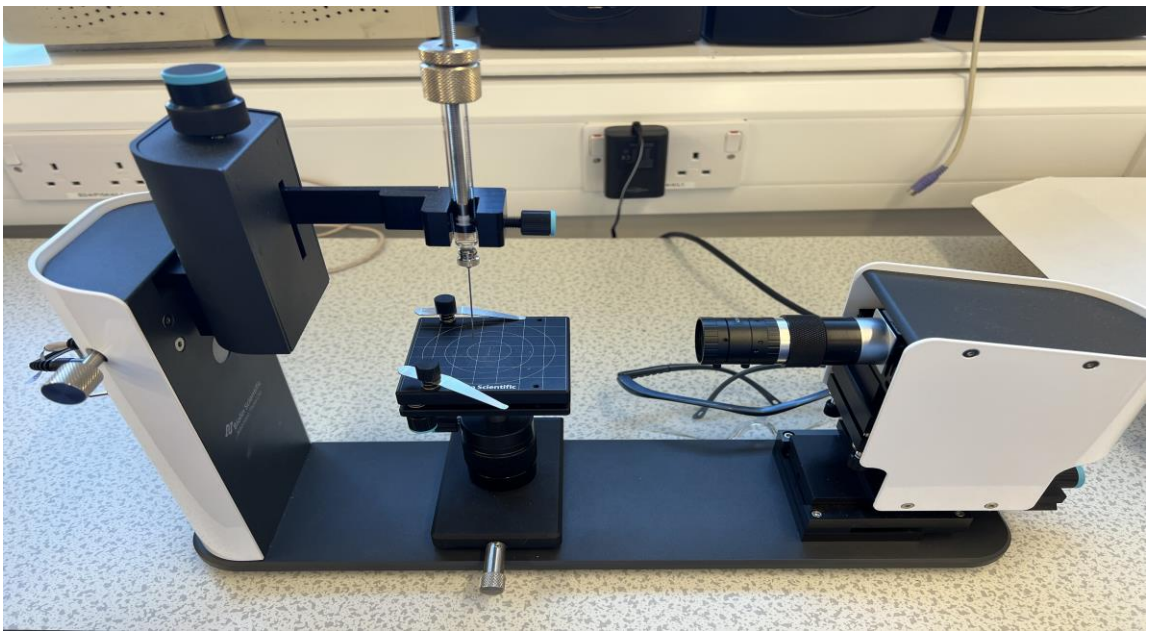

Figure 18 ThetaLite Optical Tensiometer

An intrusive characterisation method was carried out called physisorption. The gas sorption analyzer shown in **Figure *19*** was used to determine the nitrogen adsorption/desorption rates. This physisorption may produce different types of isotherms. The membrane sample to be analyzed were ground into powdered form using a sanitized mortar and pestle. The sample cells were washed, oven dried and weighed before and after sample introduction. Prior to the analysis, the sample was crushed, placed in a sample cell and weighed as shown in **Figure *20***. The sample was then degassed by loading the insulated sample containing cell into the degassing station of the equipment to remove any moisture and impurities. Degassing was done carried out for 3 hours at 300^{o}C using an inert gas (helium) after which the degassed samples were re-weighed and moved to the analysis station where the dewar containing liquid nitrogen lifts up and the sample containing cell is immersed into the liquid nitrogen and analyzed at 77K providing results which were evaluated using the computer attached to the analyzer.

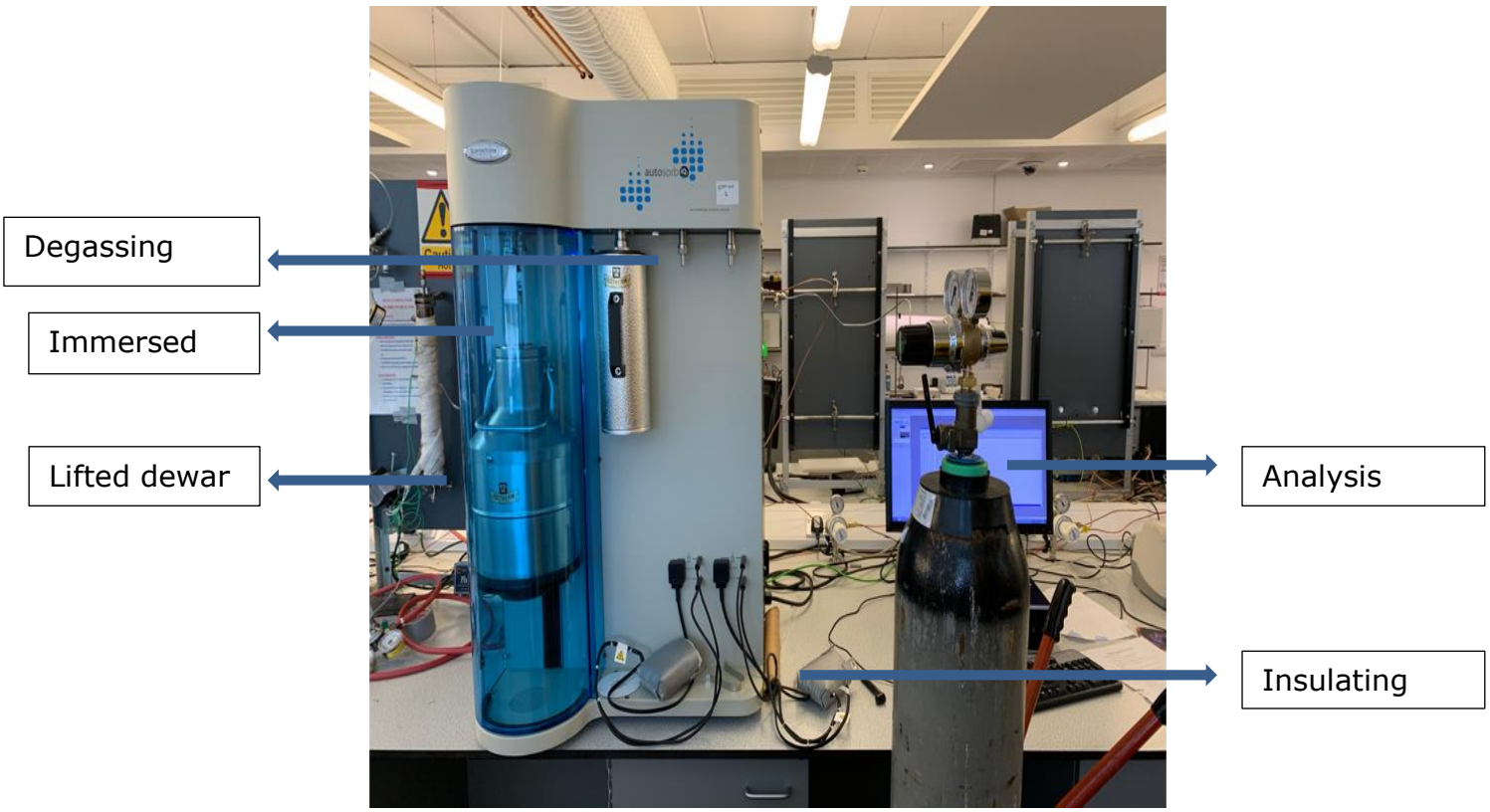

Figure 19 Gas sorption Analyzer

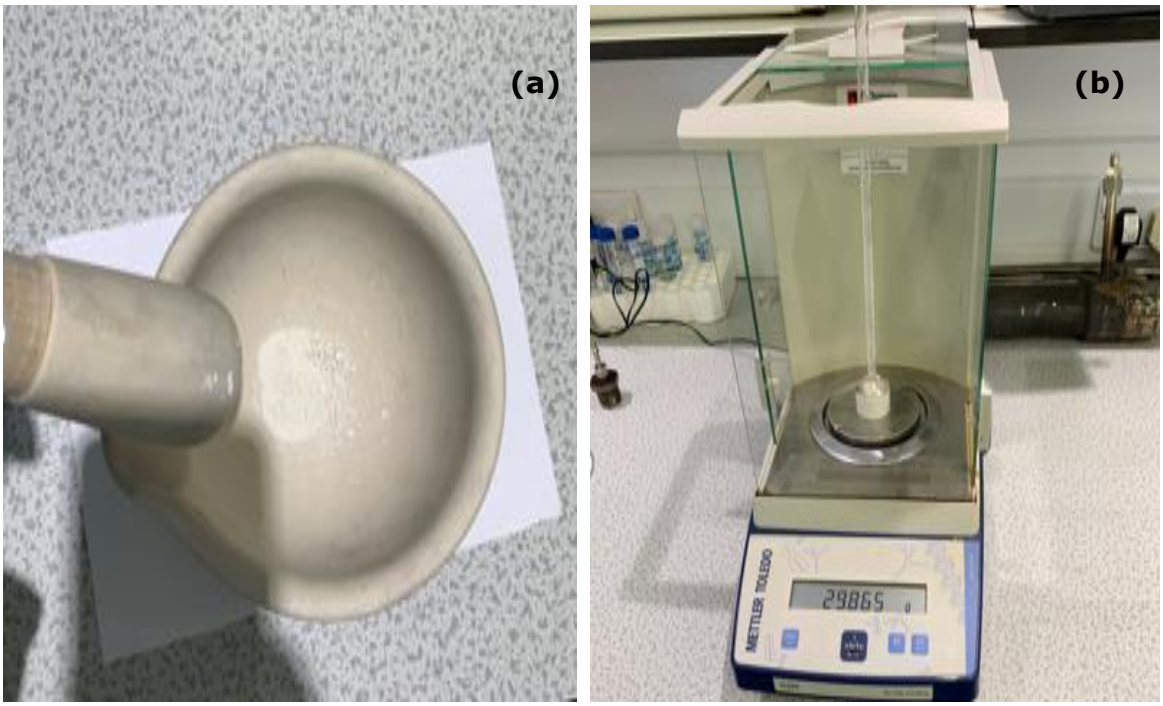

Figure 20 Physisorption sample being (a) crushed and (b) weighed

Nitrogen adsorption/desorption isotherms were obtained at 77K on a Quantachrome gas sorption analyser. The samples were thoroughly degassed to remove any moisture or impurities that may be present and then nitrogen is dosed into the analysis tube at predetermined relative pressures where the complete adsorption of gas is allowed to reach a steady-state and the volume at each pressure is recorded and shown on the adsorption isotherm.

The adsorption isotherm shows the quantity of gas adsorbed on a solid at various relative pressures, P/P_o (where P is the applied pressure and Po is the saturation pressure) and is a function of the pore size and surface area of the solid and hence can provide important information about the two parameters. The adsorbed and desorbed nitrogen volumes at constant temperature and relative pressures between 0.001 and 0.995 are recorded to provide an adsorption isotherm which may be of type I to VI as shown in **Figure *21*** according to the IUPAC definitions. This is depending on the membrane structure and intermolecular interaction between the gas molecules and its surface (Lee et al. 2006).

- Type I isotherm also known as the Langmuir type isotherm is characterised by adsorption in the non-porous microporous region at a low relative pressure
- Type II isotherm is characterised by non-porous or microporous adsorbents with the multilayer formation of the adsorbate on the adsorbent
- Type III isotherm is characterised by a non-porous or microporous layer with weak interaction between the adsorbate and the adsorbent
- Type IV isotherm is characterised by a microporous material with mono or multi-layer formation and a mesoporous surface with capillary condensation and the formation of several hysteresis loops based on the shape of the pores
- Type V isotherm is characterised by a mesoporous material having weak interaction between the adsorbate and the adsorbent
- Type VI isotherm is characterised by a very uniform adsorbent surface

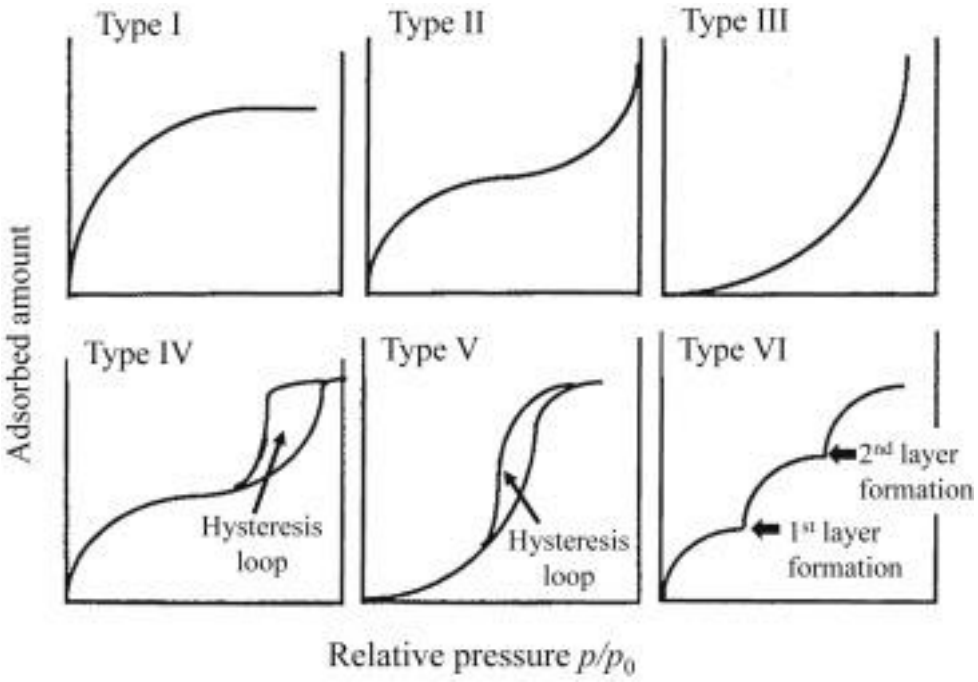

Figure 21 Adsorption isotherms

This study uses a couple of the static and dynamic characterisation techniques to give a collective indication of membrane characteristics as described in **Table *4***.

Table 4 Summary of characterisation techniques

Characterisation Method	**Application to Gas Separation**
Stereology (Scanning Electron Microscopy)	Image representation and analysis of the membrane pore structure or presence of defects
Physisorption	Description of the membrane's pore size distribution (macro-, meso-, or microporous)
Fourier Transform Infrared Spectronomy	Indication of the functional groups and elemental composition of the membrane
Tensiometer	Provides the degree of hydrophilicity or hydrophobicity of the membrane
Permeation tests	Identify the absorptivity of specific gases and separation capacity

3.4 EXPERIMENTAL PROCEDURE FOR MEMBRANE PREPARATION

The synthesis of a silica membrane was carried out by a dip-coating technique to deposit a uniform layer on the surface of the membrane support. The membrane support is shown in **Figure *22***. A schematic of the dip coating processes are shown in **Figure *23*** and **Figure *24*** . Previous research by GB Sun et al shows that the uniformity of the layer coating plays a critical role in obtaining a membrane with excellent properties and the dip coating technique is advantageous as it allows for easy manipulation/control of parameters and results in a thin layer of deposition with high surface area that maintains the membranes' high permeability (Sun, Hidajat and Kawi 2006).

Figure 22 Measurement and image of a membrane support

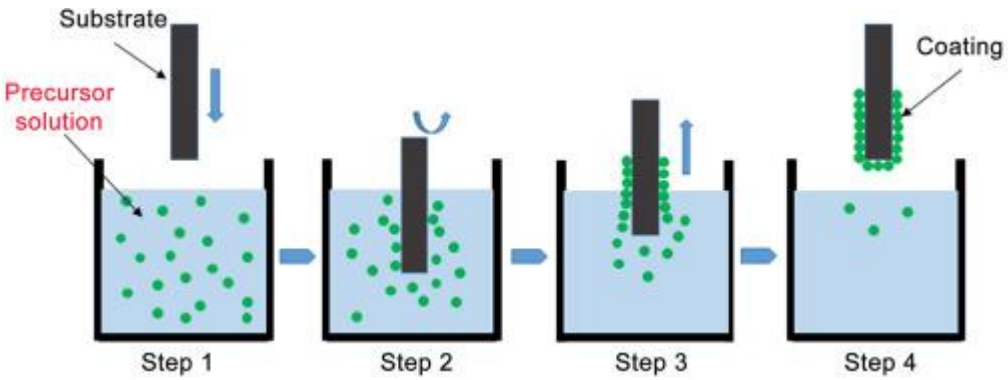

Figure 23 Schematic of the dip coating process (Neacşu et al. 2016)

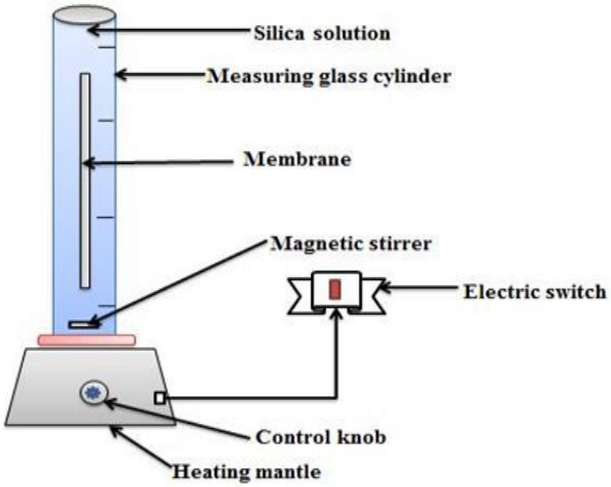

Figure 24 Schematic of silica dip coating set up

The preparation procedure involved producing a solution by dissolving the elastomer in 2 methyl-butane and adding a curing agent. The mixture contained 2 methyl-butane, silicon elastomer and curing agent in the ratio 90:10:1. The mixture was continuously stirred in a beaker using a magnetic stirrer at room temperature for 20 minutes to achieve clear and colourless solution and to prevent coagulation of the mixture. The membrane was securely covered at both ends with teflon tape and cling film to ensure only contact with the outer surface and then dipped into the sol for 30 minutes as shown in **Figure *25***. It was kept in central vertical position throughout the dip to ensure even coating throughout the membrane support. After dipping, the membrane was carefully withdrawn from the solution, spin dried for an hour with a rotary dryer to ensure homogeneity and oven dried at 75^{o}C for 24 hours to remove any residual solvent and for complete bonding or cross-linking as in **Figure *26***. The membrane sintering temperature of 75^{o}C is selected as appropriate for this analysis based on previous research by Berean K et al for good adhesion and crack free characteristics (Berean et al. 2014). The same process was repeated three times for subsequent coatings on the support

Figure 25 Dip coating process showing (a) solution preparation (b) membrane preparation and weighing (c) membrane dipped in solution

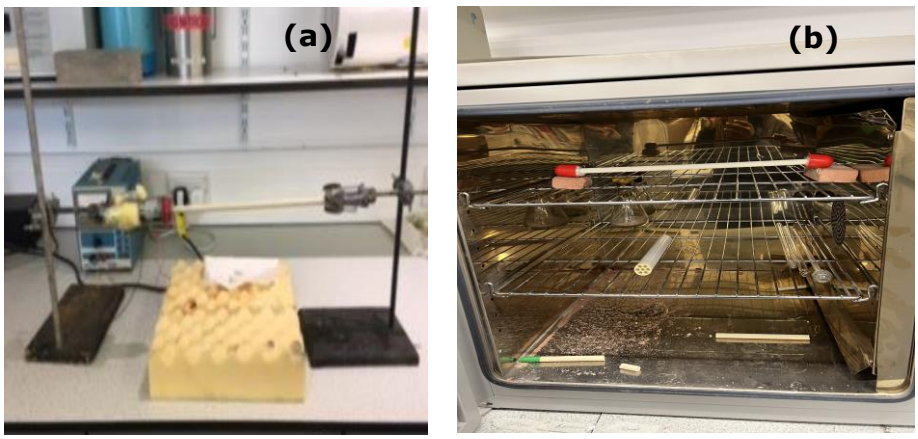

Figure 26 After dipping (a) spin drying and (b) oven drying

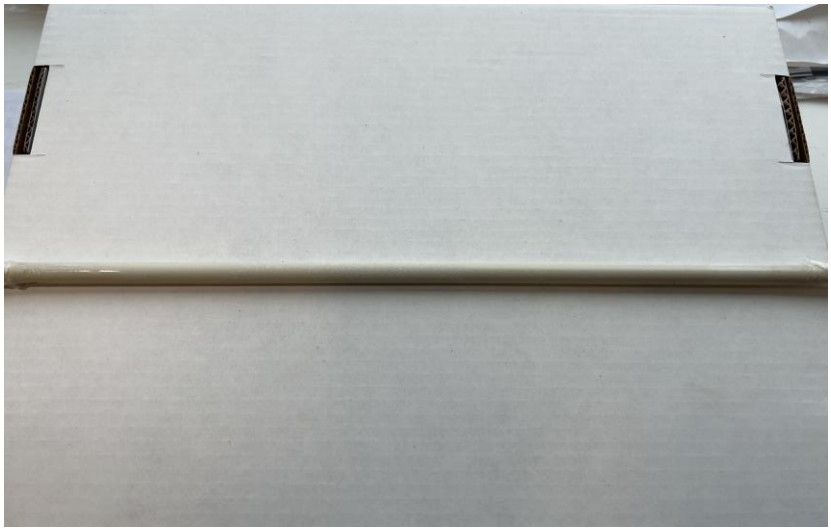

Figure 27 Prepared silica membrane

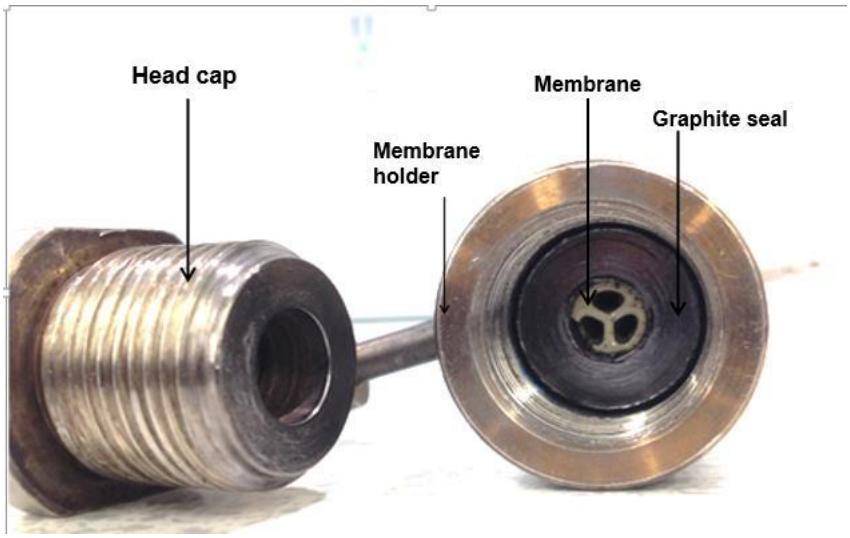

Figure 28 Membrane sealed with graphite rings in the module

The prepared silica membrane shown in **Figure *27*** was then fitted into the membrane module or core holder, sealed at the ends with compressible graphite seals to avoid gas slip (**Figure *28***) and then pressured to 5 bar with inert gas for a leak test. The membrane was characterised and the results are detailed in the following chapter.

CHAPTER 4: RESULTS

4.1 EVALUATION OF GAS TRANSPORT THROUGH A MEMBRANE SUPPORT

4.1.1 Introduction

Understanding the transport behaviour of each gas through each of the membrane core samples, under various operating conditions, is the foundation of achieving effective separation of the gases. By understanding the flow characteristics of the gas(es) of interest, the membrane perm-selectivity for the process may be evaluated.

Initial gas permeation tests were carried out to determine gas transport properties of methane and carbon dioxide through membranes having pore sizes in the mesoporous and microporous range, and the data was analysed in conjunction with observations from other characterisation techniques detailed below. A comparative analysis of the different membrane structural properties was done to ascertain the influence of these properties on fluid behaviour and flow mechanism.

4.1.2 Scanning Electron Microscopy (SEM) and Energy Dispersive X-ray Analysis (EDXA)

Analysis was done in the order of 2000x magnification and the differences in surface morphology for each sample is captured in **Figure *29*** below. From the SEM images, it is clear that the 15nm and 200nm core samples contain more closely-knit pore structures than that of the 6000nm core sample. Although each of the membranes still contain defects in their pore structures. The EDXA analysis in **Figure 30** confirms the supports to be alumina ceramic membranes.

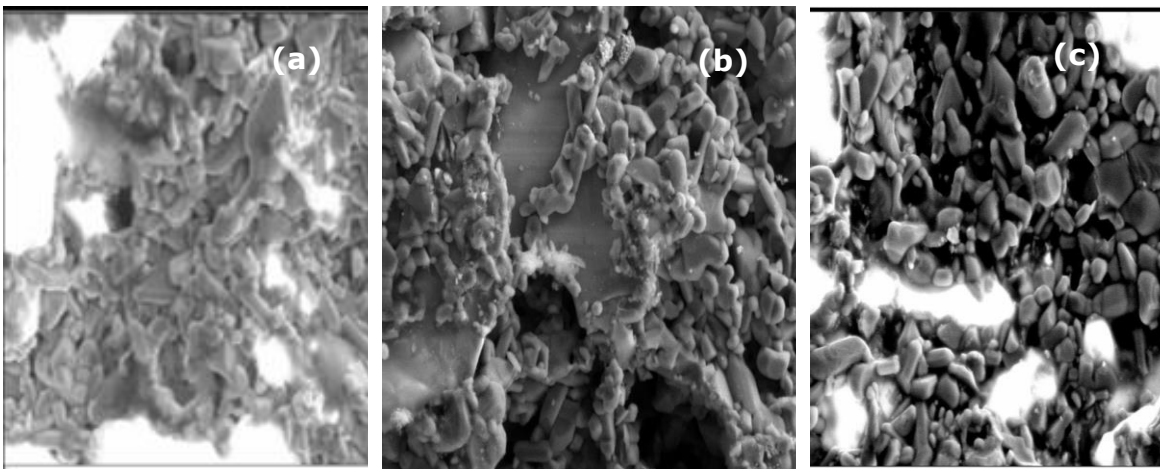

Figure 29 Outer surface SEM micrograph of (a) 15nm membrane (b) 200nm membrane (c) 6000nm membrane

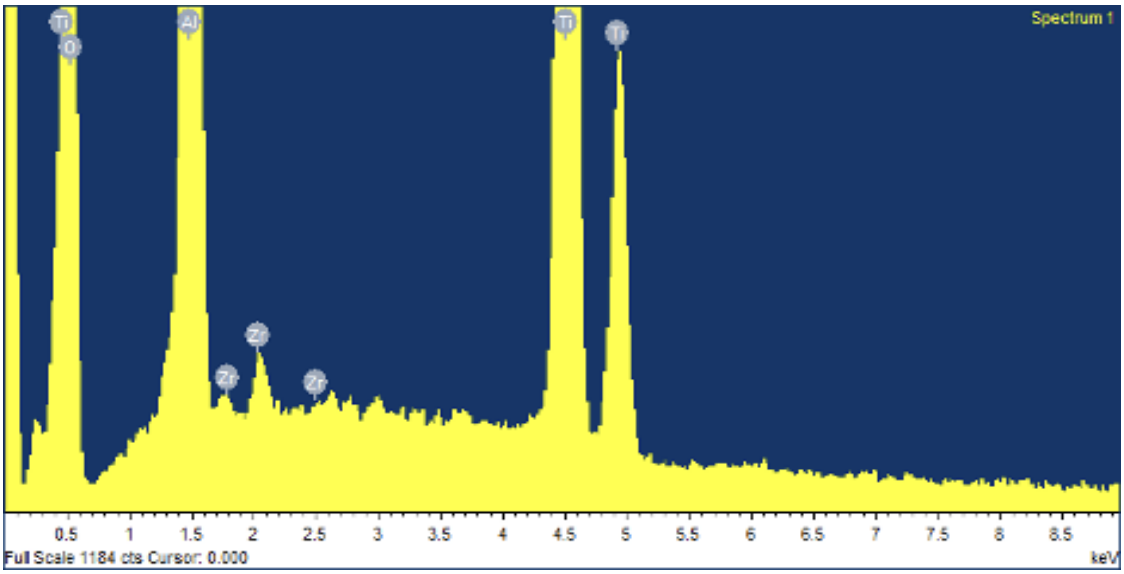

Figure 30 EDXA for ceramic membrane support

4.1.3 Physisorption Analysis

It was observed from the physisorption results in **Figure *31*** and **Figure *32*** that the N_2 adsorption/desorption isotherms are of type IV and V as they are both presented with a hysteresis loop. Although a narrow hysteresis loop is noticed for the 15nm membrane indicating smaller pores. Surface area is another physical characteristic of the membranes which determine how much adsorption area within the pores is available per gram of the material and this was estimated by Brunaver-Emmett-Teller (BET) method to be $0.247 m^2 g^{-1}$ and $1.676 m^2 g^{-1}$ for the 15nm and 6000nm membranes respectively confirming the

presence of larger pores in the 6000nm core sample that provides more area for gas adsorption.

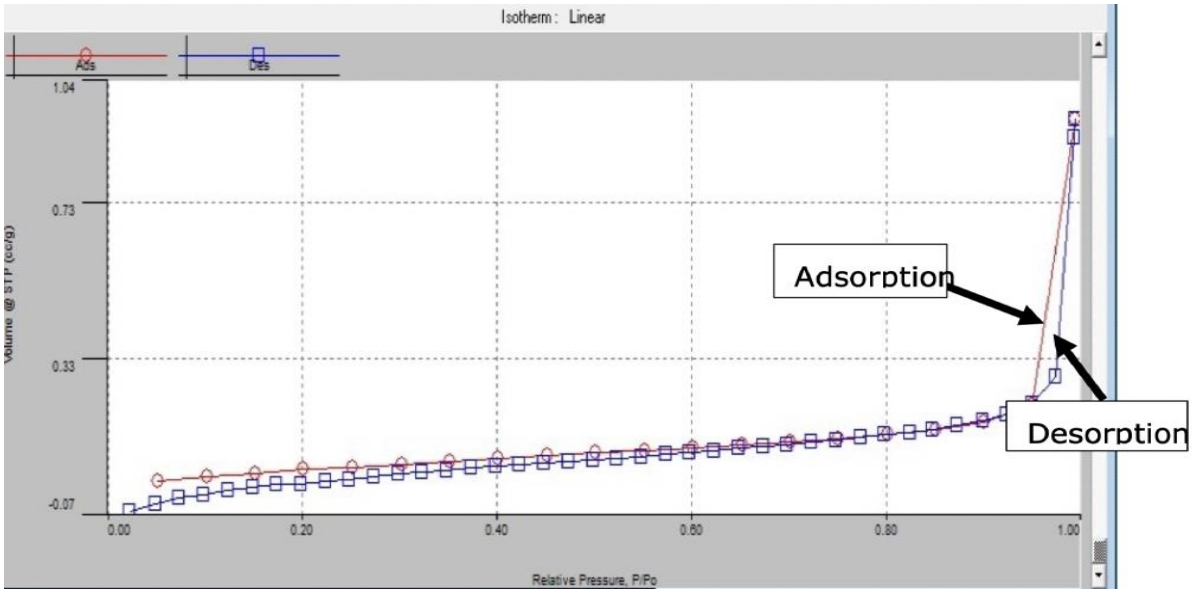

Figure 31 Adsorption/Desorption Isotherm for 15nm membrane

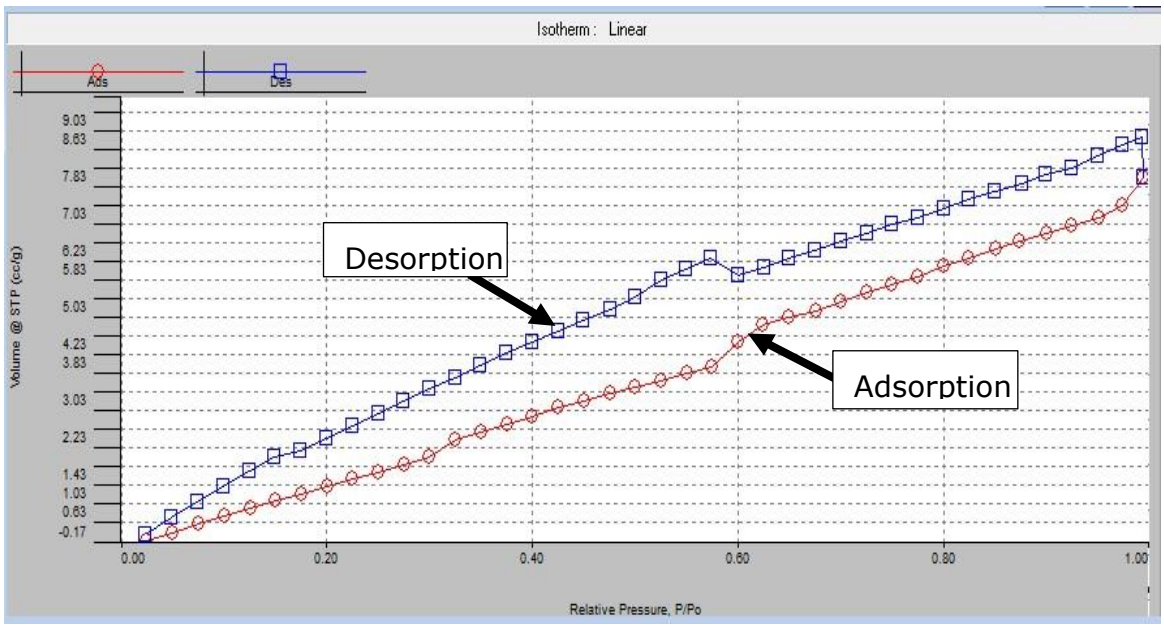

Figure 32 Adsorption/Desorption Isotherm for 6000nm membrane

4.1.4 Fourier Transform Infrared Spectronomy (FTIR) Analysis

FTIR can used to obtain an infrared spectrum of absorption or emission of a solid, liquid or gas. The spectrometer concurrently stores high-resolution

spectral data over a wide spectral range. **Figure *33*** and **Figure *34*** show that the spectra for the support membranes are somewhat similar, having amine (N-H) functional groups that appear with double peaks around a wavelength 3323 cm^{-1} which confirms the presence of alumina oxide in the support of the silica membranes produced.

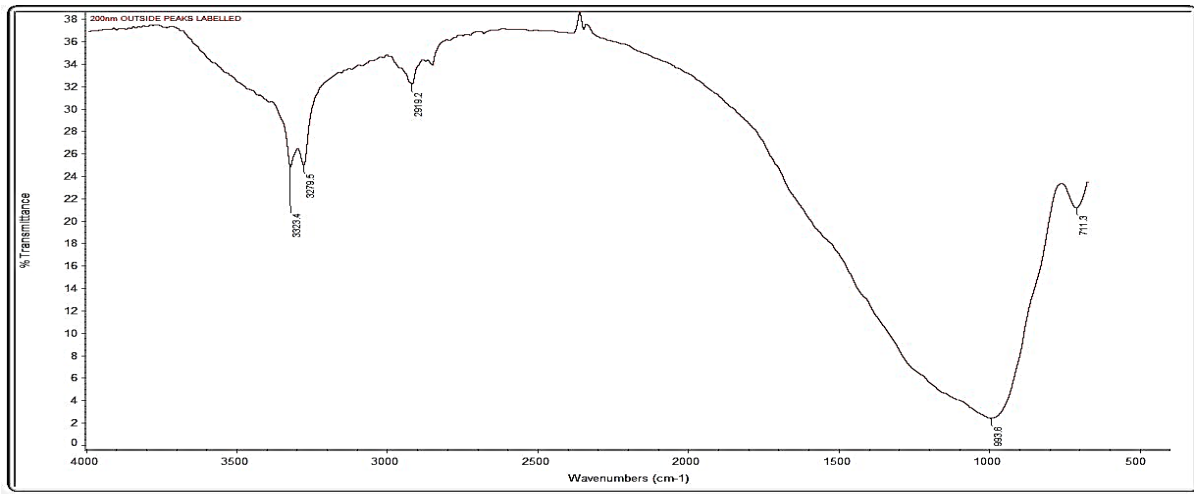

Figure 33 FTIR image for 200nm membrane

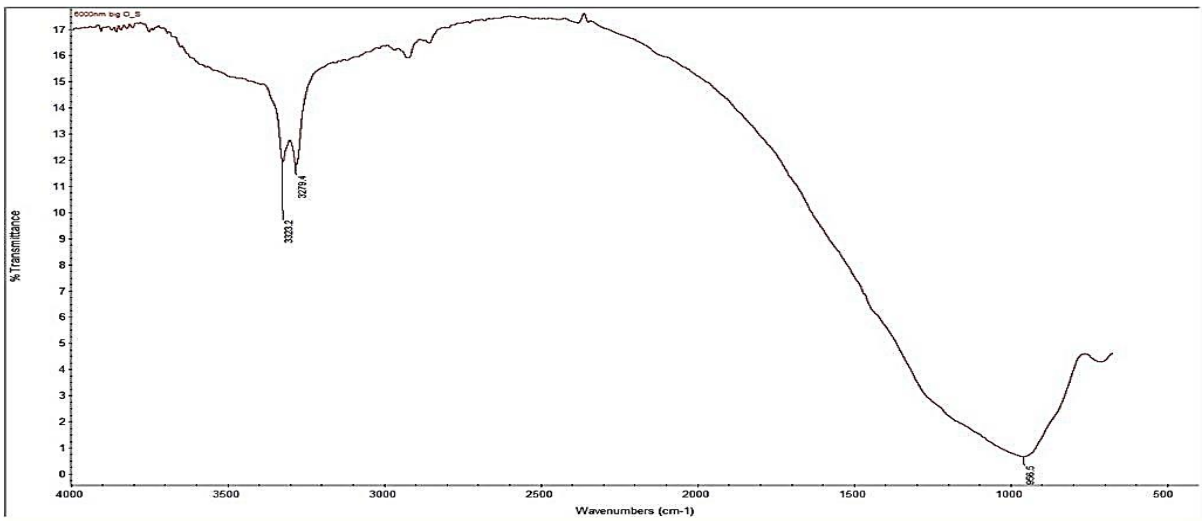

Figure 34 FTIR image for 6000nm membrane

4.1.5 Droplet permeation Measurements

Droplet permeation measurements were taken for each sample under the same conditions of approximately 5μl of droplet at 51 frame per second (FPS).

Analysis was done using distilled water for a duration of 5 seconds. Permeation images were taken with the results are shown in **Figure *35***. It is obvious from the droplet image capture that the 15nm membrane showed the highest resistance to the permeation of the distilled water compared to the 200nm and 6000nm supports confirming the pore sizes of the core samples. The results also show that the support contact angles were below 90 degrees meaning that they were hydrophilic compared to the silica membranes prepared and presented in section 4.2.4 which show that the silica membrane becomes hydrophobic thereby favouring the passage of gas and repelling water, making it more suitable for gas separation and purification applications (Valappil, Ghasem and Al-Marzouqi 2021).

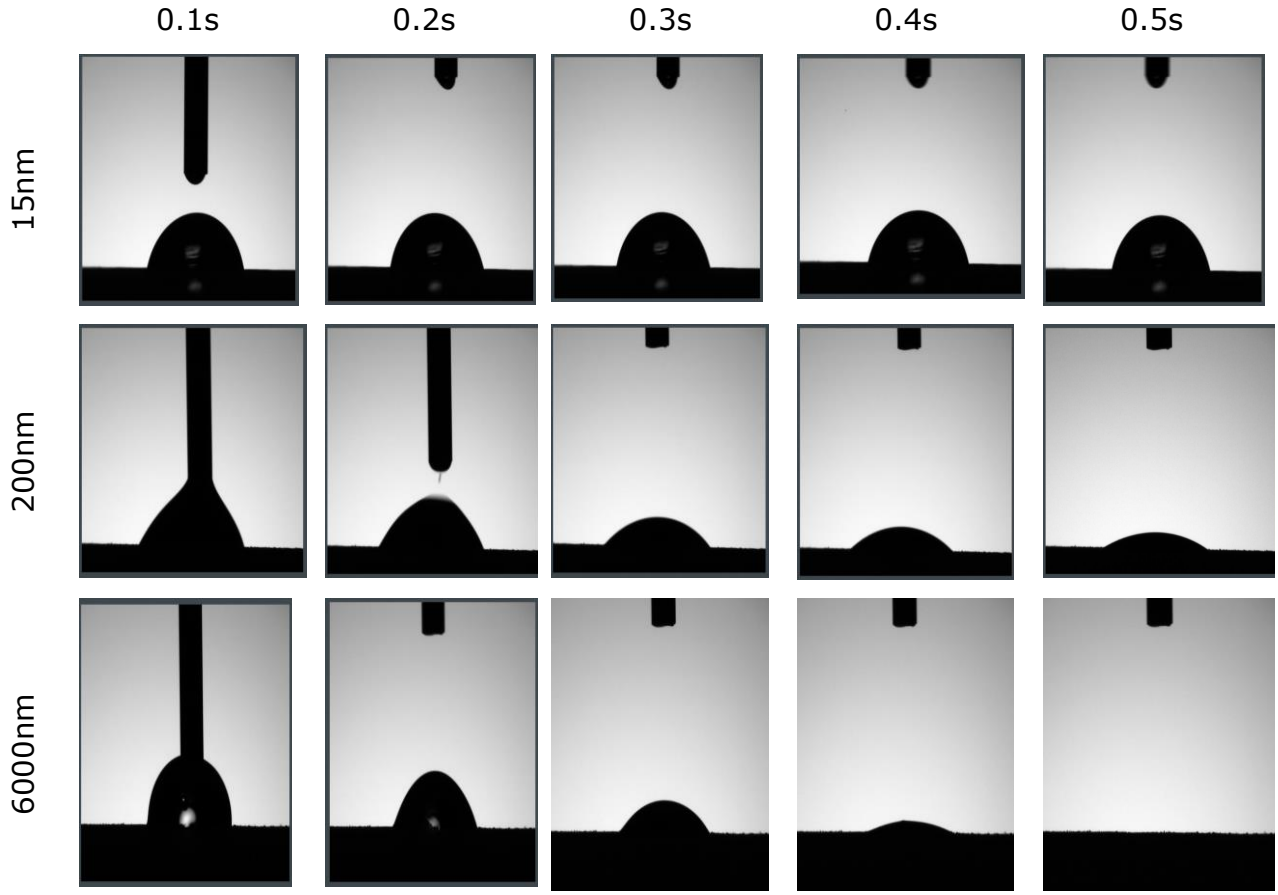

Figure 35 Droplet images for 6000nm membrane at 0.1, 0.2, 0.3, 0.4, 0.5s (left to right)

4.1.6 Gas Permeation Tests

The permeation unit was set up to investigate the behaviour of gases and membrane performance for each membrane. The effect of changes in the membrane and fluid properties are detailed in this section.

4.1.6.1 Effect of Pressure

Pressure ranges between 0.2 and 3.0 bar were studied with 0.4 bar increments (with ±0.01 bar error) as adapted from Yildirim and Hughes in their study (Yildirim and Hughes 2003). The plots below in **Figure *36*** show the behaviour of gases as a result of pressure drop across the membrane and proves that pressure is a major driving force in the rate of flow of gases through the membrane. This behaviour is characteristic of viscous flow.

What is interesting to note is the characteristic flow of each gas through the pores. It was observed that methane, CH_4 which has a smaller molecular weight, travels through the membrane at a much faster rate than CO_2 for all the operating conditions studied. This is indicative of the Knudsen flow mechanism where the flow of gases is dependent on the gas molecular mass, thus the light gases permeate faster than the heavier ones.

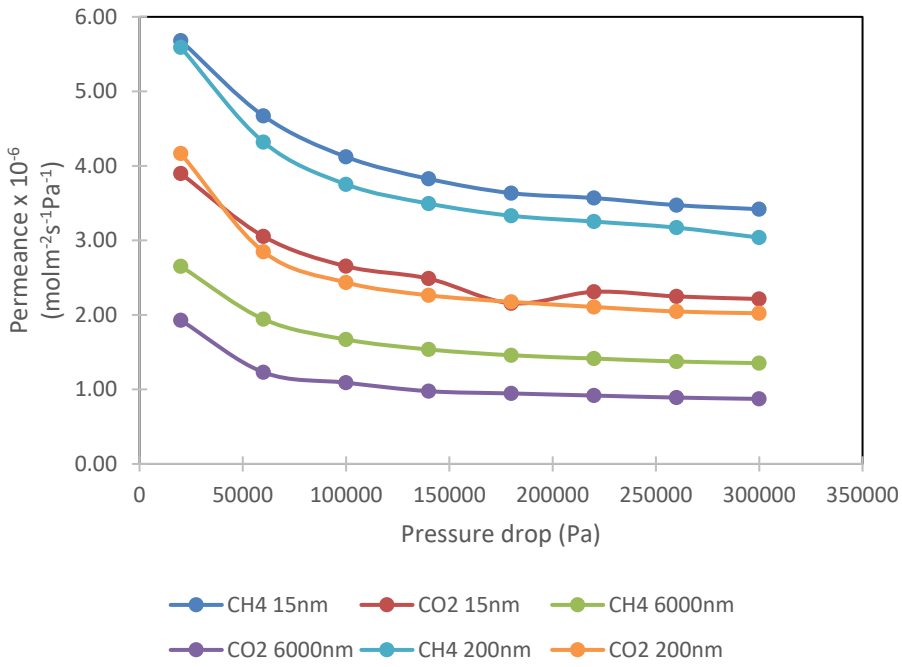

Figure 36 Isothermal effect of pressure on gas permeance for each membrane at 20 degrees Celsius

It has been identified by Pillalamarry et al. that pressure significantly affects CH_4 diffusion at lower pressure than high pressure (Pillalamarry, Harpalani and Liu 2011) and this was also confirmed in this study with a similar behaviour observed for gas diffusion. There is a linear relationship between pressure drop and permeance at these low pressures below 0.6 bar which is suggestive of laminar flow in this region following which there is a transition in diffusion behaviour and flow regimes.

4.1.6.2 Effect of Temperature

From literature, it is known that the permeating flux decreases as temperature increases in the Knudsen regime (Sedigh et al. 1998; Da Costa et al. 1999; Ghasemzadeh, Basile and Iulianelli 2019). However, within the four isothermal conditions studied, the effect of temperature was found to be negligible as shown in **Figure 37**. The analysis also showed the relationship between selectivity and temperature for each membrane which revealed that an increase in temperature to 100°C rarely improves the membrane selectivity. However, the measured selectivity ranges between 1.49 - 1.55 which is below the ideal Knudsen selectivity of 1.6. The selectivity is defined by the ratio of permeability of methane to carbon dioxide whilst the theoretical (Knudsen) selectivity is defined by the ratio of their molecular weights.

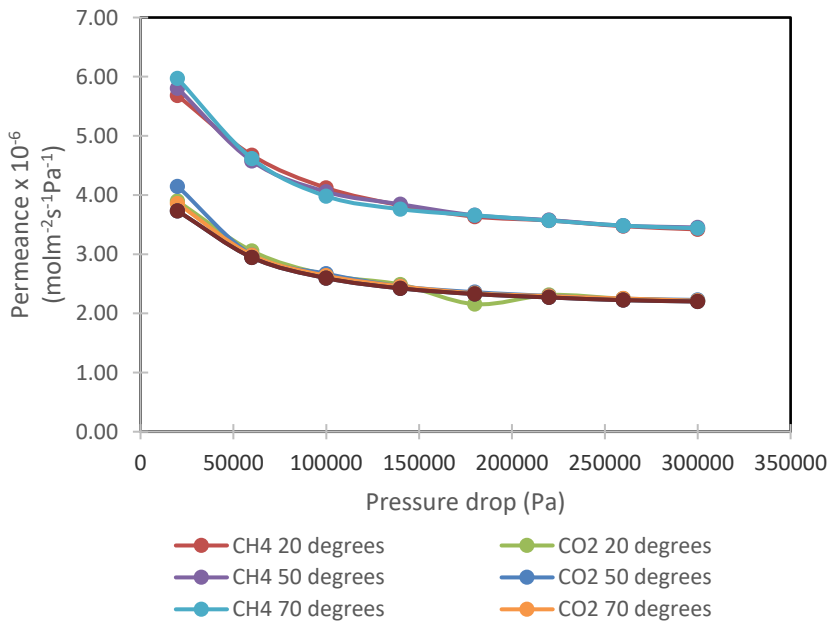

Figure 37 *Effect of temperature on methane and carbon dioxide gas permeance*

4.1.6.3 Effect of Pore Size

Membranes with different mean pore sizes were evaluated to analyse how gas flow is altered within each membrane. Gas flowrates were observed to increase as the pore size increased. For instance, through the 15nm and 6000nm membranes and under the same operating conditions of temperature and pressure, it was observed that the flowrate of each gas was greater with the 6000nm membrane than through the 15nm membrane. This observation is attributed to the very large pore sizes of the 6000nm membrane which is categorized in the macro-porous range that allows greater flow of gases.

Figure *38* shows the plots of permeance against pore size for the three pore sizes studied (15nm, 200nm and 6000nm). Assuming that when r_p is zero the permeability is zero, permeance is highest at 15nm and the order of plots confirmed that viscous flow and Knudsen transport were the experienced in the gas permeation study. A quadratic curve is noticed in the figures and this can be linked to the parallel flow model described by De Meis et al (Domenico De Meis 2017), which confirms the interplay of viscous and Knudsen diffusion within these membranes.

This study therefore confirms that a combination of viscous and Knudsen flow can occur through mesoporous and microporous membranes as described by Luis et al (Luis, Van Gerven and Van der Bruggen 2012). In this case of the mesoporous membranes, the contribution of viscous flow can be attributed to the presence of defects in the pore structure as shown from the SEM micrographs in **Figure *29***. Thus, it can be evaluated that the low selectivity obtained from these membranes is due to the presence of viscous flow limits the separation properties being initiated by Knudsen diffusion. This means that in order to achieve improved separation characteristics, there should be a reduction in the viscous contribution to flow in a manner that will allow significant interaction of the gas molecules with the pore walls. This may be achieved by reducing the pore size to the optimum region as shown on the arrows in the figure below through subsequent coating of the membrane surface.

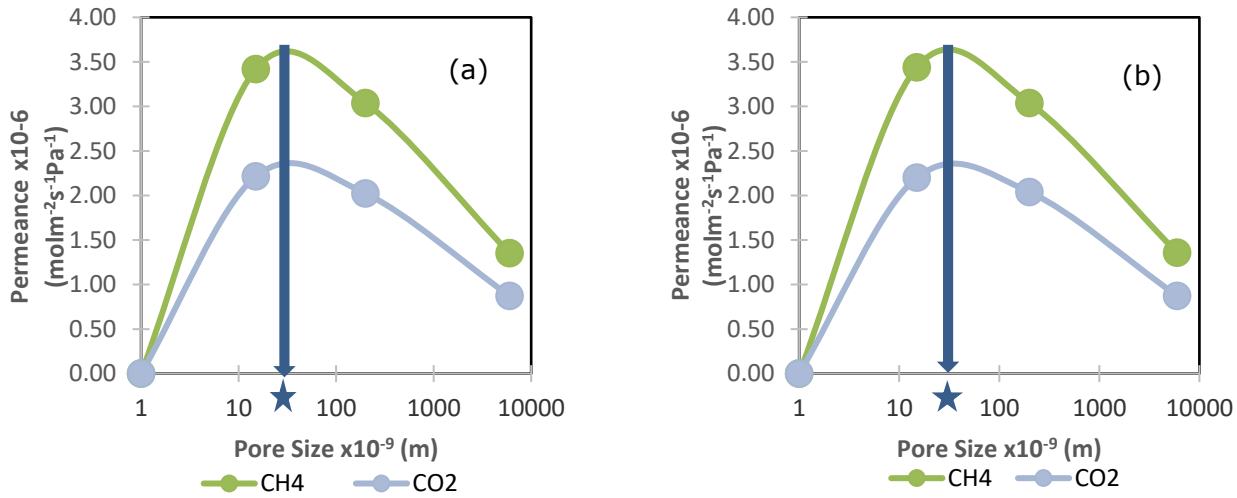

Figure 38 Effect of membrane pore size on gas permeance at (a) 20 degrees Celsius and (b) 100 degrees Celsius

4.1.6.4 Effect of Porosity

Porosity can be described as a measure of the void or free spaces in a material. It is defined as the fraction of void volume to the total volume. This study looks into how this affects the preferential flow of gas components. Samples of the different porosity were used to investigate how porosity would affect CH_4/CO_2 separation in membrane system.

The porosity of the 15nm, 200nm and 6000nm membrane were found to be 13%, 20% and 4% respectively using particulate density equation for measuring porosity ('4 Ways to Calculate Porosity' 2022). According to Julong Fu et al (Fu, Thomas and Li 2021), porosity and tortuosity are defined by an inverse relationship and this is confirmed in results on **Table *5***.

Permeance is optimized with higher porosity, thus the 200nm membrane is ideal despite having an intermediate mean pore size. This means that porosity and pore size can be mutually exclusive when dealing with membranes. In summary, permeance of gases increase with increasing porosity whilst permeance of gases decreased with increasing pore size. This means that in order to achieve optimal permeance, the membrane must have a high porosity and low pore size. This enables the investigation of the effect of loading the membrane support of high porosity with coating material that will improve the

selectivity of the membrane by reducing structural defects whilst maintaining high permeance. In section 4.2, the effect of subsequent loadings on permeance will be studied and compared with the permeance achieved from this initial support flow characteristics.

4.1.6.5 Effect of Thickness and Surface Area

Membranes having the same mean pore sizes and thickness of 3mm (15nm) and 5mm (15nmB) respectively were assessed to determine whether the thickness and surface area of the membrane plays a role in the manner in which gas is transported within the membrane. **Figure *39*** shows that both membranes followed a gradual rise in selectivity but the selectivity between 0.2 – 1.8 bar for each membrane was significantly different with the thicker membrane selectivity rising with increasing pressure and reaching the expected selectivity range around 1.8 bar. This means that the driving force for flow (i.e., pressure) had to be increased considerably in order to force the flow of gases through the pores of the thicker membrane. The results also reveal that the membrane with a larger surface area achieved higher selectivity compared with the other of smaller surface area. The improved selectivity may be due to more acting site that maximized contact between the gases and the surface of the inorganic membrane.

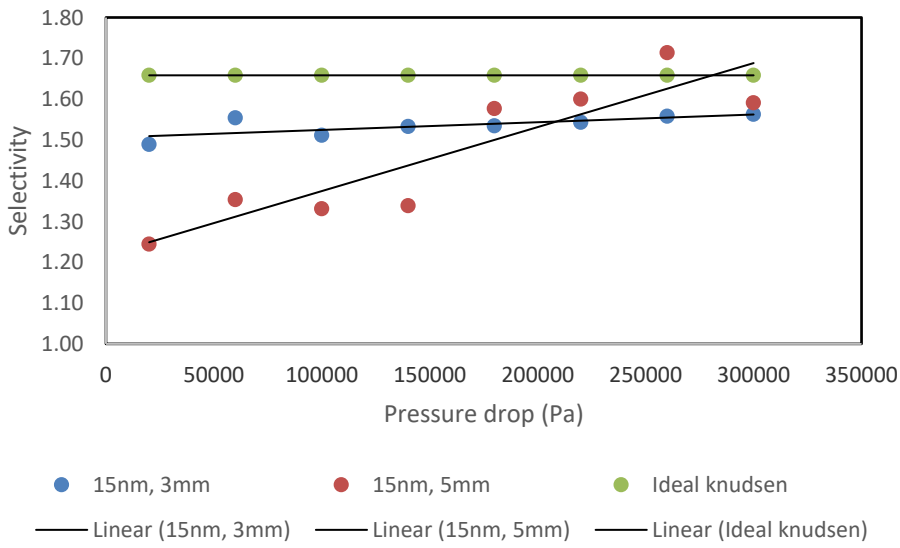

Figure 39 Comparison of selectivity performance of 15nm membranes

4.1.7 Mathematical description of flow through membranes

The experimental analysis of gas flow through the membranes studied have shown that viscous and Knudsen flow characteristics are prevalent. A mathematical description of permeation is detailed in this section. Due to the parallel flow transport mechanism observed, Darcy's law cannot be used to explain the flow behaviour of these gases. However, we will consider Darcy's law in the acceptable region (0 - 0.6 bar) as shown in **Figure *42*** and use this to estimate the mass flow in the low pressure drop range.

A two-parameter model is described to account for the effect of viscous and Knudsen flow characteristics on gas permeation rates. The model may be used as a guide to explain gas behaviour through mesoporous and microporous membranes. The mathematical model is compared with experimental results for gas transport though membrane. From the analysis, a relationship between the viscous and Knudsen flow contribution is obtained to describe how their contribution affects the results for the different pore size membranes.

4.1.7.1 TWO-PARAMETER MODEL (TPM)

The net gas transport through a membrane is a cumulative of the transport mechanisms (Van de Water and Maschmeyer 2004). Given that the membrane support pore sizes were in the mesoporous and macroporous range, the contribution of surface diffusion, capillary condensation and molecular sieving mechanisms to the net gas transport are negligible (Domenico De Meis 2017). Moreover, having shown from the gas permeation experiments that the gas flow is operating within viscous and Knudsen regime, the parallel transport equation for permeability may be written as:

$$P_T = P_{Knudsen} + P_{viscous} \tag{4.1}$$

$$P_{Knudsen} = \left[\left(\frac{4}{3}\right)\left(\frac{\sqrt{2}}{\sqrt{\pi}}\right)\left(\frac{\emptyset}{\tau}\right)\left(\frac{1}{\sqrt{RTM_a}}\right)\right] r_p \tag{4.2}$$

$$P_{viscous} = \left[\left(\frac{\emptyset}{\tau}\right)\left(\frac{P}{8\mu T}\right)\right] r_p^2 \tag{4.3}$$

by substitution,

$$P_T = \left[\left(\frac{\emptyset}{\tau}\right)\left(\frac{P}{8\mu T}\right){r_p}^2\right] + \left[\left(\frac{4}{3}\right)\left(\frac{\sqrt{2}}{\sqrt{\pi}}\right)\left(\frac{\emptyset}{\tau}\right)\left(\frac{1}{\sqrt{RTM_a}}\right)r_p\right] \quad (4.4)$$

and, with the gas permeabilities, we can evaluate the membrane selectivity by

$$\alpha_{A/B} = \frac{P_{t,A}}{P_{t,B}} \quad (4.5)$$

Ideal selectivity is obtained using the equations:

(i) for Knudsen flow:

$$\frac{P_{t,A}}{P_{t,B}} = \sqrt{\frac{M_B}{M_A}} \quad (4.6)$$

(ii) for Viscous flow:

$$\frac{P_{t,A}}{P_{t,B}} = \frac{\mu_B}{\mu_A} \quad (4.7)$$

The total permeability due to acting flow mechanisms within these membranes is written as equation (4.9) below

$$P_T = \left[\left(\frac{\emptyset}{\tau}\right)\left(\frac{P}{8\mu T}\right){r_p}^2\right] + \left[\left(\frac{4}{3}\right)\left(\frac{\sqrt{2}}{\sqrt{\pi}}\right)\left(\frac{\emptyset}{\tau}\right)\left(\frac{1}{\sqrt{RTM_a}}\right)r_p\right] \quad (4.8)$$

where,

P_T	total permeability, molmm^{-2}s^{-1}Pa^{-1}
$\emptyset$	porosity of the membrane, %
τ	tortuosity
M_a	molecular mass, g/gmol
R	gas constant, J mol^{-1} K^{-1}
T	absolute temperature, K
P	transmembrane pressure, Pa
μ	gas viscosity P_as
r_p	pore radius, m

Membrane porosity was obtained from experimental analysis in conjunction with particulate density equation written in equation (4.10) while tortuosity was obtained using equation (4.11) and checked with data from previous studies on image analysis and numerical simulations with values stated in **Table *5*** (Tanko 2018).

$$Porosity = 1 - \frac{Bulk\ Density}{Particle\ Density} \tag{4.9}$$

$$\tau = -3.3421(\text{ø}) + 3.9013 \tag{4.10}$$

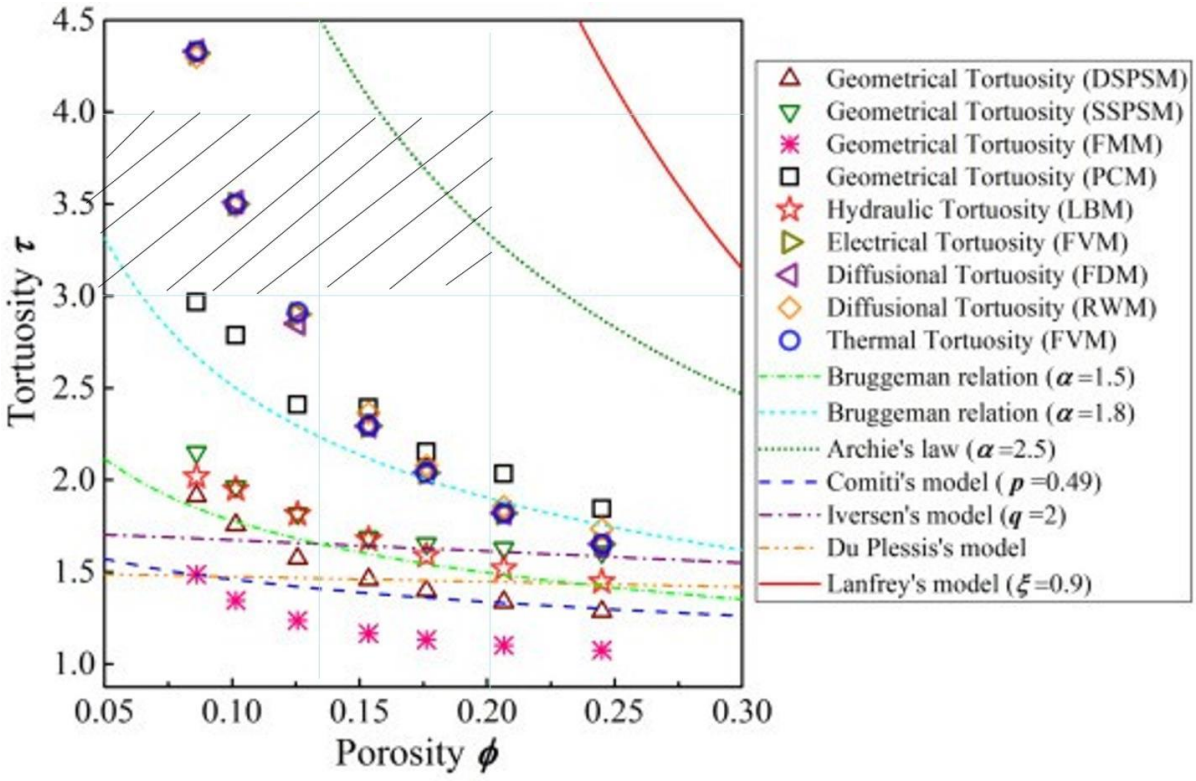

Figure 40 Tortuosity results from image analysis methods and simulations (Fu, Thomas and Li 2021)

The tortuosity values range from 3.23 to 3.77 and is shown on the porosity/tortuosity data plot derived from image analysis and physical simulation of porous media. The values obtained lie in the shaded region of **Figure *40***. The figure displays the tortuosity results calculated from different

image analysis methods, physical simulations, and porosity-tortuosity models for the set of Fontainebleau sandstone samples. It was noted that our values fall in the diffusional tortuosity (FDM, RWM) and thermal tortuosity (FVM) categories.

Table 5 Estimated porosity and tortuosity for each membrane

Membrane pore size (nm)	**Porosity (ø)**	**Tortuosity (τ)**	**$ø/\tau$**
15	0.13	3.47	0.0375
200	0.20	3.23	0.0619
6000	0.04	3.77	0.0106

From the data obtained and using equation (4.9), gas permeabilities were calculated for each gas at 20°C and 100°C with the results are presented in **Table *6*** below.

Table 6 Calculated permeabilities for each membrane at 20 and 100 degrees Celsius

Membrane Pore Size (nm)	**Temperature (°C)**	**P_t CH_4 (calculated) ($molmm^{-2}s^{-1}Pa^{-1}$)**	**P_t CO_2 (calculated) ($molmm^{-2}s^{-1}Pa^{-1}$)**
15	20	4.46E-12	3.12E-12
	100	3.23E-12	2.19E-12
200	20	8.39E-10	6.23E-10
	100	1.82E-09	1.32E-09
6000	20	1.34E-10	1.00E-10
	100	8.57E-10	6.25E-10

With the knowledge of the relationship between permeability and permeance and knowing the thickness of each support as confirmed by scanning electron microscopy, we can now show the correlation of our experimental permeation studies with the calculated values of permeance on **Table *7***.

Table 7 Experimental and calculated permeance for each membrane

Membrane Pore Size (nm)	Membrane Thickness (m)	Temperature (°C)	Ft CH4 (calculated) (molmm-2s-1Pa-1)	Ft CH4 (measured) (molm-2s-1Pa-1)	Ft CO2 (calculated) (molmm-2s-1Pa-1)	Ft CO2 (measured) (molm-2s-1Pa-1)
15	10-6	20	4.46E-06	3.42E-06	3.12E-06	2.21E-06
		100	3.23E-06	3.44E-06	2.19E-06	2.20E-06
200	10-3	20	8.39E-07	3.04E-06	6.23E-07	2.02E-06
		100	1.82E-06	3.04E-06	1.32E-06	2.04E-06
6000	10-3	20	1.34E-07	1.35E-06	1.00E-07	8.73E-07
		100	8.57E-07	1.36E-06	6.25E-07	8.73E-07

From this analysis, it is observed that the experimental gas permeance in 15 nm pore membrane are in good agreement with the measured gas permeance for both temperatures and gases. However, with an increase in the pore size, there is a deviation between the experimental gas permeance and theoretical gas permeance. The experimental gas permeance through the nanopores is generally higher than that predicted by the total permeance equation by one or two order of magnitude, as the equation underestimates gas flux in the nanoscale pores. Therefore, the transition flow characteristics should be considered when the diameter of the pores ranges from mesoporous to macroporous and flow resistance in the nanopores need be analysed to explain the phenomenon. Nonetheless, the results demonstrate that the parallel transport model is accurate in predicting the experimental results in the range of the explored working conditions, especially within the lower pores size range.

Perm-selectivities were calculated as a ratio of the permeances and shown in **Table *8***. The obtained selectivities are compared with the ratio of the square root of the inverse of the molecular weights (Knudsen selectivity) and the ratio of the viscosities (viscous selectivity). It is observed that the calculated perm-selectivities lie between the ideal Knudsen and viscous flow values.

Table 8 Comparison of calculated permselectivity, ideal Knudsen, and ideal viscous selectivity

Membrane Pore Size (nm)	Temperature (°C)	Calculated Permselectivity (CH_4/CO_2)	√MWCO2/ √MWCH4 Ideal Knudsen selectivity	$\mu CO_2/\mu CH_4$ Ideal Viscous Flow selectivity
15	20	1.43	1.66	1.34
	100	1.52	1.66	1.37
200	20	1.35	1.66	1.34
	100	1.38	1.66	1.37
6000	20	1.34	1.66	1.34
	100	1.37	1.66	1.37

4.1.7.2 DARCY FLOW MODEL

Darcy flow means that the flow of a fluid traveling through a porous medium is directly proportional to the pressure gradient, ΔP/ δ, that is, a difference in pressure ΔP over some finite distance (δ), and inversely proportional to the viscosity of the fluid or gas, μ. In Darcy flow the proportionality constant, k, is called the permeability, and is used to characterize the porous medium. The Darcy formula for linear displacement is given by equation (4.12).

$$Q = \frac{q}{A} = \frac{-k\Delta P}{\mu\delta} \tag{4.11}$$

where,

Q fluid volumetric flowrate, $m^3 s^{-1}$

q fluid volume flux, $m^3 m^{-2} s^{-1}$

A cross-sectional area of the porous medium perpendicular to the flow, m^2

k absolute permeability, m^2

ΔP pressure difference, Pa

μ fluid viscosity, Pa s

δ finite distance, m

To describe how each membrane flux varies with pressure change, experimental results were illustrated in **Figure *41***. The results show that for each gas, temperature range, and membrane studied, there are three sections of the plot. In the first section there is a linear variation of flux with trans-membrane pressure (TMP) that passes through the origin (0<TMP<60000 Pa). The gas diffusion transport characteristics resembles the typical flow in porous media postulated by Darcy showing the relationship between flux and pressure drop along the membrane and can offer design recommendations for an industrial scale gas plant. This is followed by a transition region where there is a bend (60000<TMP<100000) and then the third region where linearity does not pass through the origin (TMP>100000) and flow becomes inertial due to the momentum of the fluid as a result of increasing gas velocities. In the first region where the flux increases linearly with TMP passing through the origin, the variations of flux versus applied pressure shows a linear increase in fluxes at low pressures passing through the origin (60000 Pa). However, when the operating pressure is beyond this, there is the beginning of a deviation and the relationship is no longer linear, which suggests that the flow regime is transitioning. As more pressure is applied the relationship is transferred from the Darcy regime to the inertial flow regime where Darcy's law is no longer valid anymore (Pant, Mitra and Secanell 2012).

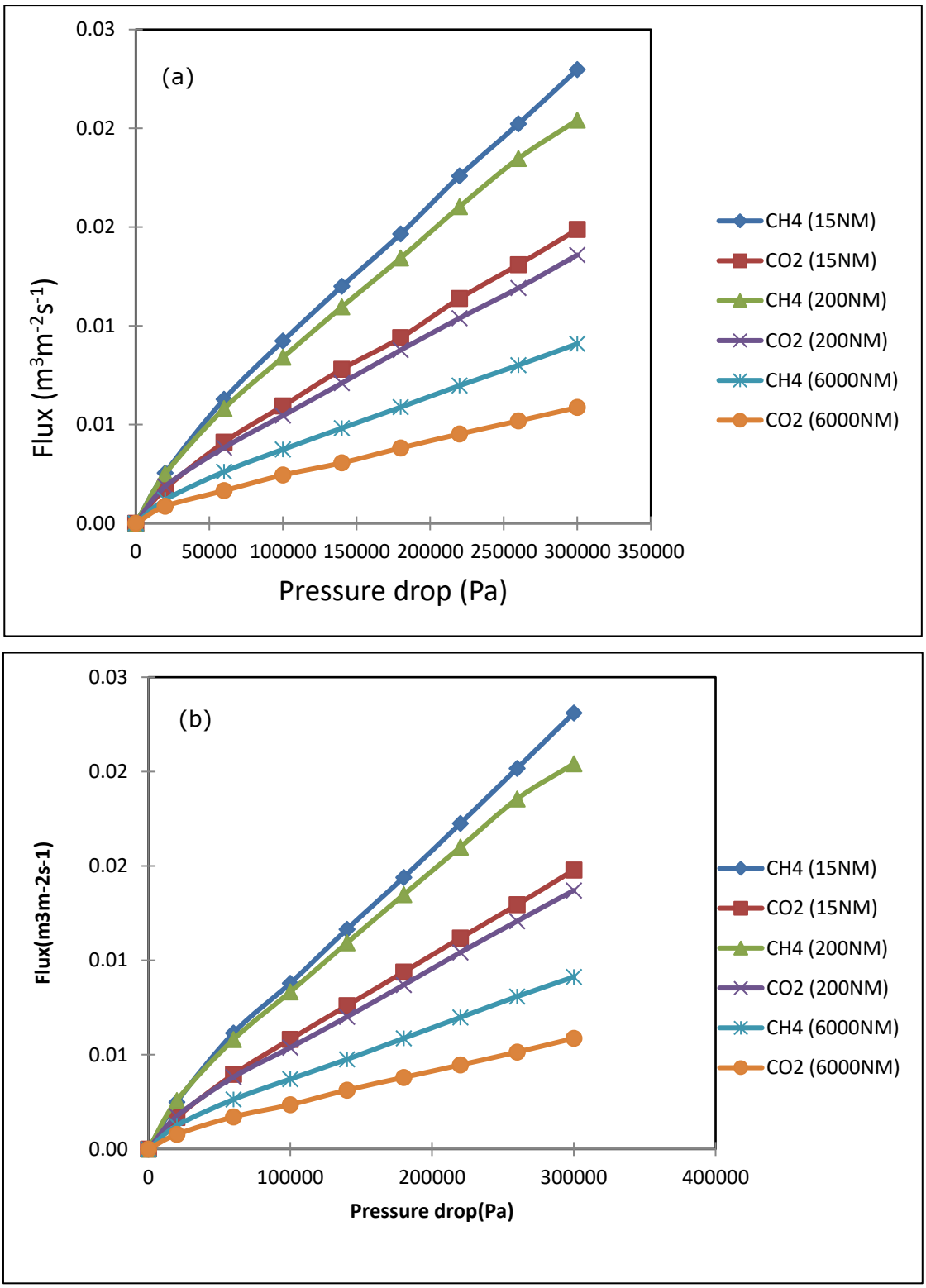

Figure 41 Variation of methane and carbon dioxide flux as a function of applied trans-membrane pressure at (a)20°C and (b) 100 °C

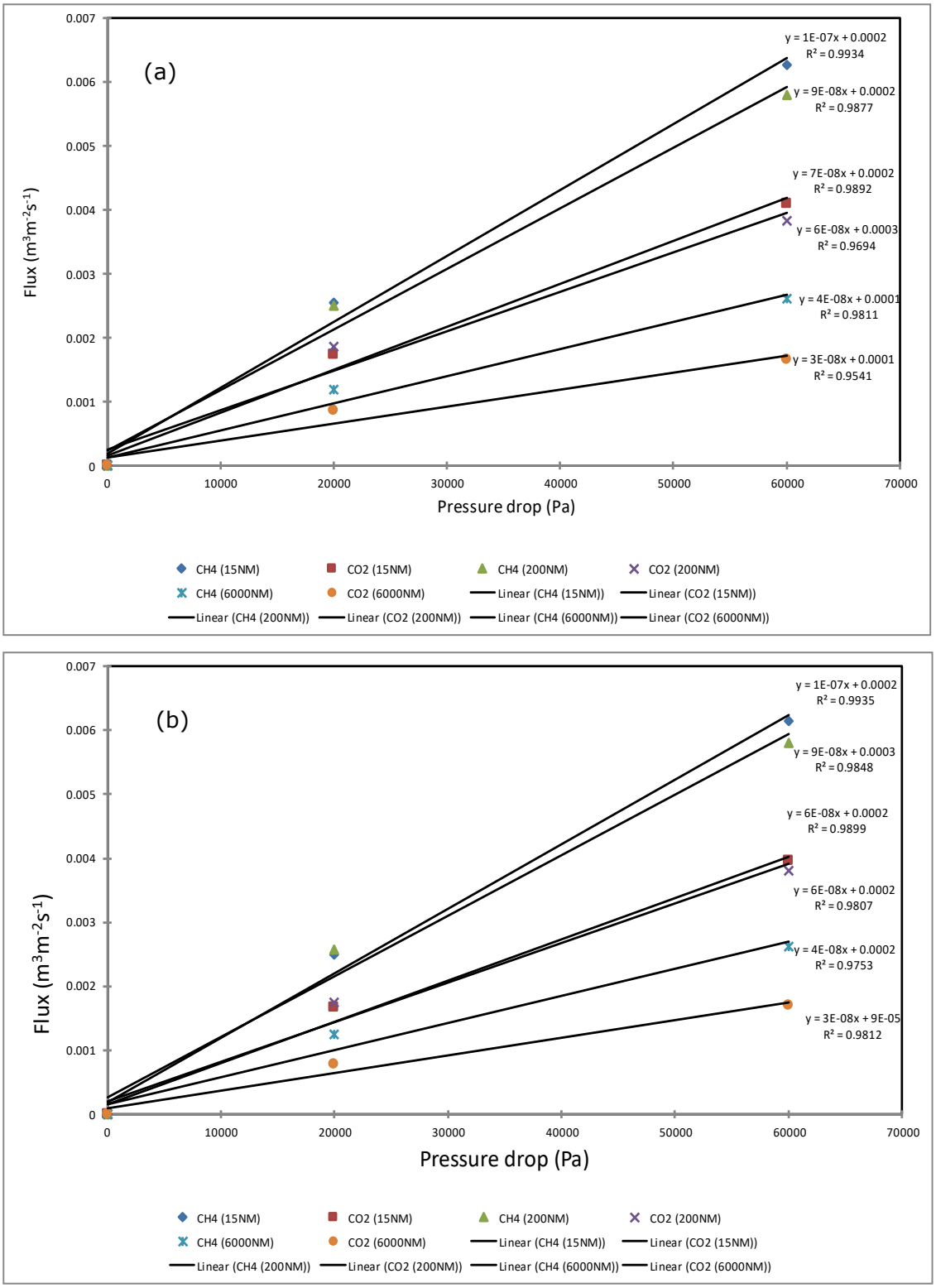

Figure 42 Flux as a function of trans-membrane pressure below 6000Pa at (a) 20°C and (b) 100°C

The variation of CO_2 and CH_4 fluxes as a function of applied transmembrane pressure for the Darcy flow regime, between a TMP of 0 to 60000 Pa and temperatures of 20 and 100 degrees Celsius, is shown in **Figure *42***. From the data evaluation, Darcy permeability was calculated for each gas with linear flow as shown in the tables below.

Table 9 Calculation of Darcy permeability for carbon dioxide gas

Membrane pore size (nm)	**Temperature (°C)**	**Thickness (m)**	**Slope= $\frac{k}{\mu\delta}$ (m/Pa-s)**	**Darcy Permeability (k) = $slope \times \mu\delta$ (m^2)**
15	20	10^{-6}	7E-08	1.0E-18
	100	10^{-6}	6E-08	1.1E-18
200	20	10^{-3}	6E-08	8.8E-16
	100	10^{-3}	6E-08	1.1E-15
6000	20	10^{-3}	3E-08	4.4E-16
	100	10^{-3}	3E-08	5.6E-16

Table 10 Calculation of Darcy permeability for methane gas

Membrane pore size (nm)	**Temperature (°C)**	**Thickness, (m)**	**Slope=$\frac{k}{\mu\delta}$ (m/Pa-s)**	**Darcy Permeability (k) = $slope \times \mu\delta$ (m^2)**
15	20	10^{-6}	1E-07	1.1E-18
	100	10^{-6}	1E-07	1.4E-18
200	20	10^{-3}	9E-08	9.9E-16
	100	10^{-3}	9E-08	1.2E-15
6000	20	10^{-3}	4E-08	4.4E-16
	100	10^{-3}	4E-08	5.4E-16

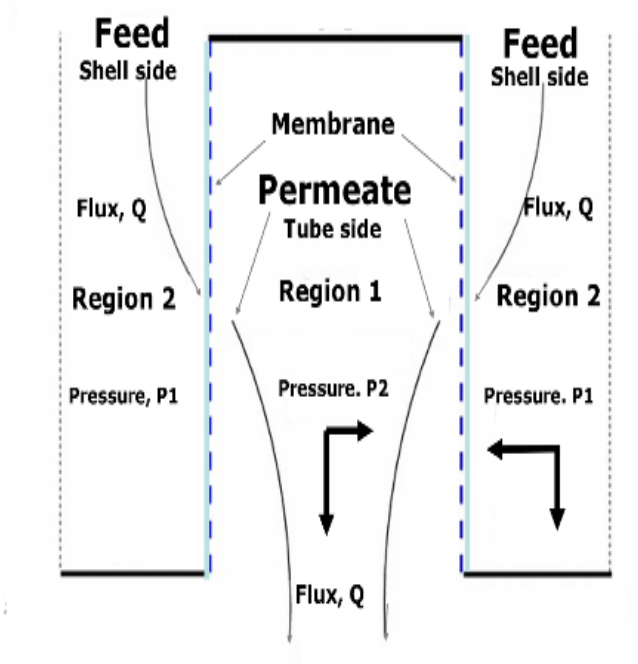

Figure 43 Schematic of the gas flow through membrane chamber

A schematic of the flow within a single direct-flow 2D channel is presented in **Figure *43*** with the shell (region 2) and tube (region 1) with solid lines indicating impermeable walls, blue dashed lines indicating permeable walls, and the dotted line indicating the stainless-steel outer shell. It consists of a tubular channel surrounded by a porous membrane. Fluid enters the shell side at a fixed flux, Q, which passes through the membrane side walls, and into the tube side permeate region. Flux through the membrane may also be in the radial direction, hence the Darcy equation is used to account for this from equation (4.13)

$$Q = \frac{q}{A} = \frac{k}{\mu}\frac{dP}{dr} \tag{4.12}$$

where,

μ gas viscosity, Pa s

k permeability of the membrane, m^2

In the case of the tubular membrane, the curved surface area is written as,

$$A = 2\pi rl \tag{4.13}$$

where,

l length of the membrane, m

r outer radius of the membrane, m

hence, equation (4.13) can be re-written as

$$\frac{q}{2\pi rl} = -\frac{k}{\mu}\frac{dP}{dr} \tag{4.14}$$

$$dP = \frac{q\mu}{2\pi kl}\frac{dr}{r} \tag{4.15}$$

integrating, we get that

$$\int_{P_w}^{p_e} \mathrm{dP} = \int_{r_w}^{r_e} \frac{q\mu}{2\pi kl}\frac{dr}{r} \tag{4.16}$$

$$P_e - P_w = \frac{q\mu}{2\pi kl} ln\frac{r_e}{r_w} \tag{4.17}$$

$$q = \frac{2\pi kl(P_e - P_w)}{\mu ln {}^{r_e}/_{r_w}} \tag{4.18}$$

Table 11 Calculation of Darcy permeability for carbon dioxide using radial flow

Membrane pore size (nm)	**Temperature, (°C)**	**ln[r_e/r_w] (m)**	**Slope = $\frac{2\pi kl}{\mu ln {}^{r_e}/_{r_w}}$ (m^3/Pa-s)**	**Darcy Permeability (k) = $\frac{slope \times \mu ln {}^{r_e}/_{r_w}}{2\pi l}$ (m^2)**
15	20	0.3531	7E-08	1.7E-13
	100	0.3531	6E-08	1.9E-13
200	20	0.3180	6E-08	1.4E-13
	100	0.3180	6E-08	1.7E-13
6000	20	0.2224	3E-08	4.9E-14
	100	0.2224	3E-08	6.1E-14

Table 12 Calculation of Darcy permeability for methane using radial flow

Membrane pore size (nm)	**Temperature, (°C)**	**ln[r_e/r_w] (m)**	**Slope = $\frac{2\pi kl}{\mu ln^{r_e}/_{r_w}}$ (m^3/Pa-s)**	**Darcy Permeability (k)= $\frac{slope \times \mu ln^{r_e}/_{r_w}}{2\pi l}$ (m^2)**
15	20	0.3531	1E-07	1.8E-13
	100	0.3531	1E-07	2.2E-13
200	20	0.3180	9E-08	1.5E-13
	100	0.3180	9E-08	1.9E-13
6000	20	0.2224	4E-08	4.9E-14
	100	0.2224	4E-08	6.0E-14

4.1.7.3 EVALUATION OF MASS TRANSFER CHARACTERISTICS

A mathematical approach to demonstrating how the flow of gases respond to pressure profile changes in the low TPMD region is shown for the membrane system with the experimental operating conditions. **Figure *44*** shows a description of external mass transfer rates in a membrane system. The impact of changes on the permeation rate were evaluated by calculating the gas mass transfer flux J_I, to the membrane surface as described in the figure below (Nagy 2019).

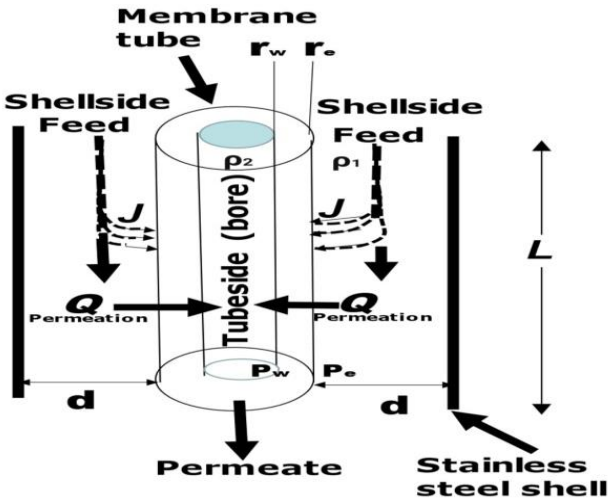

Figure 44 A visual description of mass transfer rates through membranes

From Fick's law, the amount of mass transferred is proportional to the mass transfer coefficient and concentration difference. Hence,

$$J_i = k(\rho_1 - \rho_2) \tag{4.19}$$

where,

k is the mass transfer coefficient

and

k = f (S_h,D_{ei})

$$J_i = (\rho_1 - \rho_2) S_h \, {}^{D_{ei}}/_{d} \tag{4.20}$$

where,

ρ_1	molar gas density on the shell side, gmol/cm^3
ρ_2	molar gas density on the tube side, gmol/cm^3
D_e	diffusivity of gas in the shell-side, cm^2/s
d	the annular diameter, cm
S_h	Sherwood number

$$S_h = 1.86\ (R_e)^{0.33} (S_c)^{0.33} \tag{4.21}$$

where,

R_e	Reynolds number
S_c	Schmidt number

The Schmidt number is obtained from

$$S_c = \frac{\mu}{\rho D_e} \tag{4.22}$$

where,

μ	viscosity of gas, Pa s
ρ	density of the gas, Kg/m^3

The Reynolds number is obtained from

$$R_e = \frac{\rho V D}{\mu} \tag{4.23}$$

And,

$$V = \frac{R_e \mu}{\rho D} \tag{4.24}$$

where,

V	superficial fluid velocity, m/s
ρ	fluid density, kg/m^3
D	characteristic distance, m
μ	dynamic viscosity, Pa s

S_h = f (R_e, S_c)

Reynold's number is a dimensionless number comprised of the physical characteristics of the flow given by the ratio of inertial forces to viscous forces and is used for predicting if a flow condition will be laminar or turbulent. Schmidt's number is another dimensionless number given by the ratio of viscous diffusion rate to molecular mass diffusion rate. From the analysis of experimental data and adherence to Darcy Law as shown in the high correlation coefficients observed in **Figure *42***, it can be deduced that the flow is laminar with Reynolds number is less than 2000. Hence, to calculate the fluid velocity, v, Reynolds number values of 1, 1000 and 2000 were used as shown in the tables below. All calculated data have been summarised in **Tables 13-16 and Appendix A5-A8**.

Table 13 Superficial velocities of methane gas at 20 degrees Celsius

CH_4 at 20°C	**Reynolds Number, R_e**	**Gas Velocity, *V* (m/s)**
15nm	1	3.49E-09
	1000	3.49E-06
	2000	6.97E-06
200nm	1	3.67E-09
	1000	3.67E-06
	2000	7.35E-06
6000nm	1	1.12E-09
	1000	1.12E-06
	2000	2.25E-06

Table 14 Superficial velocities of methane gas at 100 degrees Celsius

CH_4 at 100°C	**Reynolds Number, R_e**	**Gas Velocity, *V* (m/s)**
15nm	1	5.45E09
	1000	5.45E-06
	2000	1.09E-05
200nm	1	5.74E-09
	1000	5.74E-06
	2000	1.15E-05
6000nm	1	1.75E-09
	1000	1.75E-06
	2000	3.51E-06

Table 15 Superficial velocities of carbon dioxide gas at 20 degrees Celsius

CO_2 at 20°C	**Reynolds Number, R_e**	**Gas Velocity, *V* (m/s)**
15nm	1	1.69E-09
	1000	1.69E-06
	2000	3.39E-06
200nm	1	1.79E-09
	1000	1.79E-06
	2000	3.57E-06
6000nm	1	5.46E-10
	1000	5.46E-07
	2000	1.09E-06

Table 16 Superficial velocities of carbon dioxide gas at 100 degrees Celsius

CO_2 at 100°C	**Reynolds Number, R_e**	**Gas Velocity, *V* (m/s)**
15nm	1	2.72E-09
	1000	2.72E-06
	2000	5.43E-06
200nm	1	2.86E-09
	1000	2.86E-09
	2000	5.72E-06
6000nm	1	8.74E-10
	1000	8.74E-07
	2000	1.75E-06

The gas mass transfer flux from the bulk gas in the shell-side to the membrane outer surface, J, was estimated. The range for J was calculated from Reynolds numbers between 1-2000. However, it is unlikely that a *R*e value as low as 1 would be of any significant practical application in membrane separation and therefore *R*e values closer to 2000 are more realistic. As shown in Appendix A9 – A12, *J* values obtained for *R*e = 2000 were found to be always greater than the permeation flux, *Q,* and therefore, the gas stream velocity changes the rates of transfer of gas to the membrane surface are sufficient to sustain its permeation through the membrane for the two transmembrane pressure drops and temperatures studied. Furthermore, the analysis reveals that, under the same pressure drop across the membrane, the mass/volume flux in porous membrane can be over four orders of magnitude higher than in a dense membrane reported by Merkel et al in their study (Merkel et al. 2000).

This method has demonstrated a simple but effective way to estimate mass transfer from bulk gas to the membrane surface and compared that with permeation rate by integrating porous membranes with different porosities and pore sizes. The study has also compared the performance of our porous systems with that of a classical dense membrane composed of a transparent polymer and our porous systems have shown that the dense system is limited by the low permeability. In all situations of temperature and pressure drops investigated in this study, the mass transfer rate from the bulk gas stream to the membrane surface was significantly greater than the permeation rate which confirms that mass transfer conditions are not limiting.

4.2 EVALUATION OF GAS TRANSPORT THROUGH A MODIFIED SILICA MEMBRANE

4.2.1 Introduction

This section contains a description of the design, fabrication, and characterization of the coating applied on the membrane support surface to eliminate defects and achieve an ideal separation mechanism for improved performance. This method would achieve a composite membrane that offers better separation properties than the conventional membranes previously used (Ji et al. 2010). The incorporation of this coating layer is suggested to improve the gas diffusion characteristics through the membrane via selective permeation of one gas component. The ideal technique should minimize the coating thickness on the membrane surface to limit resistance to permeation and improve the selectivity performance (Xomeritakis et al. 2003).

The objective is to prepare an organic/inorganic composite membrane that combines the advantages of polymeric (silicon) and inorganic (ceramic) membranes. This would be achieved by effectively combining the high permeability of inorganic (ceramic) membranes and a thin polymer layer with good separation properties that work together to enhance the membranes' selectivity for the target gas. The ceramic support will provide a good mechanical support for the top layer. The 200nm membrane was selected for further analysis based on results from the initial gas permeation studies with its high porosity that offers more gas permeation channels and limits gas diffusion resistance.

Silicon membranes are some of the best performing ceramic membranes for CH_4/CO_2 gas separation and have been studied over time in many fluid forms (such as tetraethoxysilane and 1,2-Bis(triethoxysilyl)ethane) to achieve good permeability and selectivity (Richard et al. 2001). However, it was identified that tetraethoxysilane (TEOS) membranes are hydrothermally unstable due to the reactivity of silanol groups in the matrix. 1,2-Bis(triethoxysilyl)ethane (BTESE) were studied to overcome this limitation as it is a hydrothermally stable organosilica material with organic-inorganic structure, however, low selectivity were discovered as a result of their relatively open network compared to TEOS (ten Hove et al. 2017).

There has been little research into elastomeric materials for gas separation, even though studies show that rubbery polymers have very high gas fluxes compared with glassy polymers (Duval et al. 1994). Polydimethylsiloxane (PDMS) is a part of the siloxane family comprising silicon, oxygen, and alkane. It is the most permeable mineral-organic polymer that contains primarily carbon and silicon (Merkel et al. 2000). Silicon elastomer was chosen as coating material because of its properties being an amorphous, non-crystallizing thermally stable agent with high tensile strength and suitable adhesion. It has a very low glass transition temperature (-129^{o}C) compared to other polymers which indicates a very flexible polymer backbone with long-range segmental motion that provides strong mechanical characteristics. Furthermore, it is economical, easily accessible, environmentally friendly, and its high crosslink density reduces the swelling capacity which in turn reduces the effect of plasticisation (Sadrzadeh et al. 2009, 2009; Shamsabadi, Kargari and Babaheidari 2014). Plasticisation is an increase in the penetrant diffusivity caused by greater polymer local segmental motions from the presence of penetrant molecules at high pressure and temperature in the polymer matrix (Sadrzadeh et al. 2009).

This modification was done using dip coating technique which is a simple, low-cost, reliable and reproducible method that allows for controlled mono- or multi-layer deposition to form a coating layer of desired thickness by simply varying parameters such as the viscosity of the solution and dipping time (Pakizeh, Omidkhah and Zarringhalam 2007a; Karakiliç et al. 2017). The thickness and other surface parameters were monitored as these characteristics influence the rate of permeability (Tosti et al. 2006; Santucci et al. 2013). The dip coating technique has many advantages including delivering high surface area, high pore volume and covering very large defects. The method is controlled to avoid non-uniform deposition which limit other deposition techniques found in literature such as electroless plating and chemical vapour deposition (CVD) that cause inhibited permeability, selectivity or mechanical stability (Leenaars, Keizer and Burggraaf 1984; Cho, Han and Lee 1995; Santucci et al. 2013; Maneerung, Hidajat and Kawi 2014; Shamsabadi, Kargari and Babaheidari 2014).

4.2.2 Scanning Electron Microscopy (SEM) and Energy Dispersive X-ray Analysis (EDXA)

SEM analysis was carried out to observe any changes in the microstructure and surface morphology due to the coating. The membrane was also characterised with EDXA to identify changes in the elemental composition of the membrane after dipping. The analysis was carried out in a similar manner to what has been previously described and the SEM results of the coated membrane shows good adhesion and a homogeneous film layer free of defects as in **Figure *45***. EDXA analysis as depicted in **Figure *46*** proves that the silica particles penetrated the pores and successful deposition is established.

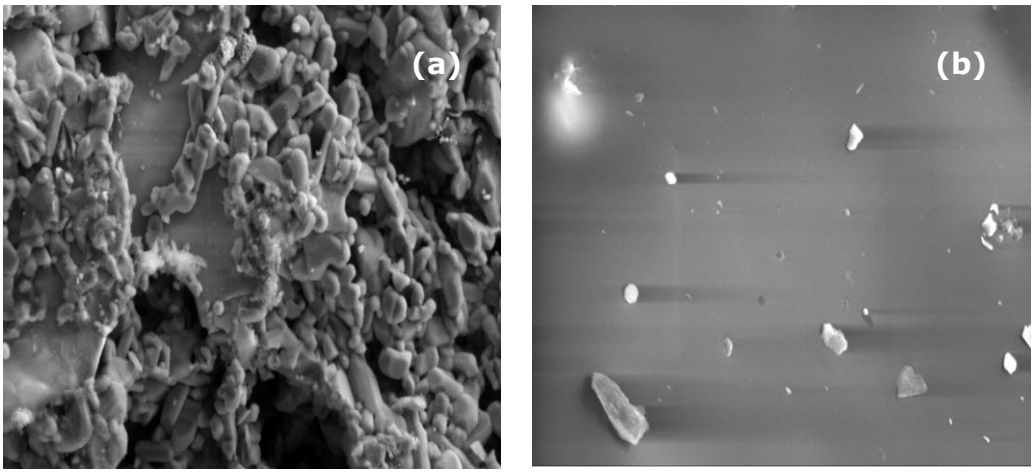

Figure 45 Outer surface SEM micrograph of (a) support (b) coated membrane

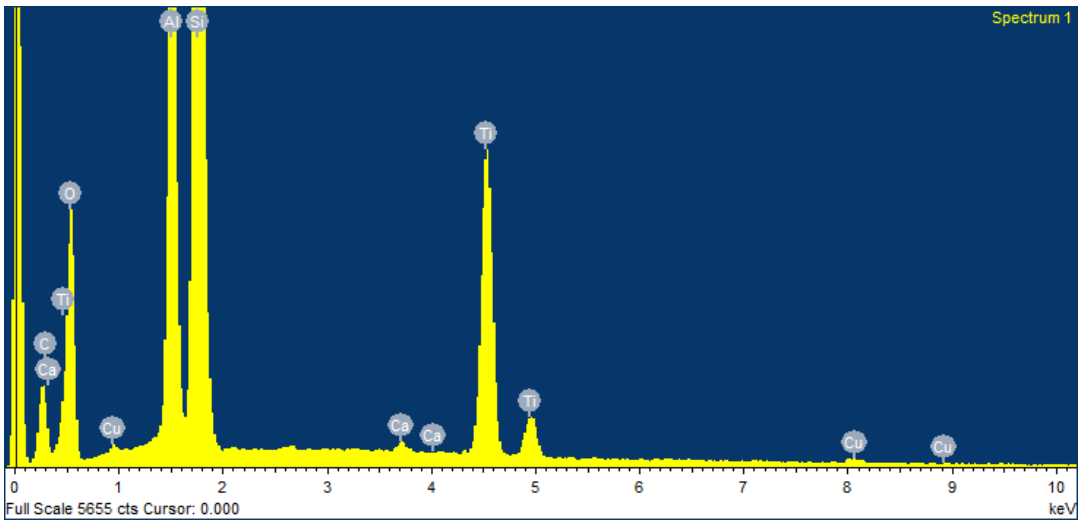

Figure 46 EDXA for silica coated membrane

4.2.3 Fourier Transform Infrared Spectronomy (FTIR) Analysis

The functional groups, intermolecular interactions and modification extent of the membrane are determined using an attenuated total reflection (ATR) Nicolet i S 10 FT-IR spectrometer in the range 400-4000cm^{-1} to show the different bonds present in a compound. By coating the membrane support, an alkyl group (C-H) has been introduced to the spectrum (peak intensity at 2962.5 cm^{-1}) which originally only had a Amine (N-H) group, this shows the incorporation of an organic polymer such as polydimethylsiloxane (PDMS) and confirms the successful production of an organic/inorganic composite membrane. The spectra for the support before coating is shown in **Figure *47*** whilst the coated sample spectrum shows the introduction of a Si-CH_3 band in **Figure *48***.

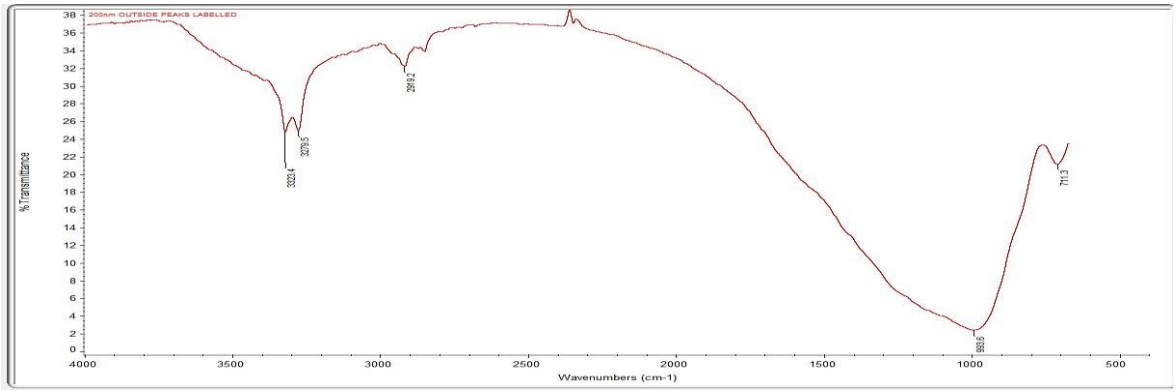

Figure 47 FTIR spectra for 200nm membrane support

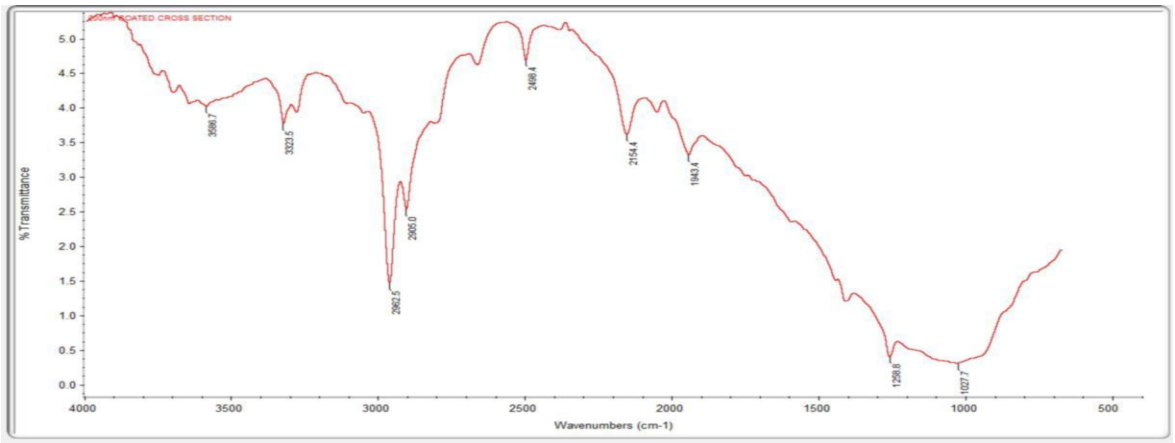

Figure 48 FTIR spectra of 200nm silica coated membrane

4.2.4 Droplet Permeation Measurements

Droplet permeation measurements were observed for the support and coated membrane under the same conditions of approximately 5µl of droplet at 51 frame per second (FPS) using distilled water. The coated membrane had a higher mean contact angle with higher permeation time confirming the deposition of hydrophobic silica layer on the support material as shown in **Figure *49*** and **Figure *50***. It was observed that by coating the support membrane, the droplet permeation time was much greater with nearly complete permeation at 0.5s for the support compared to the silica membrane with very high resistance to permeation and incomplete permeation of the droplet even after 120 seconds.

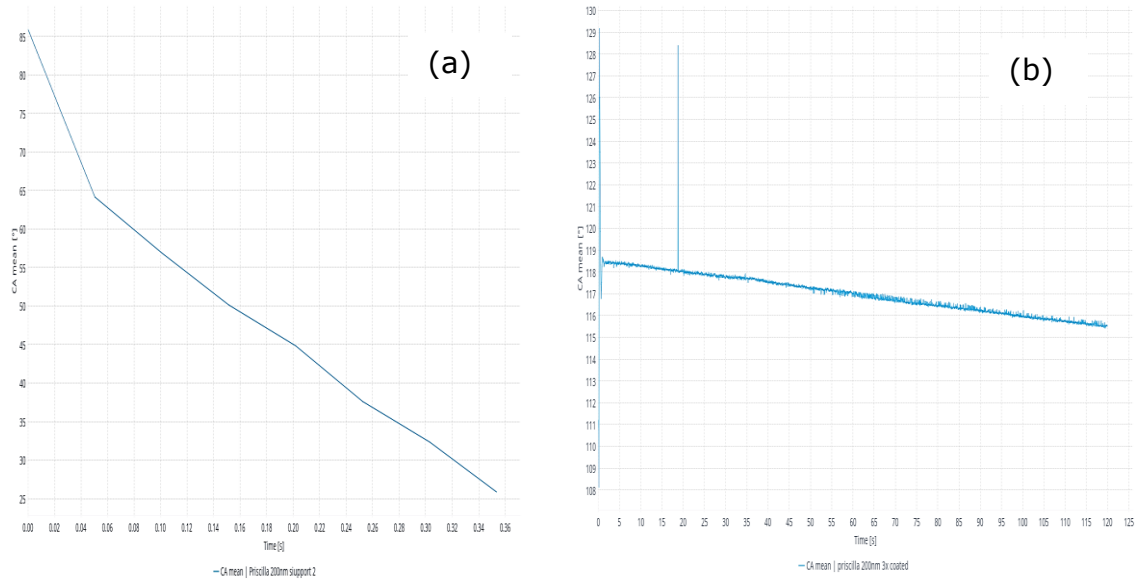

Figure *49* *Mean contact angle plot for (a) support and (b) coated membrane*

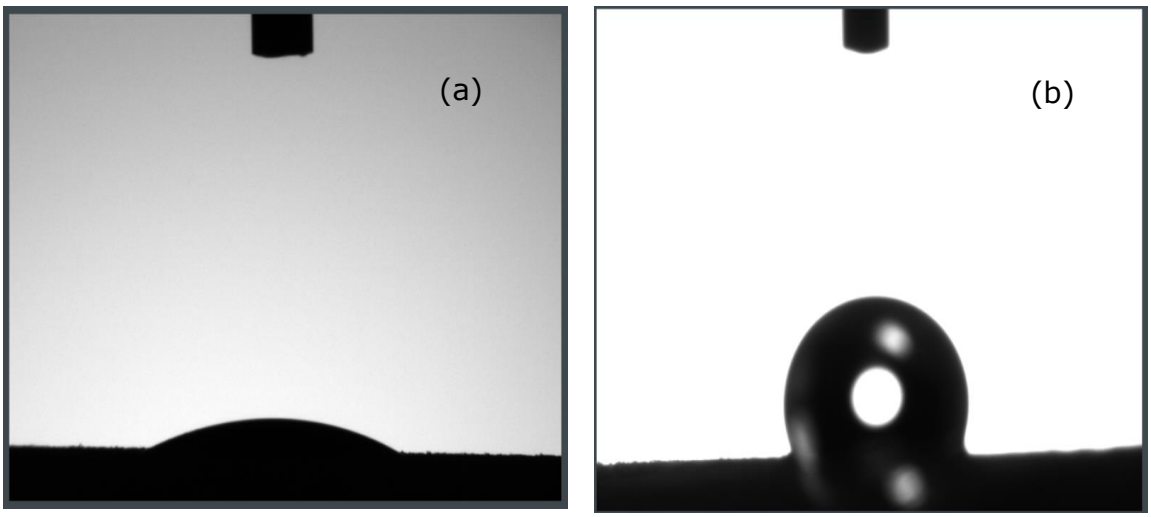

Figure *50* *Droplet image at 0.5s for the (a) support and (b) coated membrane*

4.2.5 Gas Permeation Test

The membrane unit was set up again to investigate the flow of gases and membrane performance for the coated membrane. Gas permeation measurements were taken and analysed for single and binary gas mixtures to test the membrane effectiveness and behaviour of gases.

4.2.5.1 Single gas permeation

Figure *51* shows the effect of pressure on single gas permeation for the support and silica membranes at 20 degrees Celsius. The reduction in permeation rates confirms a change in pore size as a result of the silica coating. Nonetheless, through both membranes, methane gas remains more permeable through the pores compared to carbon dioxide gas for the operating conditions studied. This mechanism of flow is characteristic of the Knudsen regime where gas molecules flow through the pores at a rate proportional to the inverse of their molecular weight.

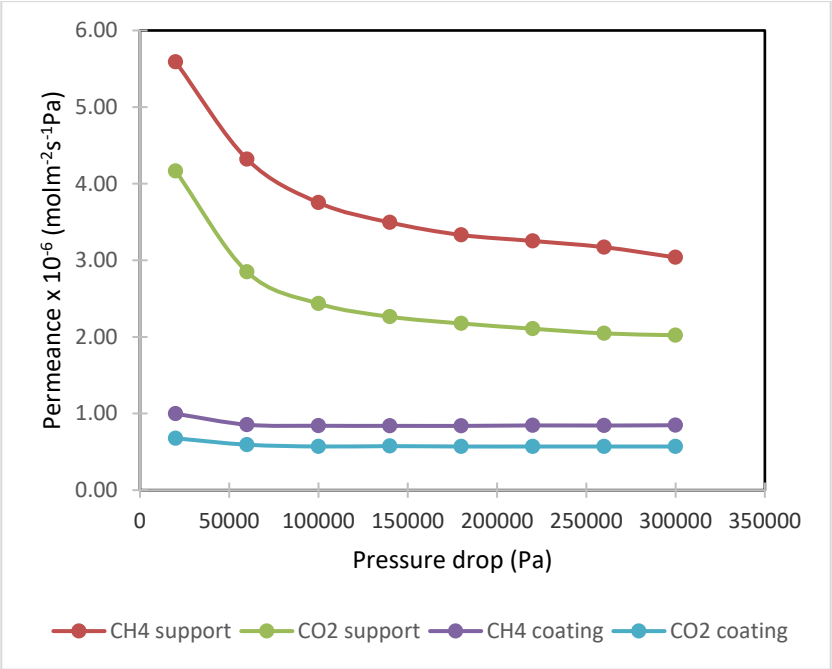

Figure 51 Effect of pressure drop on permeance for support and coated membrane

In the previous chapter (section 4.1.7.1), it was confirmed that gases flowed through the support membrane with a combination of viscous flow and Knudsen flow contributions. However, due to the reduction in pore size by the silica coating, it is expected that the contribution of viscous flow through the membrane will diminish. This is because the coating would successfully reduce the pore size and conceal any defects present in the membrane. Viscous flow is a function of pressure and the squared of the pore radius (from equation 2.19) and a reduction in pore radius will invariably reduce the permeation due to viscous flow. From the experimental data, it was observed that there is a dependence of permeation on pressure for the support compared to the coated membrane which has a relatively constant permeation rate irrespective of changes in pressure. This confirms that the reduction in pore size reduced the viscous flow contribution making Knudsen the dominant flow mechanism through the coated membrane.

Furthermore, it was observed that there is a difference between the temperature effect on permeation rate for the support and coated membrane. The coated membrane shows a noticeable reduction in permeation rate with increasing temperature which is typical of gas behaviour in the Knudsen regime. This effect was dampened from gas characterisation results for the membrane

support because of the lower contribution of Knudsen flow. In addition, there was an improvement in the methane selectivity of the coated membrane obtained at 100 degrees (1.62) towards the ideal Knudsen selectivity compared to the support selectivity (1.47).

Table 17 Permeation results for support and coated membrane

	Permeance (x10^{-6})			
	Support Membrane		**Coated Membrane**	
	CH_4	CO_2	CH_4	CO_2
20 degrees	5.59	4.17	0.99	0.68
100 degrees	5.73	3.88	0.46	0.28

Further analysis was done to estimate the pore size of the coating layer where Knudsen flow is dominating. The influence of the coating on the gas permeation rates was studied using a series model. It was assumed that overall resistance to permeation is a sum of the resistance due to the support and top layer. The reciprocal of the permeance is the resistance. Therefore, we can write equation (4.26).

$$\frac{1}{P_{total}} = \frac{1}{P_{top-layer}} + \frac{1}{P_{support}} \qquad (4.25)$$

where,

$\frac{1}{P_{total}}$ = resistance of the membrane

$\frac{1}{P_{top-layer}}$ = resistance of the coating/top layer

$\frac{1}{P_{support}}$ = resistance of the support

From the experimental data of the support and silica membrane permeation characteristics, the top layer permeation can be calculated.

Table 18 Summary of obtained permeance results

	Permeance x 10^{-6} (mol/m^2sPa)	Resistance x10^6 (m^2sPa/mol)
Total	0.99	1.00
Support	5.59	0.18
Top-layer	1.20	0.83

From the model equations (4.2) to (4.5) in the previous chapter (section 4.1.7.1), permeation through the support can be expressed as the sum of Knudsen and viscous flow contributions as in equation (4.27) below

$$P_{support} = \alpha_s + \beta_s \quad (4.26)$$

where,

knudsen contribution to flow, α_s	3.34x10^{-11}
viscous contribution to flow, β_s	8.06x10^{-10}

Then, the pressure at the interface of the support and silica layer was calculated from equation (4.28) (De Lange et al. 1995)

$$P_i = \frac{-\alpha_s + [\alpha_s^2 + \beta_s(\beta_s . P_1^2 + 2.\alpha_s . P_1 + 2.\frac{\emptyset}{S}]^{1/2}}{\beta_s} \quad (4.27)$$

where,

α_s	knudsen flow contribution to flow
β_s	viscous flow contribution to flow
P_1	permeate pressure, P_a
$\emptyset$	Molar flow rate, mol s^{-1}
S	permeation area, m^2

Hence, the pore radius of the top layer was obtained from (Islam and Khan 2013)

$$P_e = \frac{8 r_{p,top-layer}(\Delta P)}{3\delta\sqrt{2\pi MRT}} \quad (4.28)$$

from where,

$$r_{p,top-layer} = \frac{P_e . 3 . \delta . \sqrt{2\pi MRT}}{8\Delta P} \quad (4.29)$$

where,

δ	Membrane thickness, m
M	Gas molar mass, g mol^{-1}
R	Universal gas constant, J mol^{-1} K^{-1}
T	Temperature, K
ΔP	Pressure drop, P_a

Thus, the average pore radius was calculated. The calculated value was 18nm and thus a pore diameter of 36nm was obtained for the silica layer. In this pore size range, Knudsen diffusion is the dominating the flow mechanism which confirms the hypothesis of acting flow regime and its effect of gas behaviour and separation characteristics. This shows that the intrinsic gas properties make the gases flow distinctively through the membrane and separation may therefore be achieved because of the difference in their molecular weight and gas velocities. This is in good agreement with the calculated velocities of each gas from the mass transfer model in the previous section, with methane gas velocity having higher values than carbon dioxide.

4.2.5.2 Mixed gas permeation

Experimental results of mixed gases show a similar trend to the pure gases with a higher methane permeation through the silica membrane than carbon dioxide gas. A CO_2/CH_4 binary mixture was studied to imitate the selectivity of the membrane for biogas, it was observed that higher separation factors were obtained following Knudsen behaviour with selectivity ranging from 1.82 - 3.31 as shown in **Table *19***. CH_4 gas mixture 40% CO_2 is fed into the membrane system and exits the permeate with a concentration of 23.31% as seen in **Table *20***. This is 42% reduction in the CO_2 concentration.

Table 19 Permeance and selectivity values for CO2/CH4 mixture through the coated membrane

Feed	Permeance temperature (°C)	Permeance x 10^{-6} (mol m^{-2} s^{-1} Pa^{-1})		Selectivity
		CH_4	CO_2	CH_4/CO_2
40% CO_2	20	2.26	1.24	1.82
	100	2.73	0.83	3.31

These experiments have shown that separation by Knudsen mechanism can occur through silica membranes to obtain improved selectivity. It also confirmed that by adding amino groups to facilitate transport, enhanced membrane performance can be achieved (Habib et al. 2020).

Table 20 Gas analyser permeate log for 40%CO2/60%CH4

Gas temperature (°C)	88.7
Cell temperature (°C)	88.8
CO_2(%)	23.31

4.3 CARBON SEQUESTRATION APPLICATION

4.3.1 Introduction

This section explores membranes as a porous media to analyse the core properties for its application in carbon sequestration. Reservoir entities can be classified into geological, geometrical, and fluidic categories. To complicate matters, reservoirs are usually set in geological layers that possess some heterogeneity, such that each layer interacts differently with injected and resident fluids. Consequently, CO_2 injection must effectively couple with these reservoir entities individually and collectively to achieve CO_2 sequestration optimisations. Hence, this study explores the CO_2 sequestration optimisation subject area in light of its response to reservoir entities and heterogeneity, and aims to expand on this subject area.

A comprehensive technical screening and evaluation are required to identify reservoirs with characteristics that can support the CCS scheme. This

study used ceramic membranes as reservoir rock analogues to investigate Carbon Sequestration (CS) response to characteristic reservoir parameters. CO_2 permeation was adopted as a criterion for evaluating CS since a reliable CS site is one that prevents CO_2 from permeating further, thereby acting as a seal and storage site. **Figure 52** depicts a reservoir system with multiple sections of varying properties with the potential to be CS sites. Site A has the largest grain but the smallest pores. When CO_2 molecules permeate those tiny pores, they may become trapped or sealed due to displacement and capillary pressure effects. However, the volume of trapped CO_2 may be small compared to what Site B (large grain but largest pore size) can accommodate. CS engineers are faced with the challenge of screening and selecting from sites like these to ensure maximum CS volume and seal integrity. A rigorous experimental method has been applied to investigate this engineering dilemma (Abunumah et al. 2022). From the study, we have evaluated some reservoir petrophysical quantities that can be used by engineers to screen reservoirs for CCUS application.

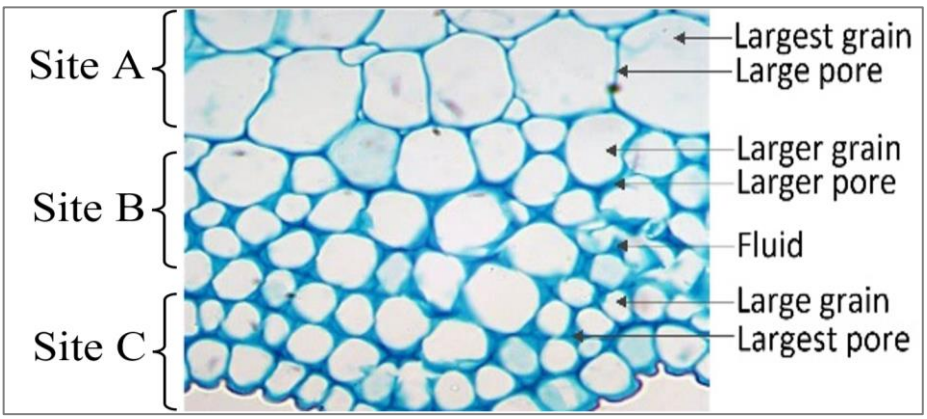

Figure 52 Reservoir porous structure for CO2 permeation and carbon storage potential site options

4.3.2 Analysis

For a site to be suitable for CS, it has to act as a seal to securely prevent the further permeation or flow of CO_2 beyond the boundary. Therefore the technique used to evaluate the structural mix of a potential seal, is to observe the change (increase or decrease) in each of the petrophysical quantities that enable a decrease in CO_2 permeation for a series of pore systems.

There are five main quantities that have been evaluated from a number

of parameters that directly relate to the CCUS site efficiency with their effects shown in **Figure *53*** below. To evaluate the structural mix of an ideal site, CO_2 gas was injected into the membrane core samples and permeation measured when steady-state was attained in each potential site to observe the conditions that facilitates gas sequestration. The results show the impact of a site's geological properties (pore density and specific surface area); geometrical properties (number of pores); and fluid properties (displacement pressure and gas density) on CO_2 permeation.

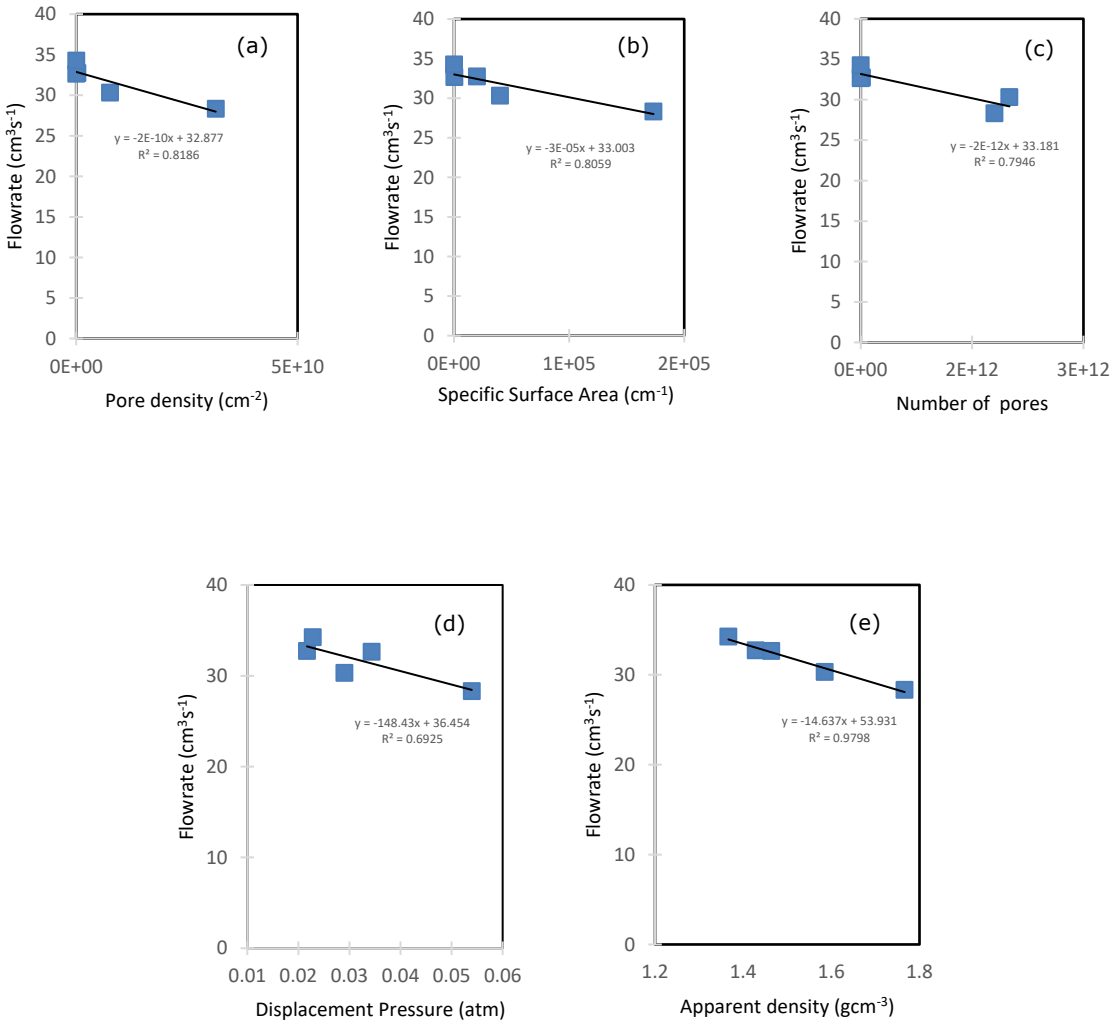

Figure 53 CS response to (a) pore density; (b)specific surface area; (c) pore number; (d) displacement pressure; (e) gas apparent density

A linear relationship is observed for these quantities, and we can see that CS improves with an increase in each of these factors. This implies that injecting the CO_2 in the direction of increasing pore density, specific surface area, pore number, displacement pressure, and CO_2 density causes an eventual linear decrease in the permeation of CO_2 which is ideal for CCUS. The strongest linear regression correlation for the investigated structural quantity is between CS and fluid density. This indicates that majority of the changes in CS can be explained by the variation in fluid density across the reservoir.

4.4 SUMMARY

A comparative analysis was done for membranes with varying pore sizes and it was observed that each membrane followed their characteristic flow mechanism according to their pore sizes consistent to the previous work carried out in this field(Sridhar, Bee and Bhargava 2014). However, these studies did not highlight the effect of pinholes which are commonly present on membrane surfaces and how these pinholes impact the pore size and overall performance of the membranes. This study showed that although the 15nm mesoporous membranes exhibited Knudsen diffusion as categorized in their pore size range in **Figure *10***, the pinholes present on its surface instigated the influence of another flow mechanism known as viscous flow. The phenomena of parallel flow mechanism with membranes experiencing viscous and Knudsen flow simultaneously based on their structural properties was identified. These membranes showed viscous and Knudsen flow characteristics with changes in temperature and pressure during permeation tests (Ghasemzadeh, Basile and Iulianelli 2019). Furthermore, a two-parameter model (TPM) confirmed numerically a cumulative combination of viscous and Knudsen flow to permeation (Van de Water and Maschmeyer 2004).

It was also confirmed that even at low pressure ranges, mass transfer conditions were not limiting, and effective mass transport can be achieved with these membranes. Moreover, flux values more than four times higher than similar membranes was achieved by Merkel et al (Merkel et al. 2000). Results from **Figure *38*** reveal that optimum permeance for these membranes is achievable between 30-40nm, hence, silica membranes were prepared following

recommendations by Xomeritakis et al by consequent dip coating stages to achieve a pore size of 36nm (Xomeritakis et al. 2003; Tosti et al. 2006; Santucci et al. 2013; Karakiliç et al. 2017). Gas permeation tests showed an increase in the membrane selectivity of up to 42% with negligible changes to permeance. This confirmed the successful production of defect free silica membranes for biogas separation that overcome the barrier of perm-selectivity compromise experienced by previous studies (Robeson 1991; Liu et al. 2006; Li et al. 2012).

In addition, membranes were tested to observe the effect of geological, geometric, and fluid properties on carbon sequestration applications. It was observed that there is a proportional relationship between the storage or sequestration capacity of a porous permeable solid with its pore density, specific surface area, pore number, displacement pressure, and gas density, thus addressing site screening criteria for channeling the effluent CO_2 from the upgrading process.

CHAPTER 5: CONCLUSION AND RECOMMENDATIONS

5.1 CONCLUSIONS

This report gives an overview of membrane technology and its application to biogas upgrading. The first chapter introduces biogas as an alternative source of energy that is produced from waste products. The different methods of upgrading biogas were highlighted and membranes were identified as an ideal technique that can be utilised with low energy requirements to separate gases based on the operating gas flow mechanism. This study began with characterising the membranes and observing the effects of different structural and fluid properties on gas transport through the pores.

1. From the experimental analysis, it was observed that a parallel flow mechanism of viscous and Knudsen flow was operating within the membrane support. Using the TPM model, a mode of estimating the viscous and Knudsen diffusivity of the porous structure has been shown. In addition, the two-parameter model (TPM) was applied to explain viscous and Knudsen transport and this can be used to estimate the permeability of CH_4 and CO_2 through similar membranes. It may be used to estimate gas behaviour at other operating temperature and pressure ranges to proffer viability of membrane systems for a given operation.
2. Darcy flow was obtainable with gases in the low transmembrane pressure drop region and the membrane mass transfer characteristics were evaluated. The membrane system involves a mass transfer section on the shell side, permeation through the membrane and a gas removal section on the tube side (bore). In the annular space section, a high mass transfer rate is established and used to generate the strong concentration gradient for gas permeation into membrane which is then transported through the membrane structure until complete removal from the tube side.
3. In the cases studied, the gas flow mechanism was dependent on the gas molecular weight as the lighter methane gas permeates the membrane at a much faster rate than the heavier carbon dioxide gas which is in line with Grahams law of diffusion that states the rate of flow of gases is inversely proportional to the square root of its molecular weight. The results show that the measured viscous and Knudsen selectivity agree

well with theory and it can be inferred that one way of achieving better membrane selectivity is though decreasing pore size to a microporous level.

4. A reduction in pore size was achieved by successful deposition of a silica layer on the mesoporous support. The membrane was fabricated by dip coating the support and then were characterized by static and dynamic methods to ensure the successful deposition of a coating layer. Gas permeation studies were also carried out to measure the permeability and selectivity of gases through ceramic support and silica coated membranes. It was found that the gas flow mechanism through the membranes was a critical parameter in improving the membrane performance. The support membrane exhibited a higher degree of viscous flow contribution due to its pore size and defects on the surface. The silica coating decreased the influence of viscous flow making Knudsen the more dominant flow regime and allowing gas separation according to this mechanism.
5. There was a 42% reduction in CO_2 concentration using the modified membrane and it can be established that a membranes' selectivity performance was dependent on an interplay of factors including (i) the structural effect which filters gases based on their interaction with pores (ii) the thermodynamic equilibrium effect having to do with operating conditions (iii) the kinetic effect which considers the different diffusion rates of gas components making them permeate quicker than others.
6. An experimental method was applied to investigate one of the solutions to climate change, Carbon storage (CS). An ideal CS site should have a large number of pores to contain the gas but tighter pore structures to restrict its permeation. Analysis was done to establish the applicability of the membrane core properties to carbon sequestration. Five main geometric, geologic and fluid quantities that can be directly related to the CCUS site effectiveness were identified and these quantities can be used to classify reservoir carbon storage capabilities. The results revealed that CS is responsive to these geological, geometrical, and fluid quantities. Simple linear equations can describe the relationship of CS to 5 of the quantities including pore density, specific surface area, pore number, displacement pressure, and gas density. Based on the outcome of this

study, CS engineers can apply knowledge to practice by screening reservoirs and selecting storage sites or layers with relatively high pore density, specific surface area, pore number, and displacement pressure. Such screening decisions will save implementation costs and reduce technical complications.

5.2 RECOMMENDATIONS FOR FUTURE WORK

Further research may be conducted in the following areas to improve on the study so far.

1. This study was carried out in the temperature range where biogas is normally produced (below 100^{o}C). Future work may be done to observe whether higher temperature ranges would significantly impact the membrane perm-selectivity. This would be advantageous for use in applications where very high purity methane is required.
2. Experimental analysis may also be carried out for testing membrane performance on a real biogas mixture instead of a synthetic mixture to observe the impact of other gas impurities on the membrane performance and effectiveness.
3. It would also be interesting to test these membranes for other gas permeation studies. Particularly, a resourceful gas like hydrogen with a much lower molecular weight, to observe whether higher perm-selectivities can be achieved based on Knudsen diffusion.
4. An investigation and comparison of the effect of utilising membrane supports in the microporous range having the same porosity on the membrane flow mechanism and perm-selectivity.
5. Supplementary experimental analysis may be carried out to describe the effect of incorporation of additional coating layers on the membrane and to observe changes in the gas diffusion characteristics.
6. A techno-economic study could also be carried out to ascertain the cost-energy benefit of this technology.

CHAPTER 6 : REFERENCES

4 Ways to Calculate Porosity, 2022. [online]. wikiHow. Available from: https://www.wikihow.com/Calculate-Porosity [Accessed 1 Sep 2022].

ABUNUMAH, O. et al., 2022. Experimental determination of carbon capture and sequestration response to reservoir quantities.

AKOREDE, M.F. et al., 2012. Mitigating the anthropogenic global warming in the electric power industry. *Renewable and Sustainable Energy Reviews*, 16(5), pp. 2747–2761.

AL MAMUN, M.R. and TORII, S., 2016. Enrichment of Methane Concentration by Removing Contaminant Gases from Biogas Mixtures Based on Chemical Purification Processes. *International Journal of Transport Phenomena*, 14(3).

AL SEADI, T., 2008. *Biogas handbook*. Odense, Denmark: Syddansk Universitet.

AN, W. et al., 2011. Selective separation of hydrogen from C1/C2 hydrocarbons and CO2 through dense natural zeolite membranes. *Journal of Membrane Science*, 369(1–2), pp. 414–419.

ANGELIDAKI, I. et al., 2018. Biogas upgrading and utilization: Current status and perspectives. *Biotechnology Advances*, 36(2), pp. 452–466.

Australia Bushfires: Cause, Impact, and Restoration, 2020. [online]. One Tree Planted. Available from: https://onetreeplanted.org/blogs/stories/australia-bushfires [Accessed 11 Nov 2020].

AWE, O.W. et al., 2017. A Review of Biogas Utilisation, Purification and Upgrading Technologies. *Waste and Biomass Valorization*, 8(2), pp. 267–283.

BAENA-MORENO, F.M. et al., 2019. Review: recent advances in biogas purifying technologies. *International Journal of Green Energy*, 16(5), pp. 401–412.

BEIL, M. and BEYRICH, W., 2013. Biogas upgrading to biomethane. In: *The Biogas Handbook*. Elsevier. pp. 342–377. Available from: https://linkinghub.elsevier.com/retrieve/pii/B9780857094988500154 [Accessed 6 May 2019].

BENITO, J. et al., 2005. Preparation and characterization of tubular ceramic membranes for treatment of oil emulsions. *Journal of the European Ceramic Society*, 25(11), pp. 1895–1903.

BEREAN, K. et al., 2014. The effect of crosslinking temperature on the permeability of PDMS membranes: Evidence of extraordinary CO2 and CH4 gas permeation. *Separation and Purification Technology*, 122, pp. 96–104.

BHAVE RAMESH, R., 1991. Inorganic membranes synthesis, characteristics and applications. *Chapman & Hall*, pp. 289–291.

BRUNETTI, A. et al., 2010. Membrane technologies for CO2 separation. *Journal of Membrane Science*, 359(1–2), pp. 115–125.

BURGGRAAF, A.J. and COT, L., 1996. *Fundamentals of inorganic membrane science and technology*. Elsevier.

CAPPENBERG, T.E., 1975. A study of mixed continuous cultures of sulfate-reducing and methane-producing bacteria. *Microbial Ecology*, 2(1), pp. 60–72.

CHANG, X. et al., 2006. Match of thermal performances between the membrane and the support for supported dense mixed-conducting membranes. *Journal of Membrane Science*, 285(1–2), pp. 232–238.

CHEN, G. et al., 2020. Effect of pore size on CH4/N2 separation using activated carbon. *Chinese Journal of Chemical Engineering*, 28(4), pp. 1062–1068.

CHENG, J. et al., 2020. Nitrogen-doped microporous carbon material decorated with metal nanoparticles derived from solid Zn/Co zeolitic imidazolate framework with high selectivity for CO2 separation. *Fuel*, 265, p. 116972.

CHO, Y.-K., HAN, K. and LEE, K.-H., 1995. Separation of CO2 by modified γ-Al2O3 membranes at high temperature. *Journal of Membrane Science*, 104(3), pp. 219–230.

Climate change and health, 2022. [online]. Available from: https://www.who.int/news-room/fact-sheets/detail/climate-change-and-health [Accessed 31 Aug 2022].

CLIMENHAGA, M.A. and BANKS, C.J., 2008. Anaerobic digestion of catering wastes: effect of micronutrients and retention time. *Water Science and Technology*, 57(5), pp. 687–692.

Could climate change lead to a shortage of food? - CBBC Newsround, n.d. [online]. Available from: https://www.bbc.co.uk/newsround/49725155 [Accessed 11 Nov 2020].

DA COSTA, J.D. et al., 1999. Novel composite membranes for gas separation: preparation and performance. *Journal of Porous Materials*, 6(2), pp. 143–151.

DAI, Z. et al., 2016. Combination of ionic liquids with membrane technology: A new approach for CO2 separation. *Journal of Membrane Science*, 497, pp. 1–20.

DAMLE, A., 2014. An introduction to the utilization of membrane technology in the production of clean and renewable power. In: *Membranes for Clean and Renewable Power Applications*. Amsterdam: Elsevier. pp. 3–43. Available from: https://linkinghub.elsevier.com/retrieve/pii/B978085709545950001X [Accessed 23 May 2019].

DE LANGE, R. et al., 1995. Formation and characterization of supported microporous ceramic membranes prepared by sol-gel modification techniques. *Journal of Membrane Science*, 99(1), pp. 57–75.

DE MEIS, D., 2017. Liquid filtration through ceramic membranes. *COMITATO NAZIONALE PER LA RICERCA E PER LO SVILUPPO DELL'ENERGIA NUCLEARE E DELLE ENERGIE ALTERNATIVE. ENEA-RT/DISP*.

DEEPANRAJ, B., SIVASUBRAMANIAN, V. and JAYARAJ, S., 2014. Biogas generation through anaerobic digestion process-an overview. *Research Journal of Chemistry and Environment*, 18, p. 5.

Delivering clean growth: CCUS Cost Challenge Taskforce report, n.d., p. 64.

DINCĂ, M. et al., 2014. The influence of heavy metals on biogas production during the anaerobic digestion process. Proceedings of the 3rd International Conference on Thermal Equipment, Renewable Energy and Rural Development, 2014. pp. 12–14.

DOMENICO DE MEIS, 2017. *Gas-transport-through-porous-membranes*. Rome, Italy: Frascati Research Center.

DUVAL, J. et al., 1994. Preparation of zeolite filled glassy polymer membranes. *Journal of Applied Polymer Science*, 54(4), pp. 409–418.

FAIN, D.E., 2000. Mixed gas separation technology using inorganic membranes. *Membrane Technology*, 2000(120), pp. 9–13.

FISCHER, C. and NEWELL, R.G., 2005. *Environmental and technology policies for climate change and renewable energy*.

FU, J., THOMAS, H.R. and LI, C., 2021. Tortuosity of porous media: Image analysis and physical simulation. *Earth-Science Reviews*, 212, p. 103439.

GARDNER, T., 2019. Climate change's fingerprints are on U.S. Midwest floods: scientists. *Reuters*, 22 Mar [online]. Available from: https://uk.reuters.com/article/us-usa-weather-climatechange-idUKKCN1R22I8 [Accessed 11 Nov 2020].

GHASEMZADEH, K., BASILE, A. and IULIANELLI, A., 2019. Progress in Modeling of Silica-Based Membranes and Membrane Reactors for Hydrogen Production and Purification. *ChemEngineering*, 3(1), p. 2.

HABIB, N. et al., 2020. Development of highly permeable and selective mixed matrix membranes based on Pebax® 1657 and NOTT-300 for CO2 capture. *Separation and Purification Technology*, 234, p. 116101.

HARVEY, F. and CORRESPONDENT, F.H.E., 2019. Climate crisis topping UK election agenda is 'unprecedented' change. *The Guardian*, 21 Nov [online]. Available from: https://www.theguardian.com/environment/2019/nov/21/climate-crisis-topping-uk-election-agenda-is-unprecedented-change [Accessed 31 Aug 2022].

HAVAS, D. and LIN, H., 2017. Optimal membranes for biogas upgrade by removing CO2: High permeance or high selectivity? *Separation Science and Technology*, 52(2), pp. 186–196.

TEN HOVE, M. et al., 2017. Hydrothermal stability of silica, hybrid silica and Zr-doped hybrid silica membranes. *Separation and Purification Technology*, 189, pp. 48–53.

HSIEH, H.P., 1996. *Inorganic Membranes for Separation and Reaction*. Elsevier.

Infographic: IPCC: Pull the Emergency Brake on Global CO2 Emissions, 2020. [online]. Statista Infographics. Available from: https://www.statista.com/chart/15737/global-co2-emissions-ipcc-targets/ [Accessed 12 Feb 2020].

ISLAM, M. and KHAN, M., 2013. *The petroleum engineering handbook: sustainable operations*. Elsevier.

ISMAIL, A.F., KHULBE, K.C. and MATSUURA, T., 2015. Gas separation membranes. *Switz. Springer*, 10, pp. 973–978.

JI, P. et al., 2010. Impacts of coating condition on composite membrane performance for CO2 separation. *Separation and Purification Technology*, 71(2), pp. 160–167.

JULBE, A. and RAMSAY, J., 1996. Methods for the characterisation of porous structure in membrane materials. In: *Membrane Science and Technology*. Elsevier. pp. 67–118.

KANELLOPOULOS, N.K., 2000. *Recent Advances in Gas Separation by Microporous Ceramic Membranes*. Elsevier.

KARAKILIÇ, P. et al., 2017. Sol-gel processed magnesium-doped silica membranes with improved H2/CO2 separation. *Journal of Membrane Science*, 543, pp. 195–201.

KIM, J. et al., 2013. New materials for methane capture from dilute and medium-concentration sources. *Nature Communications*, 4(1), pp. 1–7.

KINYUA, M.N., CUNNINGHAM, J. and ERGAS, S.J., 2014. Effect of solids retention time on the bioavailability of organic carbon in anaerobically digested swine waste. *Bioresource Technology*, 162, pp. 14–20.

KRISHANIA, M. et al., 2012. Opportunities for improvement of process technology for biomethanation processes. *Green Processing and Synthesis*, 1(1), pp. 49–59.

KUYLENSTIERNA, J. et al., 2011. Near-term climate protection and clean air benefits: Actions for Controlling Short-Lived Climate Forcers.

LASHOF, D.A. and AHUJA, D.R., 1990. Relative contributions of greenhouse gas emissions to global warming. *Nature*, 344(6266), p. 529.

LAWRENCE, A.W. and MCCARTY, P.L., 1965. The role of sulfide in preventing heavy metal toxicity in anaerobic treatment. *Journal (Water Pollution Control Federation)*, pp. 392–406.

LEE, H.-J. et al., 2006. Influence of adsorption on the gas permeation performances in the mesoporous alumina ceramic membrane. *Separation and Purification Technology*, 49(1), pp. 49–55.

LEENAARS, A., KEIZER, K. and BURGGRAAF, A., 1984. The preparation and characterization of alumina membranes with ultra-fine pores. *Journal of Materials Science*, 19(4), pp. 1077–1088.

LI, K., 2007. *Ceramic Membranes for Separation and Reaction*. John Wiley & Sons.

LI, L. et al., 2012. A high CO2 permselective mesoporous silica/carbon composite membrane for CO2 separation. *Carbon*, 50(14), pp. 5186–5195.

LIU, G. et al., 2009. Effect of feed to inoculum ratios on biogas yields of food and green wastes. *Bioresource Technology*, 100(21), pp. 5103–5108.

LIU, Q. et al., 2006. Zeolite married to carbon: a new family of membrane materials with excellent gas separation performance. *Chemistry of Materials*, 18(26), pp. 6283–6288.

LIU, X. and HE, X., 2017. Effect of pore characteristics on coalbed methane adsorption in middle-high rank coals. *Adsorption*, 23(1), pp. 3–12.

LUIS, P., VAN GERVEN, T. and VAN DER BRUGGEN, B., 2012. Recent developments in membrane-based technologies for CO2 capture. *Progress in Energy and Combustion Science*, 38(3), pp. 419–448.

MANEERUNG, T., HIDAJAT, K. and KAWI, S., 2014. Ultra-thin (< 1 μm) internally-coated Pd–Ag alloy hollow fiber membrane with superior thermal stability and durability for high temperature H2 separation. *Journal of Membrane Science*, 452, pp. 127–142.

MCCARTY, P.L. and MCKINNEY, R.E., 1961. Volatile acid toxicity in anaerobic digestion. *Journal (Water Pollution Control Federation)*, pp. 223–232.

MERKEL, T. et al., 2000. Gas sorption, diffusion, and permeation in poly (dimethylsiloxane). *Journal of Polymer Science Part B: Polymer Physics*, 38(3), pp. 415–434.

MICHALOPOULOS, S., 2018. EU Parliament ends palm oil and caps crop-based biofuels at 2017 levels. *www.euractiv.com* [online]. Available from: https://www.euractiv.com/section/agriculture-food/news/eu-parliament-ends-palm-oil-and-caps-crop-based-biofuels-at-2017-levels/ [Accessed 11 Nov 2020].

MINDE, G., MAGDUM, S. and KALYANRAMAN, V., 2013. Biogas as a sustainable alternative for current energy need of India. *Journal of Sustainable Energy & Environment*, 4, pp. 121–132.

NAGY, E., 2019. Chapter 3 - Mass Transport Through a Membrane Layer. In: E. NAGY, ed. *Basic Equations of Mass Transport Through a Membrane Layer (Second Edition)*. Elsevier. pp. 21–68. Available from: http://www.sciencedirect.com/science/article/pii/B9780128137222000030 [Accessed 30 May 2019].

NEACŞU, I.A. et al., 2016. Inorganic micro-and nanostructured implants for

tissue engineering. In: *Nanobiomaterials in Hard Tissue Engineering*. Elsevier. pp. 271–295.

NIESNER, J., JECHA, D. and STEHLÍK, P., 2013. Biogas upgrading technologies: state of art review in European region. *Chemical Engineering Transactions*, 35(86), pp. 517–522.

VAN OLDENBORGH, G.J. et al., n.d. Human contribution to the record-breaking June 2019 heat wave in France, p. 32.

OYAMA, S.T., 2011. Review on mechanisms of gas permeation through inorganic membranes. *Journal of the Japan Petroleum Institute*, 54(5), pp. 298–309.

OZEN, H.A. and OZTURK, B., 2019. Gas separation characteristic of mixed matrix membrane prepared by MOF-5 including different metals. *Separation and Purification Technology*, 211, pp. 514–521.

PACHAURI, R.K. et al., 2014. *Climate change 2014: synthesis report. Contribution of Working Groups I, II and III to the fifth assessment report of the Intergovernmental Panel on Climate Change*. Ipcc.

PAKIZEH, M., OMIDKHAH, M. and ZARRINGHALAM, A., 2007a. Synthesis and characterization of new silica membranes using template–sol–gel technology. *International Journal of Hydrogen Energy*, 32(12), pp. 1825–1836.

PAKIZEH, M., OMIDKHAH, M. and ZARRINGHALAM, A., 2007b. Study of mass transfer through new templated silica membranes prepared by sol–gel method. *International Journal of Hydrogen Energy*, 32(12), pp. 2032–2042.

PANT, L.M., MITRA, S.K. and SECANELL, M., 2012. Absolute permeability and Knudsen diffusivity measurements in PEMFC gas diffusion layers and micro porous layers. *Journal of Power Sources*, 206, pp. 153–160.

PENG, Z. and LI, X., 2018. Improvements of the permeability experiment in coalbed methane. *Arabian Journal of Geosciences*, 11(11), pp. 1–4.

PETERSSON, A. and WELLINGER, A., 2009. Biogas upgrading technologies–developments and innovations. *IEA Bioenergy*, 20, pp. 1–19.

PILLALAMARRY, M., HARPALANI, S. and LIU, S., 2011. Gas diffusion behavior of coal and its impact on production from coalbed methane reservoirs. *International Journal of Coal Geology*, 86(4), pp. 342–348.

PROTOCOL, K., 1997. United Nations framework convention on climate change. *Kyoto Protocol, Kyoto*, 19.

QUADRELLI, R. and PETERSON, S., 2007. The energy–climate challenge: Recent trends in CO2 emissions from fuel combustion. *Energy Policy*, 35(11), pp. 5938–5952.

RACKLEY, S.A., 2017. 8 - Membrane separation systems. In: S.A. RACKLEY, ed. *Carbon Capture and Storage (Second Edition)*. Boston: Butterworth-

Heinemann. pp. 187–225. Available from: http://www.sciencedirect.com/science/article/pii/B9780128120415000088 [Accessed 30 May 2019].

RICHARD, V. et al., 2001. Experimental study of hydrogen, carbon dioxide and nitrogen permeation through a microporous silica membrane. *Chemical Engineering Journal*, 84(3), pp. 593–598.

ROBESON, L.M., 1991. Correlation of separation factor versus permeability for polymeric membranes. *Journal of Membrane Science*, 62(2), pp. 165–185.

ROUQUEROL, J. et al., 1994. Recommendations for the characterization of porous solids (Technical Report). *Pure and Applied Chemistry*, 66(8), pp. 1739–1758.

RUBIN, E. and DE CONINCK, H., 2005. IPCC special report on carbon dioxide capture and storage. *UK: Cambridge University Press. TNO (2004): Cost Curves for CO2 Storage, Part*, 2, p. 14.

RYCKEBOSCH, E., DROUILLON, M. and VERVAEREN, H., 2011. Techniques for transformation of biogas to biomethane. *Biomass and Bioenergy*, 35(5), pp. 1633–1645.

SADRZADEH, M. et al., 2009. Gas permeation through a synthesized composite PDMS/PES membrane. *Journal of Membrane Science*, 342(1–2), pp. 236–250.

SAHOTA, S. et al., 2018. Review of trends in biogas upgradation technologies and future perspectives. *Bioresource Technology Reports*, 1, pp. 79–88.

SAINAN, L. et al., 2013. Ceramic supported PDMS and PEGDA composite membranes for CO2 separation. *Chinese Journal of Chemical Engineering*, 21(4), pp. 348–356.

SANTUCCI, A. et al., 2013. Testing of dense Pd–Ag tubes: Effect of pressure and membrane thickness on the hydrogen permeability. *Journal of Membrane Science*, 444, pp. 378–383.

SCHELL, W.J. and HOUSTON, C., 1983. Use of membranes for biogas treatment. *Energy Prog.;(United States)*, 3(2).

SCOTT, K. and HUGHES, R., 2012. *Industrial membrane separation technology*. Springer Science & Business Media.

SEDIGH, M.G. et al., 1998. Experiments and simulation of transport and separation of gas mixtures in carbon molecular sieve membranes. *The Journal of Physical Chemistry A*, 102(44), pp. 8580–8589.

SENEVIRATNE, S.I. et al., 2016. Allowable CO 2 emissions based on regional and impact-related climate targets. *Nature*, 529(7587), pp. 477–483.

SHAMSABADI, A.A., KARGARI, A. and BABAHEIDARI, M.B., 2014. Preparation, characterization and gas permeation properties of PDMS/PEI composite asymmetric membrane for effective separation of hydrogen from H2/CH4 mixed

gas. *International Journal of Hydrogen Energy*, 39(3), pp. 1410–1419.

SHEKHAWAT, D., LUEBKE, D.R. and PENNLINE, H.W., 2003. A review of carbon dioxide selective membranes: A topical report.

SHIMEKIT, B. et al., 2009. Ceramic membranes for the separation of carbon dioxide—a review. *Transactions of the Indian Ceramic Society*, 68(3), pp. 115–138.

SHIMEKIT, B. and MUKHTAR, H., 2012. Natural gas purification technologies-major advances for CO2 separation and future directions. *Advances in Natural Gas Technology*, 2012, pp. 235–270.

SHINDELL, D. et al., 2012. Simultaneously mitigating near-term climate change and improving human health and food security. *Science*, 335(6065), pp. 183–189.

SOKOLOV, A.P. et al., 2009. Probabilistic forecast for twenty-first-century climate based on uncertainties in emissions (without policy) and climate parameters. *Journal of Climate*, 22(19), pp. 5175–5204.

SRIDHAR, S., BEE, S. and BHARGAVA, S., 2014. Membrane-based gas separation: principle, applications and future potential. *Materials Science*.

STAFFORD, D.A., 1982. The effects of mixing and volatile fatty acid concentrations on anaerobic digester performance. *Biomass*, 2(1), pp. 43–55.

STERN, S.A., 1994. Polymers for gas separations: the next decade. *Journal of Membrane Science*, 94(1), pp. 1–65.

SUN, G., HIDAJAT, K. and KAWI, S., 2006. Ultra thin Pd membrane on α-Al2O3 hollow fiber by electroless plating: high permeance and selectivity. *Journal of Membrane Science*, 284(1–2), pp. 110–119.

SUN, Q. et al., 2015. Selection of appropriate biogas upgrading technology-a review of biogas cleaning, upgrading and utilisation. *Renewable and Sustainable Energy Reviews*, 51, pp. 521–532.

TANKO, N.L., 2018. The effect of Porosity on Tortuosity. *International Journal of Scientific & Engineering Research, 9 (5)*, pp. 2163–2169.

TASSELLI, F., 2015. Membrane Preparation Techniques. In: E. DRIOLI and L. GIORNO, eds. *Encyclopedia of Membranes*. Berlin, Heidelberg: Springer Berlin Heidelberg. pp. 1–3. Available from: https://doi.org/10.1007/978-3-642-40872-4_1825-1 [Accessed 3 May 2019].

The Greta Effect: Global CO2 Emissions Increased By 1.9% In 2018, 2019. [online]. The Global Warming Policy Forum (GWPF). Available from: https://www.thegwpf.com/the-greta-effect-global-co2-emissions-increased-by-1-9-in-2018/ [Accessed 12 Feb 2020].

The Ten Point Plan for a Green Industrial Revolution, n.d., p. 38.

TOMA, L. et al., 2016. THE INFLUENCE OF THE TEMPERATURE ON BIOGAS PRODUCTION IN A SMALL CAPACITY PLANT. *Acta Technica Corviniensis-Bulletin of Engineering*, 9(4), p. 153.

TOMORI, O., 2012. *Feasibility study of a large scale biogas plant in Lagos, Nigeria*. PhD Thesis, Murdoch University.

TOSTI, S. et al., 2006. Long-term tests of Pd–Ag thin wall permeator tube. *Journal of Membrane Science*, 284(1–2), pp. 393–397.

TÜZÜN, F.N. and ARÇEVIK, E., 2010. Pore modification in porous ceramic membranes with sol-gel process and determination of gas permeability and selectivity. Macromolecular symposia, 2010. Wiley Online Library. pp. 135–142.

UCHYTIL, P. et al., 2003. Influence of capillary condensation effects on mass transport through porous membranes. *Separation and Purification Technology*, 33(3), pp. 273–281.

UHLHORN, R.J.R., KEIZER, K. and BURGGRAAF, A.J., 1992. Gas transport and separation with ceramic membranes. Part I. Multilayer diffusion and capillary condensation. *Journal of Membrane Science*, 66(2), pp. 259–269.

UK becomes first major economy to pass net zero emissions law, 2020. [online]. GOV.UK. Available from: https://www.gov.uk/government/news/uk-becomes-first-major-economy-to-pass-net-zero-emissions-law [Accessed 11 Nov 2020].

ULLAH KHAN, I. et al., 2017. Biogas as a renewable energy fuel – A review of biogas upgrading, utilisation and storage. *Energy Conversion and Management*, 150, pp. 277–294.

VALAPPIL, R.S.K., GHASEM, N. and AL-MARZOUQI, M., 2021. Current and future trends in polymer membrane-based gas separation technology: A comprehensive review. *Journal of Industrial and Engineering Chemistry*, 98, pp. 103–129.

VAN DE WATER, L.G. and MASCHMEYER, T., 2004. Mesoporous membranes—a brief overview of recent developments. *Topics in Catalysis*, 29(1), pp. 67–77.

VERCAUTEREN, S. et al., 1998. Porous ceramic membranes: preparation, transport properties and applications. *Journal of Porous Materials*, 5(3), pp. 241–258.

Viewpoint: Why India's Chennai has run out of water, 2019. *BBC News*, 2 Jul [online]. Available from: https://www.bbc.co.uk/news/world-asia-india-48797399 [Accessed 11 Nov 2020].

VRBOVÁ, V. and CIAHOTNÝ, K., 2017. Upgrading biogas to biomethane using membrane separation. *Energy & Fuels*, 31(9), pp. 9393–9401.

WEI, Y. et al., 2019. Controlling pore structures of Pd-doped organosilica membranes by calcination atmosphere for gas separation. *Chinese Journal of Chemical Engineering*, 27(12), pp. 3036–3042.

WIHEEB, A.D. et al., 2015. HYDROGEN PURIFICATION USING A MICROPOROUS HYDROTALCITE-SILICA COMPOSITE MEMBRANE. *Diyala Journal of Engineering Sciences*, 8(4), pp. 846–854.

WILD, M., 2018. Global dimming and brightening: A review. *Journal of Geophysical Research: Atmospheres*. [online]. Available from: https://agupubs.onlinelibrary.wiley.com/doi/full/10.1029/2008JD011470%4010.1002/%28ISSN%292169-8996.DIMBRIGHT1 [Accessed 22 Dec 2019].

XOMERITAKIS, G. et al., 2003. Organic-templated silica membranes: I. Gas and vapor transport properties. *Journal of Membrane Science*, 215(1–2), pp. 225–233.

YANG, N.-T., KATHIRASER, Y. and KAWI, S., 2013. La0. 6Sr0. 4Co0. 8Ni0. 2O3−δ hollow fiber membrane reactor: Integrated oxygen separation–CO2 reforming of methane reaction for hydrogen production. *International Journal of Hydrogen Energy*, 38(11), pp. 4483–4491.

YILDIRIM, Y. and HUGHES, R., 2003. An Experimental Study of CO2 Separation Using a Silica Based Composite Membrane. *Process Safety and Environmental Protection*, 81(4), pp. 257–261.

YUAN CHEN, X. et al., 2015. Membrane gas separation technologies for biogas upgrading. *RSC Advances*, 5(31), pp. 24399–24448.

ZENG, J., QU, J. and ZHANG, Z., 2009. Review of the international greenhouse gas emission reduction scenario programs. *Advances in Earth Science*, 4.

ZIOUI, D. et al., 2015. Membrane Technology for water treatment applications. Proceedings of the International Conference on Communication, Computing and Electronics Systems, Istanbul, Turkey, 2015. pp. 9–12.

APPENDIX

APPENDIX A: EXPERIMENTAL FORMULA AND DATA

Pressure in feed = Gauge pressure + 1atm

Pressure in permeate = 1atm

ΔP = Pressure in feed − Pressure in permeate = Gauge pressure + 1atm − 1atm

$$\text{Average pressure} = \frac{(\text{Pressure in feed} + \text{Pressure in permeate})}{2}$$

$$= \frac{\text{Gauge pressure} + 1\text{atm} - 1\text{atm}}{2}$$

$$\text{Membrane Area} = \frac{\pi L(r_1 - r_2)}{\ln {}^{r_1}/_{r_2}}$$

A1:15nm, 3mm permeation data

Inlet Pressure (Pa)	CH_4 Outlet Flowrate at 20 degrees (LPM)	CO_2 Outlet Flowrate at 20 degrees (LPM)	Molar Flowrate CH_4	Molar Flowrate CO_2	CH_4 Flux	CO_2 Flux
20000	1.37	0.94	0.0010	0.0007	0.1136	0.0779
60000	3.38	2.21	0.0025	0.0016	0.2802	0.1832
100000	4.97	3.20	0.0037	0.0024	0.4121	0.2653
140000	6.46	4.20	0.0048	0.0031	0.5356	0.3482
180000	7.89	4.68	0.0059	0.0035	0.6542	0.3880
220000	9.47	6.13	0.0070	0.0046	0.7852	0.5082
260000	10.89	7.05	0.0081	0.0052	0.9029	0.5845
300000	12.37	8.01	0.0092	0.0060	1.0256	0.6641

Inlet Pressure (Pa)	CH_4 Outlet Flowrate at 50 degrees (LPM)	CO_2 Outlet Flowrate at 50 degrees (LPM)	Molar Flowrate CH_4	Molar Flowrate CO_2	CH_4 Flux	CO_2 Flux
20000	1.40	1.00	0.0010	0.0007	0.1161	0.0829
60000	3.31	2.16	0.0025	0.0016	0.2744	0.1791
100000	4.89	3.22	0.0036	0.0024	0.4054	0.2670
140000	6.49	4.15	0.0048	0.0031	0.5381	0.3441
180000	7.94	5.12	0.0059	0.0038	0.6583	0.4245
220000	9.49	6.09	0.0071	0.0045	0.7868	0.5049
260000	10.92	7.05	0.0081	0.0052	0.9054	0.5845
300000	12.49	8.06	0.0093	0.0060	1.0356	0.6683

Inlet Pressure (Pa)	CH_4 Outlet Flowrate at 70 degrees (LPM)	CO_2 Outlet Flowrate at 70 degrees (LPM)	Molar Flowrate CH_4	Molar Flowrate CO_2	CH_4 Flux	CO_2 Flux
20000	1.44	0.93	0.0011	0.0007	0.1194	0.0771
60000	3.34	2.16	0.0025	0.0016	0.2769	0.1791
100000	4.80	3.18	0.0036	0.0024	0.3980	0.2637
140000	6.35	4.15	0.0047	0.0031	0.5265	0.3441
180000	7.94	5.08	0.0059	0.0038	0.6583	0.4212
220000	9.47	6.08	0.0070	0.0045	0.7852	0.5041
260000	10.92	7.06	0.0081	0.0053	0.9054	0.5854
300000	12.44	8.01	0.0093	0.0060	1.0314	0.6641

Inlet Pressure (Pa)	CH_4 Outlet Flowrate at 100 degrees (LPM)	CO_2 Outlet Flowrate at 100 degrees (LPM)	Molar Flowrate CH_4	Molar Flowrate CO_2	CH_4 Flux	CO_2 Flux
20000	1.34	0.90	0.0010	0.0007	0.1111	0.0746
60000	3.31	2.13	0.0025	0.0016	0.2744	0.1766
100000	4.73	3.13	0.0035	0.0023	0.3922	0.2595
140000	6.27	4.09	0.0047	0.0030	0.5199	0.3391
180000	7.75	5.05	0.0058	0.0038	0.6426	0.4187
220000	9.29	6.02	0.0069	0.0045	0.7702	0.4991
260000	10.86	6.97	0.0081	0.0052	0.9004	0.5779
300000	12.44	7.96	0.0093	0.0059	1.0314	0.6600

A2: 15nm, 5mm permeation data

Inlet Pressure (Pa)	CH_4 Outlet Flowrate at 20 degrees (LPM)	CO_2 Outlet Flowrate at 20 degrees (LPM)	Molar Flowrate CH_4	Molar Flowrate CO_2	CH_4 Flux	CO_2 Flux
20000	1.89	1.34	0.0014	0.0010	0.0331	0.0235
60000	3.84	2.46	0.0029	0.0018	0.0672	0.0431
100000	5.39	3.50	0.0040	0.0026	0.0944	0.0613
140000	6.90	4.51	0.0051	0.0034	0.1208	0.0790
180000	8.40	5.43	0.0063	0.0040	0.1471	0.0951
220000	9.88	6.38	0.0074	0.0047	0.1730	0.1117
260000	11.33	7.35	0.0084	0.0055	0.1984	0.1287
300000	12.8	8.36	0.0095	0.0062	0.2241	0.1464

Inlet Pressure (Pa)	CH_4 Outlet Flowrate at 50 degrees (LPM)	CO_2 Outlet Flowrate at 50 degrees (LPM)	Molar Flowrate CH_4	Molar Flowrate CO_2	CH_4 Flux	CO_2 Flux
20000	2.00	1.46	0.0015	0.0011	0.0350	0.0256
60000	3.77	2.49	0.0028	0.0019	0.0660	0.0436
100000	5.44	3.50	0.0040	0.0026	0.0953	0.0613
140000	6.93	4.50	0.0052	0.0033	0.1214	0.0788
180000	8.41	5.40	0.0063	0.0040	0.1473	0.0946
220000	9.92	6.44	0.0074	0.0048	0.1737	0.1128
260000	11.41	7.35	0.0085	0.0055	0.1998	0.1287
300000	12.8	8.31	0.0095	0.0062	0.2241	0.1455

Inlet Pressure (Pa)	CH_4 Outlet Flowrate at 70 degrees (LPM)	CO_2 Outlet Flowrate at 70 degrees (LPM)	Molar Flowrate CH_4	Molar Flowrate CO_2	CH_4 Flux	CO_2 Flux
20000	2.01	1.35	0.0015	0.0010	0.0352	0.0236
60000	3.86	2.39	0.0029	0.0018	0.0676	0.0418
100000	5.32	3.48	0.0040	0.0026	0.0932	0.0608
140000	6.82	4.40	0.0051	0.0033	0.1194	0.0769
180000	8.36	5.39	0.0062	0.0040	0.1464	0.0942
220000	9.91	6.29	0.0074	0.0047	0.1735	0.1099
260000	11.39	7.38	0.0085	0.0055	0.1995	0.1289
300000	12.80	8.28	0.0095	0.0062	0.2241	0.1447

Inlet Pressure (Pa)	CH_4 Outlet Flowrate at 100 degrees (LPM)	CO_2 Outlet Flowrate at 100 degrees (LPM)	Molar Flowrate CH_4	Molar Flowrate CO_2	CH_4 Flux	CO_2 Flux
20000	1.68	1.35	0.0013	0.0010	0.0294	0.0236
60000	3.33	2.46	0.0025	0.0018	0.0583	0.0431
100000	4.62	3.47	0.0034	0.0026	0.0809	0.0608
140000	5.97	4.46	0.0044	0.0033	0.1045	0.0781
180000	7.19	4.56	0.0053	0.0034	0.1259	0.0799
220000	8.48	5.30	0.0063	0.0039	0.1485	0.0928
260000	9.70	5.66	0.0072	0.0042	0.1699	0.0991
300000	11.01	6.92	0.0082	0.0051	0.1928	0.1212

A3: 200nm permeation data

Inlet Pressure (Pa)	CH_4 Outlet Flowrate at 20 degrees (LPM)	CO_2 Outlet Flowrate at 20 degrees (LPM)	Molar Flowrate CH_4	Molar Flowrate CO_2	CH_4 Flux	CO_2 Flux
20000	1.57	1.17	0.0012	0.0009	0.1118	0.0833
60000	3.64	2.40	0.0027	0.0018	0.2592	0.1709
100000	5.27	3.42	0.0039	0.0025	0.3752	0.2435
140000	6.87	4.45	0.0051	0.0033	0.4891	0.3168
180000	8.42	5.50	0.0063	0.0041	0.5995	0.3916
220000	10.05	6.51	0.0075	0.0048	0.7156	0.4635
260000	11.58	7.47	0.0086	0.0056	0.8245	0.5319
300000	12.80	8.52	0.0095	0.0063	0.9114	0.6066

Inlet Pressure (Pa)	CH_4 Outlet Flowrate at 50 degrees (LPM)	CO_2 Outlet Flowrate at 50 degrees (LPM)	Molar Flowrate CH_4	Molar Flowrate CO_2	CH_4 Flux	CO_2 Flux
20000	1.59	1.20	0.0012	0.0009	0.1132	0.0854
60000	3.64	2.37	0.0027	0.0018	0.2592	0.1687
100000	5.28	3.48	0.0039	0.0026	0.3759	0.2478
140000	6.90	4.49	0.0051	0.0033	0.4913	0.3197
180000	8.48	5.54	0.0063	0.0041	0.6038	0.3945
220000	10.08	6.50	0.0075	0.0048	0.7177	0.4628
260000	11.74	7.54	0.0087	0.0056	0.8359	0.5369
300000	12.80	8.60	0.0095	0.0064	0.9114	0.6123

Inlet Pressure (Pa)	CH_4 Outlet Flowrate at 70 degrees (LPM)	CO_2 Outlet Flowrate at 70 degrees (LPM)	Molar Flowrate CH_4	Molar Flowrate CO_2	CH_4 Flux	CO_2 Flux
20000	1.57	1.13	0.0012	0.0008	0.1118	0.0805
60000	3.61	2.33	0.0027	0.0017	0.2570	0.1659
100000	5.23	3.41	0.0039	0.0025	0.3724	0.2428
140000	6.89	4.46	0.0051	0.0033	0.4906	0.3176
180000	8.56	5.48	0.0064	0.0041	0.6095	0.3902
220000	10.14	6.53	0.0075	0.0049	0.7220	0.4649
260000	11.78	7.51	0.0088	0.0056	0.8387	0.5347
300000	12.80	8.60	0.0095	0.0064	0.9114	0.6123

Inlet Pressure (Pa)	CH_4 Outlet Flowrate at 100 degrees (LPM)	CO_2 Outlet Flowrate at 100 degrees (LPM)	Molar Flowrate CH_4	Molar Flowrate CO_2	CH_4 Flux	CO_2 Flux
20000	1.61	1.09	0.0012	0.0008	0.1146	0.0776
60000	3.64	2.39	0.0027	0.0018	0.2592	0.1702
100000	5.22	3.37	0.0039	0.0025	0.3717	0.2399
140000	6.85	4.39	0.0051	0.0033	0.4877	0.3126
180000	8.45	5.45	0.0063	0.0041	0.6016	0.3880
220000	10.03	6.53	0.0075	0.0049	0.7141	0.4649
260000	11.63	7.57	0.0087	0.0056	0.8281	0.5390
300000	12.80	8.59	0.0095	0.0064	0.9114	0.6116

A4: 6000nm permeation data

Inlet Pressure (Pa)	CH_4 Outlet Flowrate at 20 degrees (LPM)	CO_2 Outlet Flowrate at 20 degrees (LPM)	Molar Flowrate CH_4	Molar Flowrate CO_2	CH_4 Flux	CO_2 Flux
20000	1.61	1.17	0.0012	0.0009	0.0530	0.0385
60000	3.54	2.24	0.0026	0.0017	0.1166	0.0738
100000	5.07	3.31	0.0038	0.0025	0.1670	0.1090
140000	6.53	4.15	0.0049	0.0031	0.2151	0.1367
180000	7.97	5.17	0.0059	0.0038	0.2625	0.1703
220000	9.45	6.13	0.0070	0.0046	0.3113	0.2019
260000	10.85	7.03	0.0081	0.0052	0.3574	0.2315
300000	12.32	7.95	0.0092	0.0059	0.4058	0.2618

Inlet Pressure (Pa)	CH_4 Outlet Flowrate at 50 degrees (LPM)	CO_2 Outlet Flowrate at 50 degrees (LPM)	Molar Flowrate CH_4	Molar Flowrate CO_2	CH_4 Flux	CO_2 Flux
20000	1.63	1.12	0.0012	0.0008	0.0537	0.0369
60000	3.50	2.29	0.0026	0.0017	0.1153	0.0754
100000	5.11	3.25	0.0038	0.0024	0.1683	0.1070
140000	6.53	4.21	0.0049	0.0031	0.2151	0.1387
180000	7.97	5.19	0.0059	0.0039	0.2625	0.1709
220000	9.42	6.04	0.0070	0.0045	0.3103	0.1989
260000	10.91	6.96	0.0081	0.0052	0.3593	0.2292
300000	12.28	7.91	0.0091	0.0059	0.4045	0.2605

Inlet Pressure (Pa)	CH_4 Outlet Flowrate at 70 degrees (LPM)	CO_2 Outlet Flowrate at 70 degrees (LPM)	Molar Flowrate CH_4	Molar Flowrate CO_2	CH_4 Flux	CO_2 Flux
20000	1.65	1.20	0.0012	0.0009	0.0543	0.0395
60000	3.53	2.24	0.0026	0.0017	0.1163	0.0738
100000	5.01	3.22	0.0037	0.0024	0.1650	0.1061
140000	6.46	4.28	0.0048	0.0032	0.2128	0.1410
180000	7.95	5.17	0.0059	0.0038	0.2618	0.1703
220000	9.43	6.08	0.0070	0.0045	0.3106	0.2003
260000	10.83	7.00	0.0081	0.0052	0.3567	0.2306
300000	12.40	7.97	0.0092	0.0059	0.4084	0.2625

Inlet Pressure (Pa)	CH_4 Outlet Flowrate at 100 degrees (LPM)	CO_2 Outlet Flowrate at 100 degrees (LPM)	Molar Flowrate CH_4	Molar Flowrate CO_2	CH_4 Flux	CO_2 Flux
20000	1.68	1.05	0.0013	0.0008	0.0553	0.0346
60000	3.56	2.31	0.0026	0.0017	0.1173	0.0761
100000	5.02	3.18	0.0037	0.0024	0.1653	0.1047
140000	6.44	4.23	0.0048	0.0031	0.2121	0.1393
180000	7.95	5.14	0.0059	0.0038	0.2618	0.1693
220000	9.45	6.04	0.0070	0.0045	0.3113	0.1989
260000	10.95	6.96	0.0081	0.0052	0.3607	0.2292
300000	12.36	7.95	0.0092	0.0059	0.4071	0.2618

A5: Mass transfer flux from the bulk gas in the shell side to the membrane outer surface for methane gas at 0.2bar

Membrane	$(\rho 1 - \rho 2)$ Dei/d		$\underline{S}_h$		R_e		S_c X10^{-6}		Gas mass transfer flux from the bulk gas in the shell-side to the membrane outer surface (J_{CH4}), g/cm^2 s	
Pore Size (nm)	20 (°C)	100 (°C)	20 (°C)	100 (°C)	20 (°C)	100 (°C)	20 (°C)	100 (°C)	20 (°C)	100 (°C)
15	0.0589	0.0708	0.0362 – 0.4451	0.0365 – 0.4482	<=2000	<=2000	6.56	6.70	2.13E-03 – 0.0262	2.58E-03 – 0.0317
200	0.0621	0.0746	0.0362 – 0.4451	0.0365 – 0.4482	<=2000	<=2000	6.56	6.70	2.25E-03 – 0.0276	2.72E-03 – 0.0334
6000	0.0189	0.0228	0.0362 – 0.4451	0.0365 – 0.4482	<=2000	<=2000	6.56	6.70	6.84E-04 – 8.41E-03	8.32E-04 – 0.0102

A6: Mass transfer flux from the bulk gas in the shell side to the membrane outer surface for methane gas at 0.6 bar

Membrane	**(ρ1- ρ2) Dei/*d***		**S_h**		**R_e**		**S_c X10^{-6}**		**Gas mass transfer flux from the bulk gas in the shell-side to the membrane outer surface (J_{CH4}), g/cm^2 s**	
Pore Size (nm)	20 (°C)	100 (°C)	20 (°C)	100 (°C)	20 (°C)	100 (°C)	20 (°C)	100 (°C)	20 (°C)	100 (°C)
15	0.1769	0.2124	0.0329 - 0.4048	0.0332 – 0.4077	<=2000	<=2000	4.92	5.03	5.82E-03 – – 0.0716	7.05E-03 – 0.0866
200	0.1863	0.2237	0.0329 - 0.4048	0.0332 – 0.4077	<=2000	<=2000	4.92	5.03	6.13E-03 – – 0.0754	7.43E-03 – 0.0912
6000	0.0569	0.0684	0.0329 - 0.4048	0.0332 – 0.4077	<=2000	<=2000	4.92	5.03	1.87E-03 – – 0.0230	2.27E-03 – 0.0279

A7: Mass transfer flux from the bulk gas in the shell side to the membrane outer surface for carbon dioxide gas at 0.2 bar

Membrane	**(ρ1-ρ2) Dei/*d***		**$\underline{S}_h$**		**R_e**		**S_c X10^{-6}**		**Gas mass transfer flux from the bulk gas in the shell-side to the membrane outer surface (J_{CH4}), g/cm^2 s**	
Pore Size (nm)	20 (°C)	100 (°C)	20 (°C)	100 (°C)	20 (°C)	100 (°C)	20 (°C)	100 (°C)	20 (°C)	100 (°C)
15	0.1235	0.1528	0.0312 – 0.3836	0.0314 – 0.3859	<=2000	<=2000	4.18	4.26	3.85E-03 – 0.0474	4.79E-03 – 0.0589
200	0.1301	0.1610	0.0312 – 0.3836	0.0314 – 0.3859	<=2000	<=2000	4.18	4.26	4.06E-03 – 0.0499	5.06E-03 – 0.0621
6000	0.0398	0.0492	0.0312 – 0.3836	0.0314 – 0.3859	<=2000	<=2000	4.18	4.26	1.24E-03 – 0.0153	1.54E-03 – 0.0189

A8: Mass transfer flux from the bulk gas in the shell side to the membrane outer surface for carbon dioxide gas at 0.6 bar

Membrane	**(ρ1- ρ2) Dei/*d***		**$\underline{S}_h$**		**R_e**		**S_c X10^{-6}**		**Gas mass transfer flux from the bulk gas in the shell-side to the membrane outer surface (J_{CH4}), g/cm^2 s**	
Pore Size (nm)	20 (°C)	100 (°C)	20 (°C)	100 (°C)	20 (°C)	100 (°C)	20 (°C)	100 (°C)	20 (°C)	100 (°C)
15	0.3706	0.4585	0.0284 – 0.3490	0.0286 – 0.3508	<=2000	<=2000	3.14	3.19	0.0105 – 0.1293	0.0131 – 0.1608
200	0.3904	0.4830	0.0284 – 0.3490	0.0286 – 0.3508	<=2000	<=2000	3.14	3.19	0.0111– 0.1362	0.0138 – 0.1694
6000	0.1193	0.1477	0.0284 – 0.3490	0.0286 – 0.3508	<=2000	<=2000	3.14	3.19	3.39E-03 – 0.0416	4.22E-03 – 0.0518

A9: Comparison of achieved gas transfer rates in porous membrane systems used in this study with dense membrane systems for methane at 0.2bar

Membrane pore size (nm)	Thickness (m)	Permeability, k (m^2)		Pressure drop across membrane, Δp (kPa)		Mass flux, N_{CH4} (g/cm^2 s)	Permeate flux, Q_{CH4} (g/cm^2 s)		Gas mass transfer flux from the bulk gas in the shell-side to the membrane outer surface, J_{CH4} (g/cm^2 s)	
		20 (°C)	100 (°C)	20 (°C)	100 (°C)	35 (°C)	20 (°C)	100 (°C)	20 (°C)	100 (°C)
15	10^{-6}	1.8E-13	2.2E-13	20	20	0.013E-12	1.82E-04	1.78E-04	2.13E-03 – 0.0262	2.58E-03 – 0.0317
200	10^{-3}	1.5E-13	1.9E-13	20	20	0.013E-12	1.68E-04	1.83E-04	2.25E-03 – 0.0276	2.72E-03 – 0.0334
6000	10^{-3}	4.9E-14	6.0E-14	20	20	0.013E-12	0.85E-04	0.89E-04	6.84E-4 – 8.41E-03	8.32E-4 – 0.0102

A10: Comparison of achieved gas transfer rates in porous membrane systems used in this study with dense membrane systems for methane at 0.6bar

Membrane pore size (nm)	Thickness (m)	Permeability, k (m^2)		Pressure drop across membrane, Δp (kPa)		Mass flux, N_{CO2} ($g/cm^2 s$)	Permeate flux, Q_{CH4} ($g/cm^2 s$)		Gas mass transfer flux from the bulk gas in the shell-side to the membrane outer surface, J_{CO2} ($g/cm^2 s$)	
		20 (°C)	100 (°C)	20 (°C)	100 (°C)	35 (°C)	20 (°C)	100 (°C)	20 (°C)	100 (°C)
15	10^{-6}	1.8E-13	2.2E-13	60	60	0.039E-12	4.48E-04	4.39E-04	5.82E03 – 0.0716	7.05E3 – 0.0866
200	10^{-3}	1.5E-13	1.9E-13	60	60	0.039E-12	4.15xE-04	4.15E-04	6.13E-03 – 0.0754	7.43E-03 – 0.0912
6000	10^{-3}	4.9E-14	6.1E-14	60	60	0.039E-12	1.87E-04	1.88E-04	1.87E-03 – 0.0230	2.27E-03 – 0.0279

A11: Comparison of achieved gas transfer rates in porous membrane systems used in this study with dense membrane systems for carbon dioxide at 0.2bar

Membrane pore size (nm)	**Thickness (m)**	**Permeability, k (m^2)**		**Pressure drop across membrane, Δp (kPa)**		**Mass flux, N_{CO2} (g/cm^2 s)**	**Permeate flux, Q_{CO2} (g/cm^2 s)**		**Gas mass transfer flux from the bulk gas in the shell-side to the membrane outer surface, J_{CH4} (g/cm^2 s)**	
		20 (°C)	100 (°C)	20 (°C)	100 (°C)	35 (°C)	20 (°C)	100 (°C)	20 (°C)	100 (°C)
15	10^{-6}	1.7E-13	1.9E-13	20	20	0.112E-12	3.43E-04	3.28E-04	3.85E-03 – 0.0474	4.79E-03 – 0.0589
200	10^{-3}	1.4E-13	1.7E-13	20	20	0.112E-12	3.67E-04	3.41E-04	4.06E-03– 0.0499	5.06E-03 – 0.0621
6000	10^{-3}	4.9E-14	6.1E-14	20	20	0.112E-12	1.70E-04	1.52E-04	1.24E-03 – 0.0153	1.54E-03 – 0.0189

A12: Comparison of achieved gas transfer rates in porous membranes systems used in this study with dense membrane systems for carbon dioxide at 0.6bar

Membrane pore size (nm)	**Thickness (m)**	**Permeability, k (m^2)**		**Pressure drop across membrane, Δp (kPa)**		**Mass flux, N_{CO2} (g/cm^2s)**	**Permeate flux, Q_{CO2} (g/cm^2s)**		**Gas mass transfer flux from the bulk gas in the shell-side to the membrane outer surface, J_{CO2} (g/cm^2s)**	
		20 (°C)	100 (°C)	20 (°C)	100 (°C)	35 (°C)	20 (°C)	100 (°C)	20 (°C)	100 (°C)
15	10^{-6}	1.7E-13	1.9E-13	60	60	0.336E-12	8.03E-04	7.78E-04	0.0105 – 0.1293	0.0131 – 0.1608
200	10^{-3}	1.4E-13	1.7E-13	60	60	0.336E-12	7.52E-04	7.49E-04	0.0111 – 0.1362	0.0138 – 0.1694
6000	10^{-3}	4.9E-14	6.1E-14	60	60	0.336E-12	3.25E-04	3.35E-04	3.39E-03 – 0.0416	4.22E-03 – 0.0518

APPENDIX B: JOURNAL PUBLICATION ABSTRACTS

Available online at www.weentechpublishers.com

WEENTECH Proceedings in Energy 5 (2019) 195-205

4th International Conference on Energy, Environment and Economics, ICEEE2019, 20-22 August 2019, Edinburgh Conference Centre, Heriot-Watt University, Edinburgh, EH14 4AS, United Kingdom

Comparative evaluation of the effect of pore size and temperature on gas transport in nano-structured ceramic membranes for biogas upgrading

Priscilla Ogunlude, Ofasa Abunumah, Ifeyinwa Orakwe, Habiba Shehu, Firdaus Muhammad-Sukki and Edward Gobina*

Centre for Process Integration and Membrane Technology, School of Engineering, Robert Gordon University, Sir Ian Wood Building Garthdee Road, ABERDEEN AB10 7GJ, Tel: +441224262309

**Corresponding Author's mail: e.gobina@rgu.ac.uk*

Abstract

As a result of rising economies and environmental constraints, the demand for clean and renewable sources of energy is fast increasing. Biogas is a renewable form of energy that fits all expectations in terms of delivery, cost, and greenhouse emissions reduction. Biogas utilization is advantageous because it is a means of creating wealth from daily human, agricultural, household and municipal waste that could otherwise be polluting the environment as waste is deposited on a daily basis which are potential biogas sources; it is not dependent on weather conditions as other renewable forms (solar and wind). Biogas can also be compressed, stored and transported, and therefore easily responds to changes in demand. This paper entails the use of nano-structured membranes to upgrade biogas (which contains primarily methane and carbon dioxide). The benefits of membranes include their compact structure and ease of usage with low maintenance, their low running costs and minimal loss of the upgraded gas. 15nm, 200nm and 6000nm membranes were used to ascertain the flux of the model biogas mixture passing through it under various operating conditions. In each case, the exit flowrate of methane was higher than that of carbon dioxide and this is attributed to the pore sizes of the membrane and its ability to filter the heavier gases. The results show that the molecular weight of the gases also play a role in their permeation rate as it follows the Knudsen regime.

Keywords: Biogas upgrading; Sustainable; Nano-structured; Ceramic; Membrane; Carbon capture

https://doi.org/10.32438/WPE.8319
Manuscript History
Receipt of completed manuscript: 12 March 2019
Receipt of Revised Manuscript: 11 April 2019
Date of Acceptance: 13 April 2019
Online available from: 12 November 2019

detritus | Multidisciplinary Journal for Waste Resources & Residues

CISA

UPGRADING BIOGAS TO BIOMETHANE BY USE OF NANO-STRUCTURED CERAMIC MEMBRANES

Priscilla Ogunlude *, Ofasa Abunumah, Ifeyinwa Orakwe, Habiba Shehu, Firdaus Muhammad-Sukki and Edward Gobina

Department Centre for Process Integration and Membrane Technology, School of Engineering, Robert Gordon University, Sir Ian Wood Building, Garthdee Road, Aberdeen AB10 7GJ, United Kingdom

Article Info:
Received:
8 November 2019
Revised:
14 March 2020
Accepted:
9 April 2020
Available online:
25 July 2020

Keywords:
Biogas
Upgrading
Renewable
Nano-structured
Ceramic
Membrane
Biomethane

ABSTRACT

In order to meet the demands of growing economies while considering environmental implications, the use of clean and renewable sources of energy has increasingly become of interest. Biogas utilisation is a means by which these rising needs can be met. This involves the use of waste materials; which are deposited on a daily basis by agriculture, sewage, household, to produce energy that may be used for heating, electricity, transportation and other daily needs. This paper would look into the use of nano-structured ceramic membranes for the upgrading of biogas to a high value fuel that can be used for a variety of purposes. The use of membranes offers great advantages including low running costs, high efficiency and the elimination of the need for phase change of the gas. Experiments were carried out using membranes of different pore sizes (15nm, 200nm and 6000nm) to ascertain which would be the most suitable for use in terms of permeability and yield of product gas. The 15nm membrane showed the greatest exit flow of methane compared to carbon dioxide and a mechanism approaching an ideal knudsen regime. Taking into account the effect of molecular weight and viscosity, these results show that the smallest membrane pore size of 15nm had a greater impact on the flow mechanism and thus improvement can be made by modification of the membrane to achieve a mechanism of surface diffusion of the particles.

1. INTRODUCTION

Biogas is evolved from the anaerobic digestion of biogradable materials such as human or animal waste, food scraps, cotton, wool, wood and other organic sources. The biogas obtained can be used directly as a fuel but in order to fully harness its potential, it can be cleaned and upgraded to a point where its heating value is very high, and impurities are removed such that it can be injected into the national gas grid.

The treatment or upgrading of biogas is essential because: (i) the presence of CO_2 in the gas reduces the power output from the engine, takes up space when biogas is compressed for storage and causes freezing problems when the compressed gas undergoes expansion at valves and metering points (ii) traces of H_2S can produce H_2SO_4 which corrode pipes, fittings, etc. (iii) moisture reduces the heating value of the biogas and causes corrosion. Nonetheless, several safety aspects need to be considered during the treatment and utilization of biogas. It is very crucial to be aware of the associated risks and to minimize them. The most common risks include flammability, poisoning (due to the presence of H_2S), suffocation and the risks associated with high pressures and temperatures. However, the advantages include the fact that biogas is lighter than air and any gas leakage would rise upward. Moreover, upgraded biogas has a greater temperature of ignition than both petrol and diesel so the possibility of a fire or explosion is reduced (Svenskt Gastekniskt Center, 2012).

The advantages of utilizing biogas are numerous; biogas upgrading technology can turn the cost of waste management into a revenue opportunity. Turning waste into a renewable source of energy by this upgrading process will reduce dependence on importation of fossil fuels, reduce greenhouse gas emissions, improve environmental quality, increase local jobs and provide revenue by export thereby boosting the economies. The benefits cannot be overstretched as even the digestate from anaerobic digestion offers an opportunity to recycle nutrients in the food supply, reducing the need for both petrochemical and mined fertilizers. Research has proven that upgraded biogas shows lower carbon intensities compared to other vehicle fuel (Penev et al., 2016; Scarlat, Dallemand, & Fahl, 2018).

* Corresponding author:
Priscilla Ogunlude
email: p.ogunlude@rgu.ac.uk

Detritus / Volume 12 - 2020 / pages 73-77
https://doi.org/10.31025/2611-4135/2020.13996

ISSN 2601-8683 (Print)
ISSN 2601-8675 (Online)
European Journal of
Formal Sciences and Engineering
July - December 2022
Volume 5, Issue 2

A Study of Gas Diffusion Characteristics on Nano-Structured Ceramic Membranes

Priscilla Ogunlude
Robert Gordon University, Centre for Process Integration and Membrane Technology School of Engineering
Ofasa Abunumah
Robert Gordon University, Centre for Process Integration and Membrane Technology School of Engineering
Edward Gobina
Robert Gordon University, Centre for Process Integration and Membrane Technology School of Engineering

DOI: 10.26417/ejef.v4i1.p21-23

Abstract

The use of membranes for gas upgrading has increasingly become of interest as it has shown great potential for efficient and affective gas purification and a pathway to green energy. The emission of greenhouse gases to the atmosphere has detrimental effects on the economy in terms of global warming which has led to many natural disasters, heat waves, food shortage, loss of life and property. To combat this, studies of capturing and utilizing greenhouse gases are ongoing. In this paper, the study of biogas components (methane and carbon dioxide) diffusion through membranes are studied to employ its use as a solution for the challenge. The study involved the use of membranes of different pore sizes (15, 200 and 6000nm) to ascertain the flow characteristics and regime of the gases under different operating conditions. Single gas permeation tests were conducted, and the results show the flow of gases is dependent on factors including molecular weight, kinematic diameter and viscosity of the gas components. It was observed that pressure has a greater influence on the gas flow through membranes compared to temperature with the effect of pore size having the greatest impact. The flux of methane through the membrane is greater than that of carbon dioxide in regular pore geometry and depicts a greater potential for upgrading of biogas.

Keywords: Biogas, upgrading, emissions, nano-structured, membrane, carbon capture

Catalysis Today 388-389 (2022) 87–91

Contents lists available at ScienceDirect

Catalysis Today

journal homepage: www.elsevier.com/locate/cattod

An initial study of biogas upgrading to bio-methane with carbon dioxide capture using ceramic membranes

Priscilla Ogunlude, Ofasa Abunumah, Ifeyinwa Orakwe, Habiba Shehu, Firdaus Muhammad- Sukki, Edward Gobina *

Centre for Process Integration and Membrane Technology School of Engineering, Robert Gordon University, Garthdee Road, Aberdeen, AB10 7GJ, United Kingdom

ARTICLE INFO

Keywords:
Biogas
Upgrading
Sustainable
Membrane
Carbon dioxide capture
Biomethane

ABSTRACT

Supplement to the depleting energy resources and the stringent environmental laws regarding the atmospheric emissions of greenhouse gases, the development of clean and renewable sources of energy has been a great issue. Worldwide, energy usage is steadily increasing and would continue to increase in the coming years; the effects of global warming are also becoming more and more prevalent. Biogas holds a promising future in the sustainable supply of low-cost energy that will minimize greenhouse gas emissions. Unlike solar and wind, biogas does not rely on weather conditions. It can also be stored and transported making it easily adaptable to changes in demand. This study would utilize membrane technology for the upgrading of biogas to a clean and useful fuel replacing fossil fuels and consider the limiting factors of the process found in literature which is the trade-off between gas permeability and selectivity. In doing so, we analyse the factors that affect permeability and selectivity of ceramic membranes and then introduce methods of optimisation. Biogas components are passed through the membrane as feed gas to observe the flow characteristics at various operating conditions for membranes with different pore sizes. It was observed that for all pore sizes studied, there was a proportional rise in flowrate as the feed pressure was increased from 0.2 to 3 bar. Also, an increase in temperature from 20 °C to 100 °C favoured the membrane selectivity. In general, methane gas showed a higher flux than carbon dioxide irrespective of the operating conditions indicating that the permeation of the gases is related to their molecular weight, for example, using 15 nm membrane at 20 °C and 3 bar, a flux of 3.59 and 2.27 L/min was obtained for CH_4 and CO_2 respectively with the same trend recorded using other pore sizes, temperature and pressure ranges. It must also be noted that the pore size plays a vital role in the optimisation of membrane process as the 15 nm membrane, being the lowest mean pore size studied showed the highest separation factor of 1.60 which is close to the ideal Knudsen value. Overall, it was found that the behaviour of gases through these membranes is determined by an interplay of factors – dynamic size and diffusion rate.

1. Introduction

The emission of greenhouse gases (GHGs) have been found as a major contributing factor to global warming. These emissions are usually fostered by manmade activities such as burning of fossil fuels to provide energy, dumping at landfill sites which does not only pollute the environment but wastes vital resources including land, deforestation and many more. When greenhouse gases are released into the atmosphere, heat is trapped (that is, the heat is not allowed to dissipate into space) thereby causing an imbalance of what amount of energy that comes from the sun to the earth and back [1]. This has a massive impact on the earth surface which leads to temperature changes, drying/drought and other transformations in the ecosystem. Evidence has shown that there is a direct link between global warming and climate change, this has made the need for capturing greenhouse gases a matter of global urgency in recent decades [2].

Global warming is described as an increase in the overall air temperature near the earth's surface. In recent times, there have been unfortunate documented events of disasters directly linked to climate change. For instance, Europe experienced a terrible heat wave with Paris reaching its highest ever recorded temperature of 42.5 °C; parts of the United States of America suffered flooding; the people of Chennai in India faced droughts; Australia faced terrible wild fires; and Britain's crop shortage due to drought posed a problem in the food sector. All

* Corresponding author.
E-mail address: e.gobina@rgu.ac.uk (E. Gobina).

https://doi.org/10.1016/j.cattod.2020.11.006
Received 9 March 2020; Received in revised form 3 November 2020; Accepted 4 November 2020
Available online 8 November 2020

crystals

MDPI

Article

A Study of Gas Transport Mechanisms for CH_4/CO_2 Using Ceramic Membranes

Priscilla Ogunlude [1], Ofasa Abunumah [1], Firdaus Muhammad-Sukki [2] and Edward Gobina [1,*]

[1] Centre for Process Integration and Membrane Technology, School of Engineering, Robert Gordon University, Garthdee Road, Aberdeen AB10 7GJ, UK; p.ogunlude@rgu.ac.uk (P.O.); o.abunumah@rgu.ac.uk (O.A.)
[2] School of Engineering & the Built Environment, Merchiston Campus, Edinburgh Napier University, 10 Colinton Road, Edinburgh EH10 5DT, UK; f.muhammadsukki@napier.ac.uk
* Correspondence: e.gobina@rgu.ac.uk

Abstract: Greenhouse gas emissions (GHGs) and their effects have been a matter of global concern over the past decade. As the demand for energy grows in developing economies, there has been a challenge in harnessing and utilising sustainable forms of energy to meet these demands, and despite the effect of global warming and the problems associated with it, the use of fossil fuels is still increasing. This problem has negatively impacted the climate because greenhouse gases evolved from burning fossil fuel increase the concentration of carbon dioxide in the atmosphere and lead to global warming. This study investigates a method of channelling biogas for use as a sustainable energy source by using membrane technology. Initially, by observing the behaviour of biogas components as they travel selectively through the membrane support, the findings showed that both fluid and structural properties have significant impacts on the separation process. The next approach is to modify the membrane to obtain these optimal conditions. Furthermore, by introducing an agent that serves as an adsorptive medium for maximising contact between the pore walls and the gas molecules, this creates an adsorptive layer that preferentially draws the target gas to its surface to deliver both high permeability and selectivity of the membrane.

Keywords: biogas; upgrading; sustainable; membrane characterisation; carbon dioxide capture; biomethane

Citation: Ogunlude, P.; Abunumah, O.; Muhammad-Sukki, F.; Gobina, E. A Study of Gas Transport Mechanisms for CH_4/CO_2 Using Ceramic Membranes. *Crystals* **2021**, *11*, 1224. https://doi.org/10.3390/cryst11101224

Academic Editors: Vladislav V. Kharton and Leonid Kustov

Received: 3 September 2021
Accepted: 7 October 2021
Published: 12 October 2021

1. Introduction

A membrane may be defined as a permeable or semi-permeable layer which controls the flow of compounds and hence delivers one product with less of another component, thus resulting in the product concentration in those components [1]. This process is used in industry for the recovery of reactants and valuable gases, the isolation of products, and pollution control [2]. The flow of gases is based on their differences in permeability, which is a function of membrane properties and the nature of gases [3]. Generally, the performance of a membrane is defined by its permeability and selectivity and a good indication is with high values of both achieved for efficiency in commercial applications, but in practicality, there is a trade-off between these parameters. However, in any given process, there is an economic optimum in the combination of selectivity and permeance.

Permeance/Permeation is a measure of the amount of permeate that flows through the membrane and is evaluated by the flowrate at which a fluid passes through the area of the membrane. Selectivity refers to the ability of the membrane to separate gases and gives a measure of the purity of the permeate gas and losses. It is evaluated by the concentration of components passing through the membrane versus the concentration in the feed [4]. For single gases, it is calculated by the ratio of their permeation rates.

International Journal on Engineering, Science and Technology
Volume 4, Issue 1, 2022 ISSN: 2642-4088

Mass Transfer Characteristics through Alumina Membranes with Different Pores Sizes and Porosity

Priscilla Ogunlude
Robert Gordon University, United Kingdom

Ofasa Abunomah
Robert Gordon University, United Kingdom

Idris Hashim
Robert Gordon University, United Kingdom

Florence Aisueni
Robert Gordon University, United Kingdom

Evans Ogoun
Robert Gordon University, United Kingdom

Samuel Antwi
Robert Gordon University, United Kingdom

Muktar Ramalan
Robert Gordon University, United Kingdom

Tamunotonye Williamwest
Robert Gordon University, United Kingdom

Firdaus Muhammad Sukki
Edinburgh Napier University, United Kingdom

Edward Gobina
Robert Gordon University, United Kingdom, e.gobina@rgu.ac.uk

Abstract: Different membranes covering the macroporous to nano-pororous range and having different porosities have been used to study the mass transfer of methane and carbon dioxide single gases. The effect of flow parameters on the transport mechanisms through porous membranes were reviewed in detail. The characteristics of gas transport through the macroporous, microporous, and nano-porous membranes were investigated with several gas diffusion models in the range of 20–100 ◦C and at pressure differences ranging from 0.2 to 3 bar. The experimental gas permeation data of the membranes were analyzed using the Darcy flow model. The results clearly showed good agreement between the model analysis and the experimental data. The experimental data showed that the permeation followed a parallel flow model in which the behavior of gases was governed by viscous and Knudsen diffusion, although to varied degrees. Permeation of the gases through each membrane varies considering the viscosity of the gases at the same temperature. Furthermore, the membranes followed the configurational diffusion model in which the permeance increased with increasing pressure and decreasing temperature. For the gas flow measurements through macroporous and nano-porous membranes with diameters ranging from 6000nm to 15nm, the results indicate that the experimental flux agrees well with the calculated (model) flux through which gas flows from the bulk stream in the shell side to the membrane outer surface where viscous flow and Knudsen diffusion coexist. The study shows that experimental flux is larger than Knudsen diffusion, and the contribution of Knudsen diffusion to the experimental flux increases with the decrease in the diameter. On the other hand, the effects of gas slippage are considerable as gas velocity near the wall is higher than zero. The slip length effects are inversely proportional to pore size and with driving pressure.

Keywords: Macroporous, microporous, nano-porous, mass transfer, gas transport, mechanisms, membrane